PRODUCTION OF CONTROLLED NETWORKS AND MORPHOLOGIES IN TOUGHENED THERMOSETTING RESINS USING REAL-TIME, IN-SITU CURE MONITORING

by

Janis Michelle Brown

Dissertation submitted to the Faculty of the

Virginia Polytechnic Institute and State University

in partial fulfillment of the requirements for the degree of

DOCTOR OF PHILOSOPHY

in

Materials Engineering Science

APPROVED:

Dr. T. C. Ward, Committee Chairman

Dr. J. E. McGrath

Dr. G. L. Wilkes

Dr. A. C. Loos

Dr. R. G. Kander

April 1994

Blacksburg, Virginia

PRODUCTION OF CONTROLLED NETWORKS AND MORPHOLOGIES IN TOUGHENED THERMOSETTING RESINS USING REAL-TIME, IN-SITU CURE MONITORING

by Janis Michelle Brown

Committee Chairman: Dr. Thomas C. Ward

Materials Engineering Science

(Abstract)

Chemical and physical changes occur during the processing of toughened thermosetting resins. A number of properties are related to the type and sequence of these changes. There is a need for the development of in-situ real-time sensors to follow these changes. Once these sensors are developed, they can be used to preferentially select networks and/or morphologies by feedback-controlled "intelligent" processing.

A practical, durable, inexpensive Fourier Transform Near-Infrared (FTNIR) fiber optic sensor was developed and the cure of a model toughened cyanate as well as a commercial paste adhesive was followed with this sensor in the near-infrared. The design was suitable for many applications. A mold was designed to incorporate the fiber sensor for composite applications.

The growth of the normalized triazine (crosslink) peak appeared to follow second order kinetics. The normalized peak

reflected chemical as well as physical changes. Analysis of the individual peaks showed significant physical effects. Conversion based on triazine concentration did not follow second order kinetics.

In-situ real-time monitoring of network formation in the toughened cyanate trapped a series of novel morphologies by intelligent, interactive manipulation of the processing cycles based on real-time conversion data. Extremes in morphology were produced within reasonable cure cycle variations. These changes in morphology were also observed in a graphite reinforced laminate.

Simultaneous, in-situ monitoring of chemical and physical changes during the cure of a toughened cyanate resin were successfully demonstrated using a FTNIR fiber optic sensor in combination with a microdielectric sensor and/or a visible fiber optic sensor. This combination of these three sensors can potentially provide simultaneous monitoring degree of cure, gelation, temperature, density, phase separation, vitrification, and mobility during cure. Typically, state-of-the art in-situ sensors are used to provide information on mobility.

DEDICATION

To my family and friends, who have loved and supported me through all of this.

Also to those that have mentored and inspired me throughout my industrial and academic career.

ACKNOWLEDGMENTS

I would first like to thank my advisor, Professor T. C. Ward for his guidance in this endeavor. Thank you, Dr. Ward, for your good advice, your encouragement, for your efforts to teach me polymer physical chemistry, and for taking in a runaway from industry.

I would also like to extend my thanks to my committee for their suggestions and help, Professors McGrath, Wilkes, Kander, and Loos. I would also like to thank those that were not officially on my committee but got pulled into some of the research anyway, such as Professor Kranbeuhl, Dr. J. Hellgeth, and Mr. D. Shimp.

My thanks to the National Science Foundation Center for High Performance Adhesives and Composites and Virginia Institute for Materials Systems for funding. My thanks to General Dynamics/Ft. Worth Division for allowing me academic leave of absence while I worked on this degree. My special thanks to Mr. McKague, who taught me a lot of what I know about composites and helped arrange the academic leave.

I want to acknowledge the help of a number of other folks, without whom this would not have been possible. Thanks to Dr. S. Wilkinson for showing me the ropes when I got here to Virginia Tech. My eternal gratitude to Mr. S. Srinivasan for originating and coordinating the cyanate research and for the countless batches of resin he had to mix up for me. My thanks to Mr. A. Rau over in ESM for all the computer time trying to fit my data.

Dr. G. George at the University of Queensland offered a great

deal of help when we switched over from evanescent wave sampling to the transmission technique. My sincere thanks to Dr. George for his advice. I appreciate the kind help of the people in the Virginia Tech Fiber Optics Center (FEORG) for the great lessons and suggestions on fiber optics and the Physics Shop for a great job of machining all my strange sample holders. My thanks to Mr. S. McCartney for the scanning transmission electron micrographs. I really appreciate the trip that Mr. D. Hood made out to Tech to bring the Dek Dyne system from Williamsburg to make the simultaneous FTNIR and dielectric runs.

I want to thank the polypkem lab for making me welcome here and for the friendships I've made in the group. I also want to thank the other friends I've made here (as well as those outside of Virginia) for their friendship, help, encouragement, inspiring technical discussions and chocolate during this trying time. I especially want to thank Donna, Susan, and Pamela for their constant encouragement and moral support!

I'd also like to acknowledge my parents, Bill and Patsy Brown. Without their love, help, and encouragement I would never have made it through this adventure.

TABLE OF CONTENTS PAGE

TABLE OF CONTENTS PAGE

LIST OF FIGURES PAGE

LIST OF FIGURES PAGE

LIST OF FIGURES PAGE

LIST OF FIGURES PAGE

LIST OF FIGURES PAGE

LIST OF FIGURES PAGE

LIST OF TABLES PAGE

CHAPTER 1
INTRODUCTION

High performance thermosetting resin systems are often multi-component formulations requiring a number of complex chemical and physical changes to occur in the proper sequence to produce the appropriate mechanical properties. What seems a simple issue of processing may involve four or five different, possibly competing reactions; phase separation; and the transformation of the liquid low molecular weight material to a glassy solid. Changing the cure profile of such a thermosetting resin can drastically alter the properties through changes in the network or in the morphology. This has been repeatedly demonstrated for toughened epoxies (4-4-1 - 4-3, 4-15 - 4-33, 4-37 - 4-42) but not so clearly delineated for other reaction chemistries and tougheners.

In this study, we have demonstrated that based on knowledge of the chemical reactions and morphological changes, intentional, significant changes can be made in the morphology of a toughened dicyanate thermosetting resin through intelligent manipulation of the cure cycle and real-time knowledge of the conversion of the system as obtained by a FTNIR fiber optic sensor developed for this project. These changes were shown not only to occur within reasonable cure cycle variations for neat resin but were unintentionally induced through a processing change in a graphite reinforced composite containing this resin.

This sensor can be used alone or was demonstrated in-situ to provide simultaneous real-time complimentary chemical information to the physically information obtained from the implantable dielectric sensor typically used in industry to monitor changes in thermosetting resins during processing. Multiplexing the fiber optic signal to a visible detector can provide even more information, such as phase separation.

In doing so, a useful, practical, durable Fourier Transform near-infrared (FTNIR) fiber optic sensor has been developed. The

geometry is applicable for a number of different geometries from the inclusion in a mold to monitoring the changes in an adhesive joint. The cure of a model toughened cyanate was followed with this sensor in the near-infrared by monitoring the triazine absorbance at 4625 cm-1. Preliminary kinetic models were established but were complicated by the wealth of physical data in the spectra. Useful physical information, such as a temperature calibration and an indication of phase separation, was derived from physical changes in the peak areas and locations.

CHAPTER 2

DEVELOPMENT OF A PRACTICAL FOURIER TRANSFORM NEAR-INFRARED FIBER OPTIC PROBE FOR DETERMINING CHEMICAL CHANGES DURING THE CURE OF A TOUGHENED THERMOSETTING RESIN

2.1 INTRODUCTION

Cure of a thermosetting resin is very complex consisting of chemical reactions, physical changes such as gelation and vitrification as the network develops and, in the case of toughened systems, possibly phase separation. It is often desirable to follow both the chemical changes and the physical changes in-situ because such changes eventually determine the properties of the system. In-situ dielectric techniques (see Chapter 5) have been developed to monitor resulting physical changes. The development of techniques to directly monitor the chemical changes has been much slower. Recently, some of these techniques have evolved. So far, they have been expensive or impractical for real applications.

A practical, rugged, inexpensive FTNIR fiber optic sensor was designed for following chemical conversion during cure. The sensor was easily adapted for use in a mold, a lap shear joint, and a geometry suitable for scattering studies. The cure of a model toughened cyanate resin and a commercial cyanate adhesive were followed by monitoring the area of the peak at 4625 cm-1 due to the triazine crosslink. Monitoring the cure of a graphite reinforced toughened cyanate composite was attempted, but little data obtained since the original mold design did not place the sensor in resin rich regions. An alternate mold geometry was proposed.

The fiber optic spectroscopy techniques developed and demonstrated in this chapter will later be used to modify the morphology of the toughened cyanate by interactive conversion monitoring (Chapter 4) and combined with in-situ dielectric sensors or fiber optic visible sensors (Chapter 5) to provide simultaneous

chemical and physical information during cure.

2.2 BACKGROUND

2.2.1 Fiber Optic Probes

In a recent review of processing trends, Mijovic, et al. (2-1) described fiber optic spectroscopy as "the most promising method for in-situ monitoring of cure." A number of recent efforts (2-1 - 2-25) have been directed toward in-situ monitoring of the chemical changes in the mid-infrared fingerprint and the development of new fibers to use in monitoring. Despite the promise, these fibers have seen few real applications. To some extent, this lack of application can be blamed on the generally experimental, high attenuation, expensive, brittle, at times water soluble and/or toxic materials that have been used to obtain transmission in the mid-infrared region. Many chemical groups absorb in the near-infrared region (NIR). The near-infrared may be a more viable region for fiber optic spectroscopy than the mid-infrared. As originally shown by George, et al (2-20 - 2-25) there may be certain advantages to using more conventional, commercial fiber optic sensors in the near-infrared rather than the mid-infrared.

In 1988, Compton, et al. (2-2) pioneered the use of a chalcogenide fiber in the evanescent wave mode (like multiple internal reflectance or attenuated total reflectance) with 3 to 6 cm of the cladding removed to make real-time, in-situ measurements in the region of 1300-1800 cm^{-1} during the cure of a thermoplastic polyimide, LaRC-TPI. They also observed the cure of a graphite reinforced/ nadic terminated polyimide (PMR-15) prepreg. Later studies followed the cure of an aerospace graphite/epoxy in the region between 2500 and 3600 cm^{-1} using an unclad sapphire fiber sensors (Figure 2.1-a) in conjunction with ZrF_4 lead-in and lead-out fibers (2-2, 2-3) and proposed the use of a fiber optic sensor for "monitoring and controlling the cure and manufacture of advanced composite materials." The fiber work was extended (2-4) to actual processing conditions and monitoring the cure of the graphite/PMR-15 material (demonstrated in a press) and the graphite/epoxy

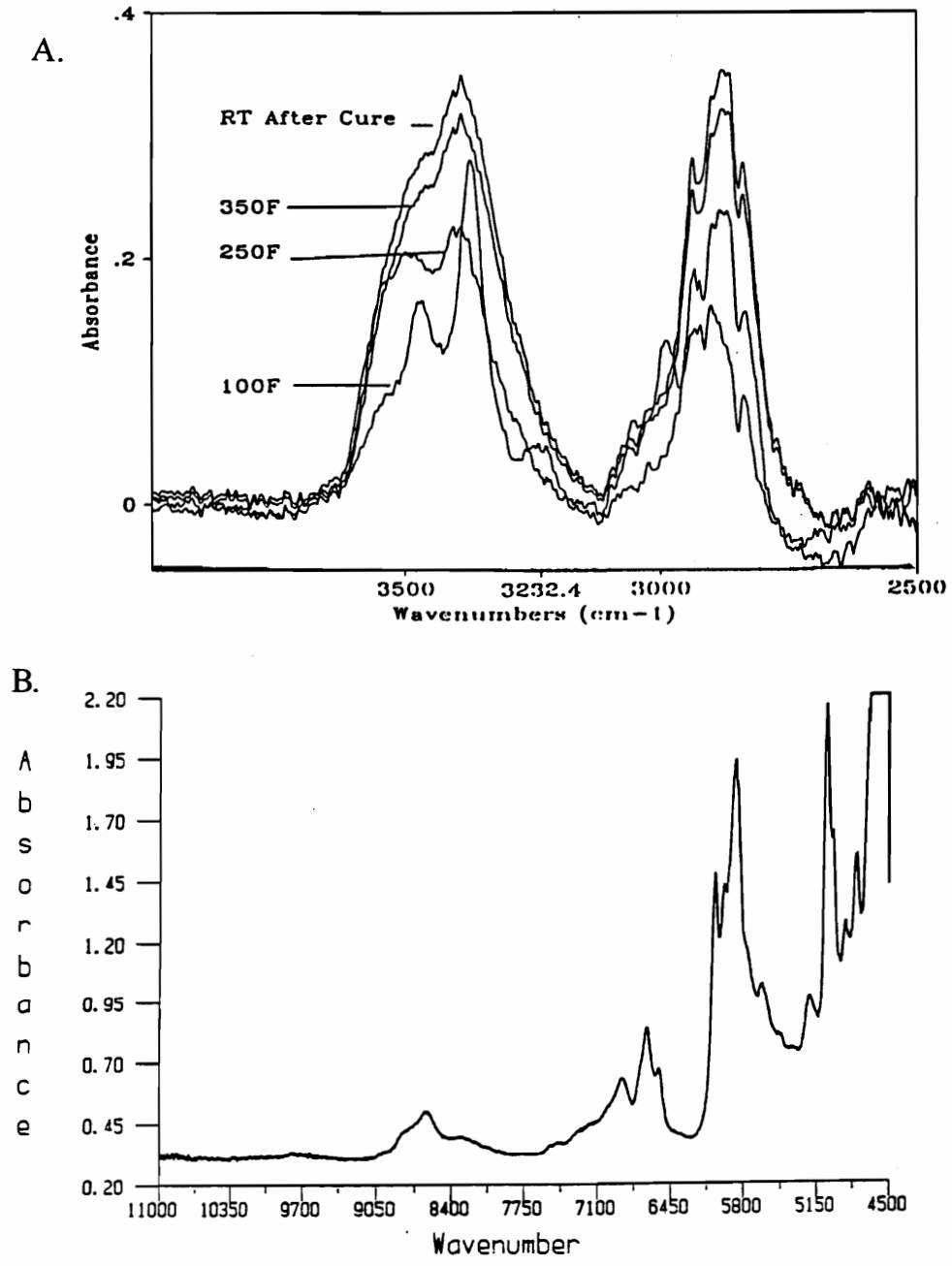

Figure 2.1. A Comparison of Fiber Optic Spectra: A. Using Evanescent Wave Technique (2-102) in the Mid-Infrared and B. Transmission in the Near-Infrared (2-20 - 2-23).

material (in an autoclave). Most recent studies have diversified, using the mid-infrared fiber optic technique in a diffuse reflectance configuration to study degree of cure and solvent retention in a melamine epoxy resin (2-6) and monitoring of urea in plasma (2-19).

Evanescent wave techniques have been explained as being similar to attenuated total reflectance. More quantitatively, as discussed by Harmer and Scheggi (2-27), citing Sutherland, evanescent wave sampling occurs when an unclad fiber (or core) is in contact with a material of lesser refractive index. The light will be retained in the core and transmitted to the detector if the angle of incidence is greater than critical angle θ_c:

$\theta_c = \sin^{-1}(n_2/n_1)$
n_1 = refractive index of core or "waveguide"
n_2 = refractive index of the surrounding liquid

An electrical field of intensity (E), which drops off exponentially with distance from the interface, will extend out into the material, thus sampling it:

$E = E_0 \exp(-z/d_p)$
E_0 = electric field at interface
z = distance from the interface
d_p = penetration depth
= distance at which E_0 is reduced by 1/e

$$d_p = \frac{\lambda}{(2 * \pi * n(\sin^2(\theta) - \sin^2(\theta_c))^{0.5}}$$

The depth of penetration is proportional to the wavelength of light. The absorbances in the higher wavelengths are very weak, requiring long path lengths of 1-10 mm or more. For UV light, silica and water at a 75 degree angle of incidence, the depth of penetration is about .0001 mm (100 nm). For evanescent curing studies, a high refractive

index fiber such as chalcogenide (r.i. = 2-3) or sapphire (r. i. = 1.7) is required with the epoxy (r. i. = 1.45. to 1.6) to take advantage of the evanescent wave sampling (2-5). A fiber such as zirconium fluoride has a refractive index (1.51) very similar to that of the epoxy. In evanescent wave mode, the light and information would be lost into the resin rather than carried down the fiber to the detector.

Chalcogenide provided an infrared window from 1200-3000 cm^{-1}. For early tests, only 3 meters of fiber could be used due to high (10-12 dB/m) attenuation of fiber (2-2 -2-3). Sapphire fiber sensors with ZrF_4 lead-in and lead-out fibers allow evanescent wave access to the region from 2400 - 4500 cm^{-1}. Combined, these two fiber optic choices can provide a great deal of information on the cure of resin systems. Other fibers (2-1) have recently been proposed that can go farther into the far infrared or have some other advantage. In general, most of the materials used for fiber optics sensors have certain disadvantages. They are often toxic, water sensitive, brittle, expensive, and even light sensitive. There is a significant need for material development in this area.

Mijovic, et al. (2-1) reviewed several different materials which have been used in the mid-IR for fiber applications: chalcogenide, group I halides, thallium halides, and silver halides. Most of the probes described by Mijovic have certain drawbacks. The chalcogenide fiber has been reported to have variable fiber quality (2-1), has certain temperature limits (2-3 - 2-6) which many current thermosetting systems may exceed during processing, and can only be considered "semi-commercial", i.e. available in small quantities. The group I halides, although promising a very good spectral range, are also non-commercial, as well as often very water soluble (2-34) or at best hygroscopic. A NaCl FTIR cell provides very good transmission in the infrared but turns into a puddle when left on the lab bench overnight. Thallium halides have been used in FTIR optics; most well known would be the KRS-5 used as a cell for attenuated total reflectance. According to the Merck index (2-32), most thallium halides are highly toxic as well as somewhat water soluble. The

thallium halides have also not been made into fibers on a commercial basis. Silver halides hold promise (2-1), although it has been reported (2-4 - 2-6) that they might not be suitable for long fibers. It is also not known what repercussions the light sensitivity (2-32) of silver halides will have.

Table 2.1 lists a number of optical materials that transmit in the infrared, near-infrared, and visible along with their ranges, refractive indices, attenuation, and comments. Some of these materials, for example zirconium fluoride, have been made into fibers, others have not. Later work by Druy (2-4 - 2-6), used these to some degree. Early work in this project also used ZrF_4 (listed as moderately water soluble at 1.32 g/100 ml (2-32) to carry light to and from an unclad sapphire fiber optic sensor. ZrF_4 is listed as being moderately water soluble at 1.32 g/100 ml (2-32). The ZrF_4 cables used in the early part of this study required heavy metal cladding to protect them from attack by atmospheric moisture. Sapphire is available as a single crystal fiber (from Galileo) in limited supply. It has a good range, theoretically covering the high frequency mid-infrared to above the visible (realistically, the fiber may not work well in evanescent wave mode in the near-infrared or visible). Sapphire is not attacked by water, or many solvents. This solvent insensitivity in conjunction with a very high melting point/use-temperature, and suitable refractive index make sapphire an extremely attractive sensor for high frequency mid-infrared to visible. The fibers are also extremely brittle, expensive, and seldom reusable if glued into a thermosetting resin. This is a drawback if one desires a rugged, disposable sensor for practical applications.

Of the other materials in the table, perhaps most attractive for future work in the mid or high frequency infrared would be some sort of modified magnesium oxide or calcium fluoride. Both are fairly innocuous, occur in large quantities in nature, and have a high enough use-temperatures that the fiber can be used in the processing of most thermosets. Magnesia (MgO) offers an attractive range from 1053 - 33,333 cm^{-1} (2-31) and a refractive index close

Table 2.1 Optical Materials (from various references)

Material	Range (cm^{-1})	R.I.	Attn (dB/m)	Fiber Mfd	Comments
Chalcogenide :Mixture of As, Ge, Se, S, Te As_xS_{x-1}	1000-3300	1.9-3.0	0.2-15	Yes	Fiber quality varies Semi-commercial. Use Temp 300°C.
Group Ia Halides: NaCl, NaI, KCl, etc	285 - 40000	1.45 - 1.79	4.2	Yes	Water Soluble. Non-commercial
Thallium Halides (KRS-5)	400 - 20,000	2.3 - 2.4	0.4 - 0.6	Yes	Very toxic. Some are water soluble. Non commercial (fibers).
Silver Halides	667 - 3000	1.96 - 2.25	0.5 - 4.0	Yes	Possible length limits and light sensitivity. Mostly non-hydroscopic. Non-toxic. Use temp: 400°C
Zinc Sulfide: Wurtzite or Sphalerite or "Irtran"	770 - 50,000	2.37 - 2.38	Not Avail	TBD	Low solubility in water. No LD_{50} reported. Sublimes at 1185°C. Possible air sensitivity.
Zirconium tetraflouride: ZrF_4	2200 - 8500	1.51 - 1.59	Not Avail	Yes	Slightly soluble in water. LD_{50} = 98 mg/kg. T_g = 250°C.
Yttria: Y_2O_3	1087 - 38,462	TBD	Not Avail	No	T_m = 2410°C

Table 2.1 Optical Materials (continued)

Material	Range (cm^{-1})	R.I.	Attn (dB/m)	Fiber Mfd	Comments
Sapphire: Al_2O_3, corundum, alumina	1333 - 66,670	1.76 - 1.78	Not Avail	Yes	Use temp >1500°C. Semi-commercial. Very low water solubility. Brittle. Expensive.
Magnesium Oxide: MgO, periclase	1053 - 33,333	1.74	Not Avail	No	Very high melt temperature, low water solubility but may absorb some water. No LD_{50} available. Hardness = 6.0
Calcium Fluoride: CaF_2	847 - 76,920	1.43	Not Avail	No	Low water solubility. Naturally occurring in large quantities. Non-toxic. Hardness = 4.0
Titania: TiO_2, brookite or anatase	1613 - 23,256	2.5 - 2.7	Not Avail	No	T_m = 1825°C.
Calcium Aluminate Glass: $CaAl_2O_4$	1818 - 25,000	1.64 - 1.67	Not Avail	No	Decomposes in water.
Fused Silica: SiO_2	2500 - 62,500	~ 1.5	Not Avail	Yes	Large -OH absorbance. Use temp <400°C. Water and solvent resistant. Commercially available.

Table 2.1 Optical Materials (continued)

Material	Range (cm^{-1})	R.I.	Attn (dB/m)	Fiber Mfd	Comments
Fused Quartz: SiO_2	2380 - 55,555	1.54 - 1.55	Low	Yes	Similar to Fused Silica.
"Low-hydroxyl" Silica	4000 - 26,310	~1.5	0.01 - 0.2	Yes	Low-hydroxyl. Numerical aperature of 0.22. Use temp <400°C. Pressure <100 kpsi. Commercial and inexpensive.

References: 2-1, 2-32, 2-2 - 2-6, 2-45, 2-35, 2-34, 2-98 2-97, 2-20 - 2-25, 2-31.

to that of sapphire, suitable for evanescent wave sampling. Synthetic MgO (periclase) has been produced and polished as a semiprecious stone (2-35). The stone is colorless and 'tough'. However, the polish is reported to dull rapidly with ambient humidity. No fibers have been reported. A blend of sapphire and magnesia has an attractive window (2-31) but there is little available information on this material.

Calcium Fluoride would be another potential fiber material. Calcium fluoride (fluorite) also provides a very attractive window from 847 - 76,920 (2-31) cm^{-1}, a reasonable melting temperature (2-32, 2-34), low water solubility (2-32, 2-34), is fairly safe (2-32), and occurs naturally in large quantities as fluorite. For the evanescent wave sampling, the low refractive index (1.434 (2-35)) of fluorite might be a drawback since evanescent wave sampling requires that the fiber have a higher refractive index than the resin being sampled. The refractive index of chalcogenide, as given in Table 2.1, is 2.0 - 3.0; sapphire is 1.7-1.8. The refractive index of epoxies varies from 1.45 - 1.6 (2-3 - 6). The bisphenol A based cyanate used in this study has a refractive index between 1.53-1.58 (2-98), changing slightly with cure. A fiber with a lower refractive index than chalcogenide could potentially be used in transmission sampling rather than evanescent wave sampling.

Although these alternate fiber materials might offer potential alternatives to the often water soluble, at times toxic, more exotic materials mentioned earlier, the materials discussed in the past few paragraphs have not been manufactured into fibers. As reported by Mijovic, et al. (2-1) and Flinn and Trojan (2-36) good quality fiber is essential and there is a substantial learning curve. Flinn and Trojan (2-36) list a number of either intrinsic material properties or processing flaws which can result in reduced light transmission in fiber optics. These include: ultraviolet electronic transitions, infrared molecular vibration, transition metals and other impurities, hydroxyl vibrations, scattering due to Rayleigh scattering by density variation, other scattering due to gross imperfections, or spontaneous Raman

and Brillouin scattering. Maturation of a fabrication process for these new fibers would most likely take a number of years, if indeed it is possible or financially rewarding. There is a lot of room and need for future development in this regime of mid and high frequency infrared transmitting fibers.

If adequate chemical data can be obtained in the near-infrared or visible, quartz or silica is a very attractive mature fiber optic material. This mineral has been widely applied as an optical material in this region and is commercially available in a number of fiber optic forms and sizes. These fibers are rugged and have a variety of refractive indices, claddings, and/or coatings. The transmission range is reported to start at about 2400 cm^{-1} (but more reasonably is 4000+) and extend far past the visible region. Pioneering work on fiber optic cure monitoring in this region was recently reported by George, et al. (2-20 -2-25) at the University of Queensland.

In 1989, Culshaw and Dakin (2-27) reviewed some of the advances in visible and near-infrared fiber optic sensors in chemical and medical testing. At that time, fiber optics were being used as sensors in the ultraviolet/visible for permeable membrane sensors for pH, pO_2, pCO_2, as well as various ions and fluorescence; to detect gas in the overtone region from 5882-8333 cm^{-1}; in Raman spectroscopy; as refractive index and liquid level sensors; for monitoring oil pollution in water and particle contamination in water by turbidity; for measuring blood oxygen by in-vivo measurements of hemoglobin (reflectance) or fluorescent quenching of dye; in glucose determination by reverse competition binding; for algae mapping; in immunological assays using evanescent wave sampling of bound antibodies; and also as physical sensors for body temperature and cardiovascular and intercranial pressure sensors, blood velocity and flow.

Of interest in curing studies would be measurements such as refractive index of a resin (which changes with cure) or turbidity (which occurs in phase separated systems). Several researchers (2-28 - 2-29) have used fiber optic refractive index measurements to

monitor cure of thermosetting resins. Turbidity in oil contaminated water has been studied by fiber optics using laser transmission and scattering. Particle size was determined by scattering angle (2-27). Changes in the intensity of scattered light gave a measure of concentration.

A very interesting series of articles by G. George, et al. (2-20 - 2-25) studied the cure of a diamine-cured aerospace epoxy in the near-infrared (NIR) by fiber optic, cuvette, or a combined FTNIR/Differential Scanning Calorimetry (DSC) techniques. As pointed out by George, NIR spectra are "less complex than those obtained in the mid-infrared region." The near-infrared is not as well characterized as the mid-infrared. The near-infrared is described as extending from 4000 to 14,790 cm^{-1} (2-33) and is a region of overtones and X-H (X = C, N, and O) stretches. Since the absorbances are much weaker in the near-infrared, not all groups can be observed. A few polymerization reactions have been studied in the NIR (2-37, 2-40). Peak shifts in some blends have also been studied in this region (2-37, 2-40). Most of the near-infrared studies (and peak identifications) relate to food, agriculture, or pharmaceutical applications (2-38 - 2-40), although there were some earlier peak assignments summarized by Colthrup (2-41).

George, et al.'s (2-2 - 2-21) earliest work used a fiber optic technique (Figure 2.1-b and 2.2) to monitor cure of a 4 4' diaminodiphenylmethane (TGDDM) 4, 4' diaminodiphenylsulfone (DDS) based epoxy with or without a boron trifluoride mono-ethylamine (BF_3MEA) catalyst at 140°C by fiber optic transmission in the near-infrared. An adapter was built which allowed the beam to be focused on the fiber optic end. A Quartz et Silice 600 micron core plastic clad silica fiber was used. The loss of primary amine at 5067 cm^{-1}, the appearance of hydroxyl groups at 6970 cm^{-1}, and loss of C-H on the epoxide peak at 8627 cm^{-1} were followed. Without the catalyst, the reaction was autocatalytic. With the catalyst, the reaction followed nth order kinetics. Later (2-21), the same resin system (no catalyst) was used with a "microcapillary cell" consisting

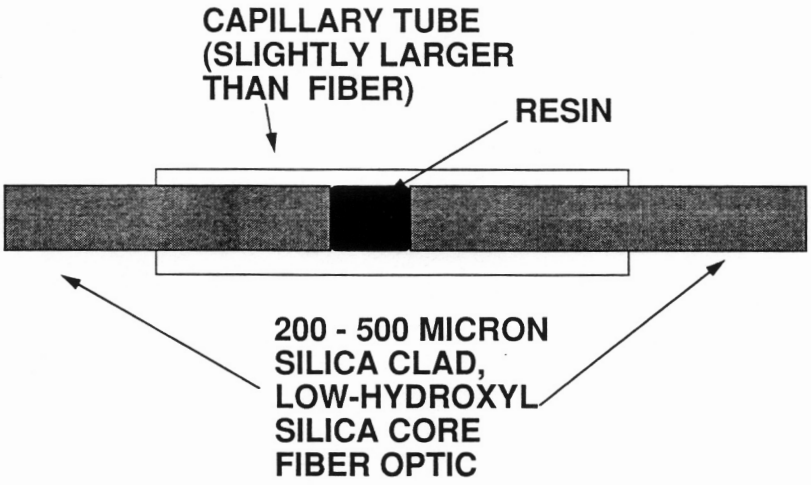

Figure 2.2. "Microcapillary Cell" used by George, et al. for Fiber Optic Transmission Spectroscopy in the Near-Infrared (2-20 - 2-23).

of two cleaved fiber optic ends inserted into a silvered capillary glass tube slightly larger than the fiber optic to observe cure at several temperatures. Prior to the insertion of the fiber ends, the resin was heated above T_g to allow flow into the cell. The 2-5 mm gap between the fiber ends was filled with this resin. The cell was then heated to the cure temperature. The fibers were used to transmit light through the resin rather than in the evanescent wave sampling mode. Data was obtained with Quartz et Silice 600W and 1000W plastic clad silica fibers, tungsten quartz-halogen lamp, an indium antinomide detector and a quartz beam splitter. A background spectra was obtained with a single fiber.

The authors looked for a suitable absorbance to provide quantitative measurements and real-time cure information. They wished to observed the hydroxyl (-OH) overtone at 7100 cm^{-1} with the PCS 1000 W but this region was inaccessible due to the strong hydroxyl absorbance in the silica fiber. The regions from 4700 to 7050 cm^{-1} and 7350 to 11000 cm^{-1} were accessible. Negative peaks due to methyl group in plastic cladding 5400 - 6000 cm^{-1} and 8400 cm^{-1} interfered with some of the peaks, such as the -CH stretch on the epoxy ring. This was eventually eliminated by the use of silica-clad 200 micron core fluorine-doped (low-hydroxyl) silica fiber (Quartz et Silice AS200/280A). A decrease in the epoxy and diamine peaks was observed along with an increase in the hydroxyl peak. The negative peaks from the original fiber made monitoring of the epoxy peak at 8627 cm^{-1} difficult. The authors wished to follow a primary amine absorbance since the primary amine should decrease throughout most of the cure. One peak combined a primary and secondary amine absorbance. When deconvoluted, this peak gave very interesting information about the primary and secondary amines, but deconvolution was impractical for real-time cure monitoring. The authors felt that the primary amine at 5067 cm^{-1} was best for quantitative monitoring of the loss of the primary amine and followed this reaction by ratioing this primary amine peak to a C-H reference peak at 5660 cm^{-1}. Qualitatively the -OH peak was

seen to increase; however, measurement of hydroxyl concentration from the -OH peak was difficult due to hydrogen bonding. The authors developed a model based on the primary amine peak and produced a program to give real-time conversion based on the primary amine concentration.

The authors then began more in-depth modeling with the same resin (2-23) using a quartz cuvette instead of the fiber. Dead zones and negative peaks due to cladding had made some of the peaks difficult to monitor with the original fiber optic. Various peaks were deconvoluted to allow calculation of secondary and tertiary amine and hydroxyl concentrations. There were still some difficulties with H-bonding of the -OH peak. For example, when hydrogen-bonded, the peak would move to lower wavenumber. They calculated free hydroxyl, measured the C-H stretch of the epoxy group, deconvoluted various groups, and observed an "excess" epoxy reaction. Concentrations were fit to empirical rate curves. The primary amine reaction was autocatalytic and not affected by viscosity. In contrast, the secondary amine reaction rate was very sensitive to physical changes, decreasing at the onset of vitrification, and finally stopping with a number of secondary amines still unreacted. For the etherification reaction of epoxy and hydroxyl, they observed two mechanisms, one possibly due to a contaminant, and developed a complex equation for total loss of epoxy.

Most thermosetting cure models are based on heat evolution by differential scanning calorimetry. These models do not distinguish between various reactions or consider substitution effects. Most recent work by George, et al. demonstrated a simultaneous FTNIR/DSC technique (2-22 - 2-24) to study determine which chemical changes coincide with the heat of reaction as observed by DSC. The maximum rate of disappearance of the epoxy peak at 4535 cm^{-1} coincided with the maximum heat evolution rate by DSC.

A very interesting joint study between D. Rogers from the University of Queensland and E. Marand of Virginia Tech in 1992 (2-99) looked at microwave cure of the epoxy described above. Using

the Nicolet 800 spectrometer and fiber optic adapter discussed in a later section along with the Quartz et Silice silica-clad, low-hydroxyl silica core fibers described above, Rogers and Marand characterized the chemical differences when the epoxy was cured using microwave instead of thermal heating. Sampling the resin with the capillary tube was quite difficult. The resin first had to be heated to flow into the capillary tube. Then it had to stay fluid long enough for the fiber ends to be inserted and the proper gap obtained while assuring that the resin did not flow out of the capillary. The capillary tube had to be suitably sealed where the edges of the capillary tube met the fiber, and the sample had to be safely inserted into the cavity. This sample preparation was further complicated by the fact that the teflon capillary tube was translucent at best. Most of these problems (and more) were later encountered when the capillary tube technique was applied to a high viscosity, toughened cyanate in this study.

According to George, et al. (2-20 - 2-25), the advantages of the fiber optic cure monitoring technique when compared with dielectric cure monitoring (beyond seeing the chemical rather than the physical changes) are that there is no interference from the electrically noisy processing environment when the fiber is used, "no reference electrode" is required, only a tiny sensor area is needed, and more than one constituent can be analyzed. NIR transmission has certain advantages over MIR chalcogenide evanescent wave techniques. The spectra are much less complex in the NIR than in the MIR. Better, much less expensive fibers can be used. The advantages of the NIR fiber optic sensor and the excellent spectral quality obtained with this technique led to our redesign of the "microcapillary cell" to a more practical geometry.

There have been several recent publications related to near-infrared fiber optic techniques. Lin and Brown (2-44) developed a temperature sensor based on shifts in the -OH peak in water at 6900 cm^{-1} with temperature. The -OH peak moves 162 cm^{-1} over a 65°C range due to changes in H-bonding. As will be discussed in Chapter

3, the location of the aromatic ring stretch at 4675 cm^{-1} could be used as an internal temperature calibration. A very exciting development in FTNIR fiber optic spectroscopy was published this year by Cassis and Lodder (2-30). They used the penetrating power of the near-infrared, a fiber optic probe, a micropositioning stage, and a super computer to record spectra as a function of position, enabling them to map concentrations much as magnetic resonance imaging can be used to map water content variations in larger items.

2.3 EXPERIMENTAL

For most of the experiments, a thermosetting resin formulated by Srinivasan (2-100, 2-104) was used, composed of 100 parts Ciba Geigy B-10 dicyanate monomer (also called the bisphenol A dicyanate or BADCy), 250 ppm aluminum acetyl acetonate (AlAcAc), 2 pph nonyl phenol with or without 25% of a reactive thermoplastic (M_n = 15K, hydroxyl-functionalized phenolphthalein-based, amorphous, polyarylene ether sulfone (PPES-OH)). The synthesis of the toughener has been described in detail elsewhere (2-100, 2-104). The thermoplastic, when used, was dissolved in the BADCy at about 104°C. The AlAcAc was dissolved in the nonyl phenol and added to the mixture. The resin was then degassed and stored at room temperature in a desiccator. The dicyanate resins have been documented to have a fairly long shelf life if kept dry (2-103). New batches were made if the resin was over 7-10 days old. Upon cooling, the BADCy monomer crystallized. Resin samples were again reheated to 104°C and mixed prior to use to insure homogeneity and immediately applied to a preheated surfaces. Some early experiments used a toughened modified bismaleimide resin based on Ciba Geigy Matrimid 5292 as shown described in Reference 2-52.

All mid-infrared or near-infrared spectra were obtained using a Nicolet 800 Fourier transform infrared spectrometer. In some cases, data was processed in real-time and transferred to a Compaq 386/30 through the Nicolet printer port (see Appendix). For mid-infrared (MIR) experiments in the bench sample chamber, a Nicolet globar source, a NaCl beam splitter and a liquid nitrogen cooled

MCTA mid-infrared detector were used. In the near-infrared (NIR) experiments in the sample chamber, a tungsten halogen white light source (GE 1982), a CaF_2 beam splitter, and a lead selenide (PbSe) detector were required. This allowed access to the region between 2400 and 9000 cm^{-1}. For both MIR and NIR in the bench top sample compartment, samples were sandwiched between two potassium bromide (KBr) salt cells. For the longer path length required for the NIR, a 2.5 mm thick steel washer was used as a spacer. Heat was provided by a Spectratech heated cell and temperature control by either a Nicolet GC7000 or a IBM PC with a DAS-8 controller board. The control program was developed by Webster for his polysulfide heating experiments (2-105). Cure cycle ramps and dwells were controlled with the DAS-8 board with input from a thermocouple imbedded in one of the KBr plates. This sample geometry was necessary since there was a significant temperature gradient across the heated cell. Isothermal experiments controlled by the Nicolet GC7000 used the temperature calibration obtained by embedding a thermocouple in the salt plates. All isothermal runs used KBr cells preheated to the desired temperature.

Fiber optic experiments utilized the Nicolet Fiber Optic Adapter shown in Figure 2.3 (2-45). Through a series of mirrors, the adapter allowed the beam to be focused down to approximately 300 micron diameter. On the detector side, an XYZ stage allowed optimum alignment of the signal coming in through the fiber with the detector. This adapter contained a dedicated liquid nitrogen cooled indium antinimide (InSb) detector which was used in conjunction with the tungsten halogen white light source and CaF_2 beam splitter previously described.

Initial experiments with the toughened bismaleimide resin used an evanescent wave sampling technique similar to that described by Compton, et al (2-2 - 2-5). Six to eight centimeters of unclad, polished 300 micron diameter single crystal sapphire (from Galileo) was used like an attenuated total reflectance cell. Metal clad ZrF_4 fibers (also from Galileo) were attached directly to the Nicolet

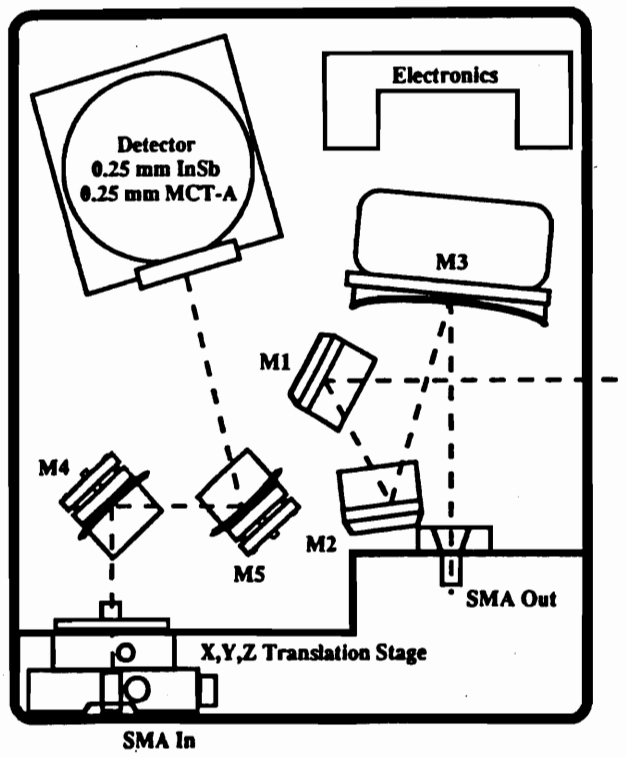

Figure 2.3. Nicolet Fiber Optic Adaptor for Nicolet 800 FTIR Spectrometer (2-45).

fiber optic adapter with SMA connectors. The ZrF_4 fibers were joined to the sapphire fiber through a reusable SMA test connector. The reusable connectors covered about 8 cm of the fiber of the 20 cm long fiber, leaving only 8-10 cm for sampling. When utilized in conjunction with the near-infrared optics, this configuration allowed access to the high frequency mid-infrared region from 2400 to 4000 cm^{-1} as shown in Figure 2.4.

The reactive groups for the dicyanate do not absorb in the region shown in Figure 2.4. According to Colthrup (2-41), there should be an overtone of the cyanate group at 5250 to 5500 cm^{-1} in the near-infrared (NIR). Evanescent wave sampling does not typically penetrate far enough into the sample in the NIR, since a longer path length is typically needed to pick up the weaker absorbances. For the majority of the work, the near-infrared transmission technique developed by George, et al. (2-22 - 2-24) was used. George and coworkers at the University of Queensland built an adapter and XYZ stage. An epoxy resin was inserted into a capillary tube. Light was transported to and from the resin by two low-hydroxyl silica fiber. The fiber ends were inserted into the capillary tube and placed 2 to 5 mm apart. The gap was filled with the resin. Data was obtained in transmission.

Limited data (Figure 2.5-b) for the cyanate were obtained with the capillary tube technique. The high viscosity of the toughened system and crystallization of the resin upon cooling made it very difficult to work in the capillary tube. An alternate geometry which would allow the preheated resin to flow between already optically aligned fibers was designed. This design is shown in Figure 2.6 and will be referred to as the "modified" or "stand-alone sensor" geometry. In this case, a 22 mm (0.875 inch) x 22 mm (0.875 inch) x 1.56 or 3.2 mm thick piece of aluminum was cut. A 0.38 mm wide x 0.5 mm deep (0.015 inch x 0.020 inch) groove was machined in the middle of the large, flat side of the sensor. Since this groove was slightly larger than the outer diameter of the fiber optic, a small piece of gas chromatography capillary tube (Polymicro Technologies

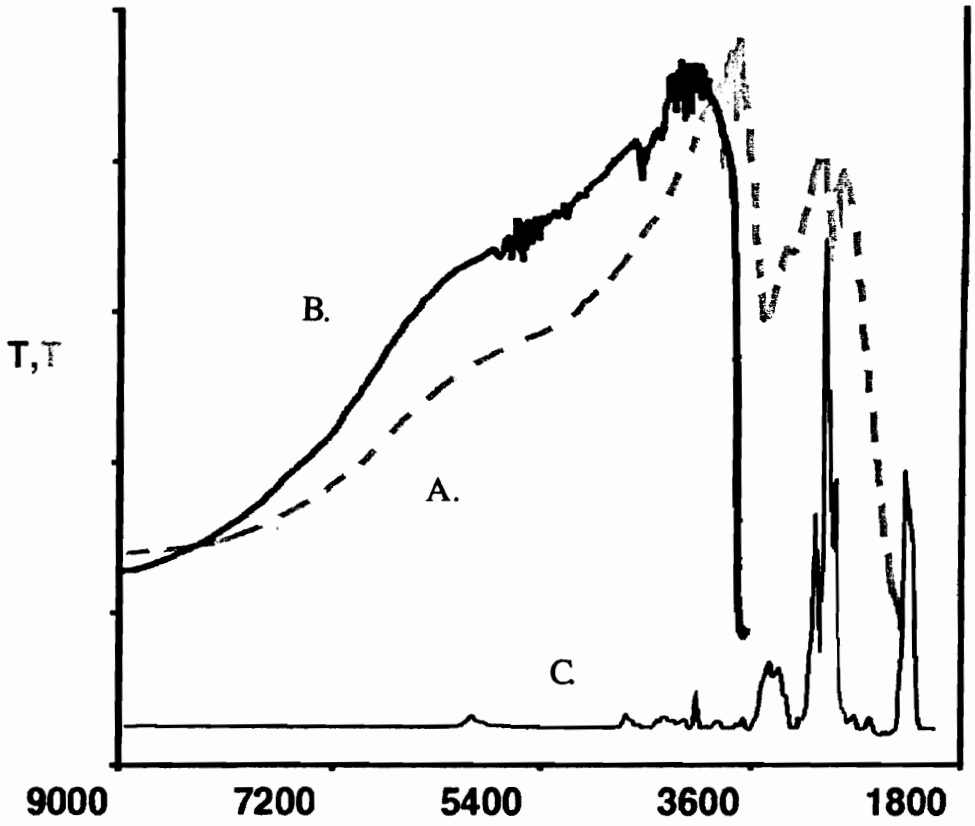

Figure 2.4. Transmission Windows for Fiber Optic Sensors: A. Sapphire in Evanscent Wave, B. Silica-Clad, Low-Hydroxyl Silica, C. Absorbance Spectra for Cyanate Monomer.

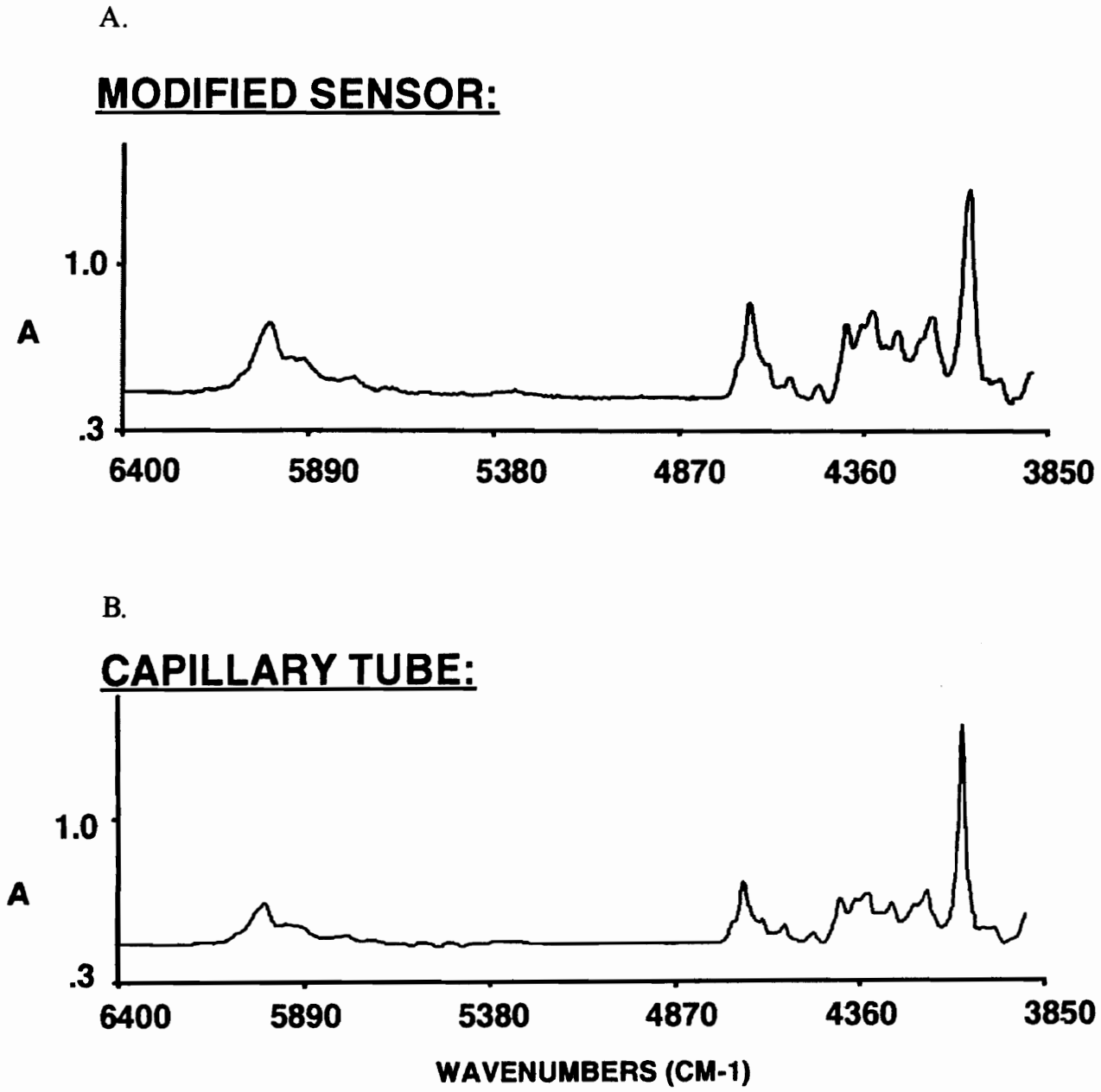

Figure 2.5. FTNIR Fiber Optic Spectra of BADCy Monomer at 104°C using A. Modified Sensor and B. Capillary Tube Technique.

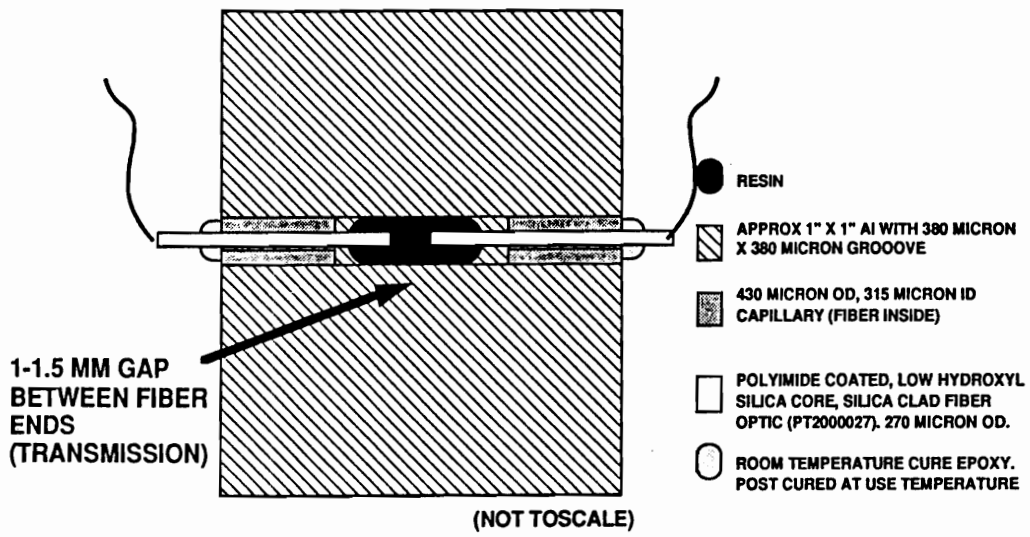

Figure 2.6. FTNIR "Modified" Sensor Based on Groove in Metallic Plate.

TSP 320450) was used to mechanically constrain the ends. Optical alignment was obtained with an XY stage to maximize the interferagram with fiber ends touching. A background spectra was obtained under these conditions either at room temperature or 100°C. The fiber ends were displaced to allow a 1-2 mm gap for the resin to flow into. Capillary tubes and fibers were then fixed with a room temperature cure epoxy. After 10-20 minutes, the whole sensor was gradually heated to slightly above the test temperature using a silicone heating blanket to postcure the epoxy. Although the epoxy did not have a lot of strength at these temperatures, in general, it was adequate to keep the fibers aligned. The Quartz et Silice fiber used by George, et al. was not readily available in this country. An alternate fiber, a single-mode, step-indexed, polyimide-coated, silica-clad, low-hydroxyl silica core from Polymicro Technologies (FIP 200240270) was used.

In some cases, alternate sensor geometries were desirable. Figure 2.7 shows geometries suitable for use in a lap shear joint (2.8 - b), a metallic mold (2.8 - c), and for scattering studies (2.8 - d). The metallic mold is described in Chapter 4; the scattering and visible light transmission in Chapter 5.

Both the resin and the sensor were preheated above the melting point of the resin. Liquid resin was allowed to flow into the gap between the fibers. Heat was supplied to the system using a SpectraTech heated cell which had been modified to allow the fibers to pass through.

The triazine ring stretch in the near-infrared was identified by doping the resin with quantities of 1,3,5-triazine (Aldrich T4,605-1).

Adhesive cure data was obtained for Bryte Technologies EX-1529 cyanate paste adhesive in the stand-alone sensor geometry. Composite monitoring used the mold described for resin castings. Data was obtained for Hercules' AS4 graphite fibers prepregged with the previously discussed 25% reactive thermoplastic toughened cyanate resin in a $[0/90]_S$ configuration with the fibers on the lower ply perpendicular to the groove in the bottom of the mold. When

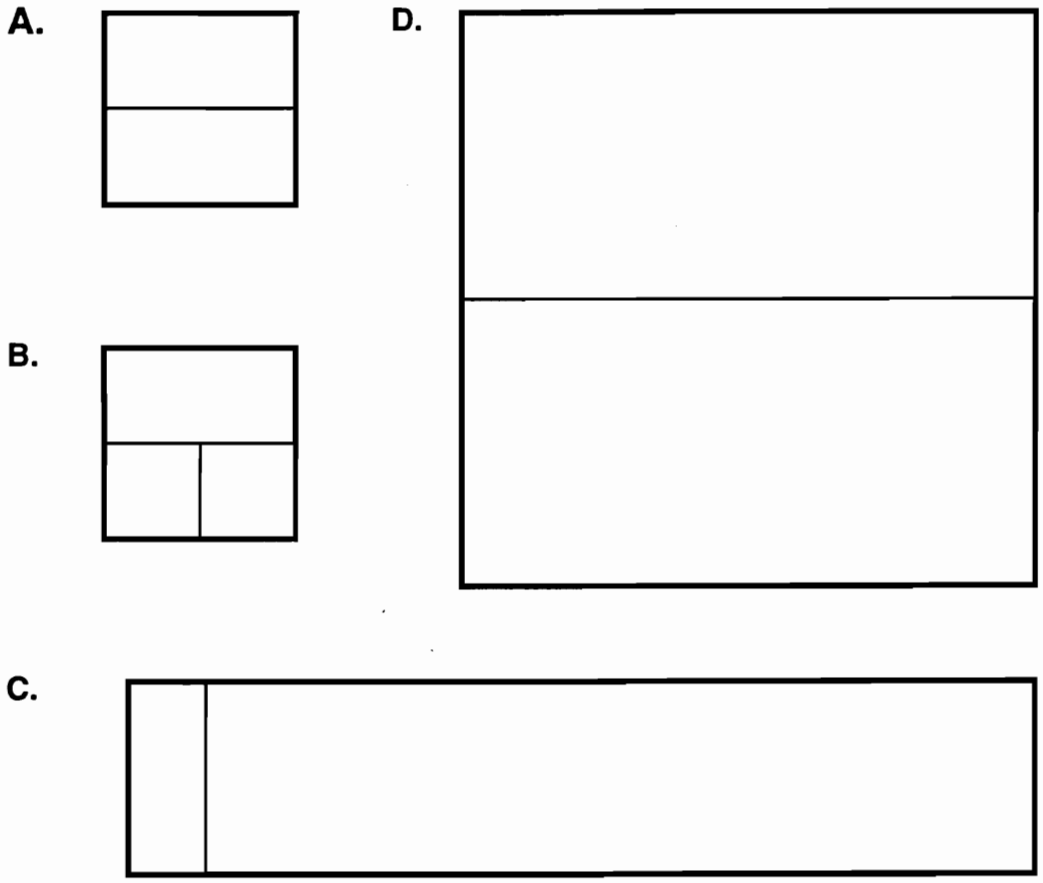

Figure 2.7. FTNIR Sensor Geometries.

placed in a (104°C) preheated mold in the oven, light contact pressure (such as from a small 2 inch x 3 inch caul plate) did not result in adequate resin flow from the prepreg to the groove. A small amount of uncured toughened cyanate resin was placed in the gap between the ends of the fiber optic and the prepreg placed on top, once again in the [0/90]s configuration with the fibers in the lower ply perpendicular to the groove. The composite was then heated at 2°C/minutes to 250°C in a forced air oven then held for 2.25 hours at 250°C. This was the same as the "control" processing cycle used in Chapter 4.

2.4 RESULTS AND DISCUSSION

2.4.1 Bismaleimide with Sapphire

Bismaleimides are attractive resins for high performance applications in composites and adhesives with a use-temperature potentially above 150°C. A number of high performance composite matrix resins and adhesives based on modified, toughened bismaleimides are commercially available. While the wide-spread use of such formulations demonstrates the obvious need to study this system, the complex chemistry of the modified bismaleimides based on Ciba Geigy Matrimid 5292 makes them a difficult model system to study. King, Chaudari, and Zahir (2-47 - 2-49) and Morgan, et al. (2-53) have proposed the possibility of at least three to five reactions occurring during the cure of the bismaleimide. These reactions are shown in Figure 2.8. One may note that as well as gaining CH_2 groups and ring closures, the mechanisms predict the loss of two double bonds producing another double bond. The reactions are still rather controversial, even after years of investigation. The purpose of this study was to apply the fiber optic sensors to a toughened thermosetting resin system, not an attempt to solve the bismaleimide controversy.

The bismaleimide resin with and without toughener was coated on 6 cm of the unclad sapphire fiber then heated to 200°C. As shown in Figure 2.9, for the untoughened system, the sapphire fiber only

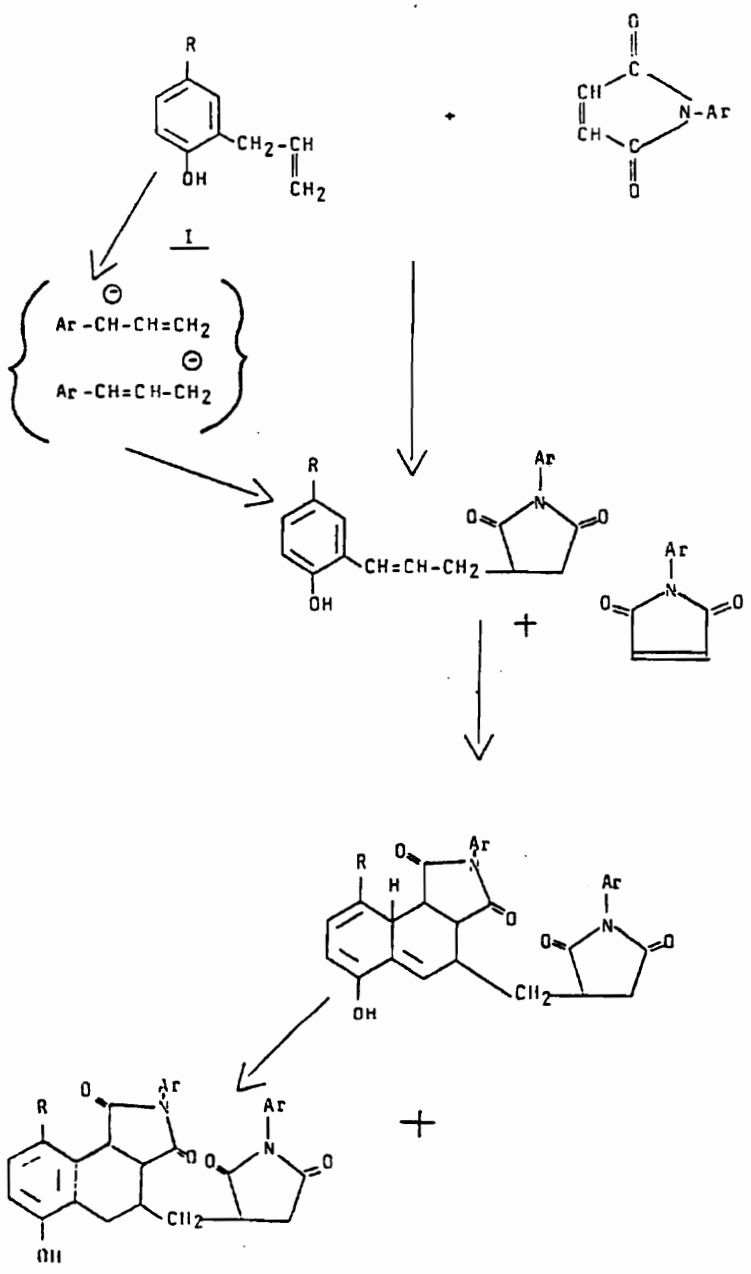

Figure 2.8. Proposed Bismaleimide Cure Mechanisms (2-47 - 2-49, 2-53 - 2-54).

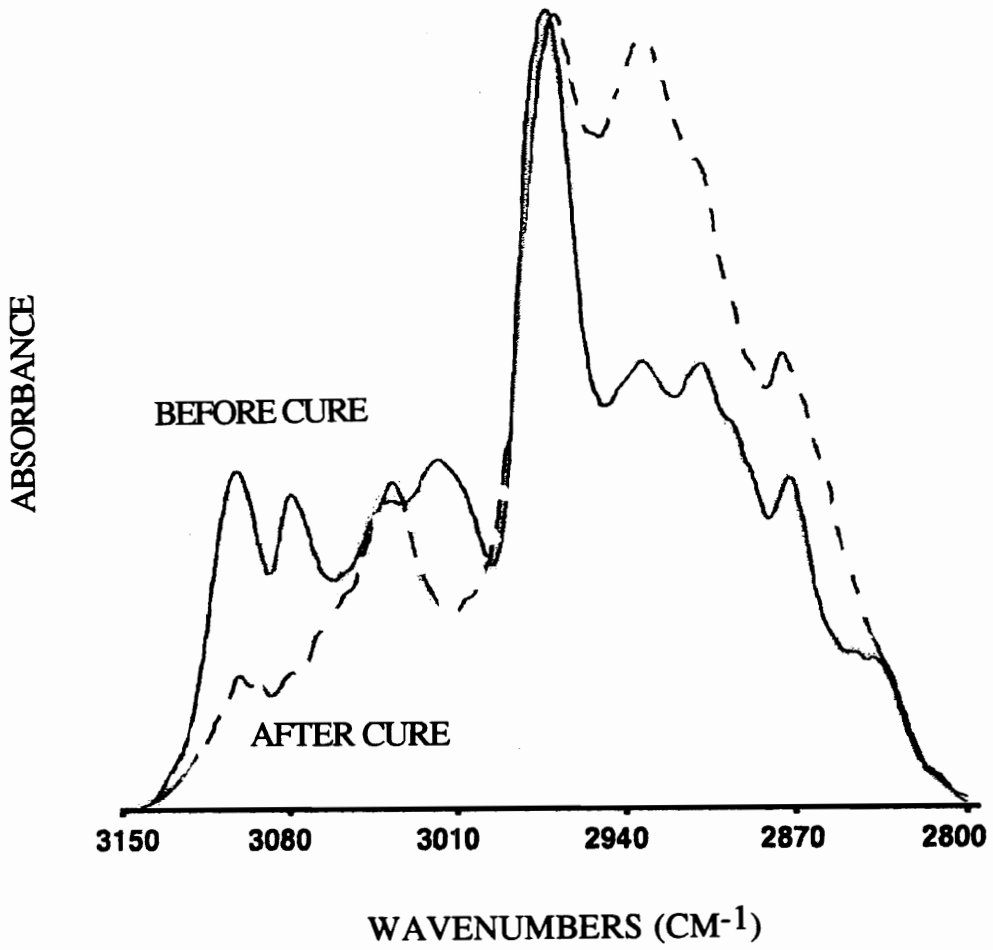

Figure 2.9. Evanescent Wave Sampling in High Frequency Mid-Infrared During Cure of Ciba Geigy Matrimid 5292 Bismaleimide at 200°C.

allowed access to one portion of the spectra. Hummel, et al. (2-46) have followed the homopolymerization of bismaleimide in this region (at 3100 cm^{-1}). The cure of the modified bismaleimide was much more complex. While double bonds could be seen to disappear and appear and CH_2 groups were formed, resolution of the information into a reasonable mechanism or kinetics based simply on this limited region of the spectra was not possible. Even heated cell studies in the mid-infrared failed to resolve the questions. A simpler resin chemistry was selected.

2.4.2 Cyanate with Low-hydroxyl Silica

A simpler resin chemistry was selected for further study. Although some side reactions are possible (2-58 - 2-68), with many catalyst systems, the cyanates proceed cleanly (greater than 85% (2-72, 2-73, 2-88)) to the triazine crosslink shown in Figure 2.11. Although not as widely used commercially as the bismaleimides, the cyanate ester resins (also called triazines or polycyanurates) offer use-temperatures between the capabilities of epoxy resin systems and bismaleimides, can be toughened, have attractive dielectric properties, and have been offered commercially by ICI/Fiberite, YLA, and Bryte Technologies. The primary monomer supplier is Ciba Geigy although Allied Signal also offers a series of monomers based on novolacs and Dow has a cycloaliphatic monomer. The Ciba Geigy resin was the topic of toughening efforts here at Virginia Tech by Srinivasan, et al. (2-100, 2-104) and was used for the rest of this study. This resin is also being used in an interdisciplinary program in the National Science Foundations' Science and Technology Center for High Performance Polymeric Adhesives and Composites. From Srinivasan's work, it was known that the BADCy monomer (catalyzed with AlAcAc and co-catalyzed with nonyl phenol) could be toughened with a series of thermoplastics. Some of the thermoplastics were soluble throughout the reaction, providing only limited toughening. PPES-OH provided further toughening due to a phase separated morphology generated during the cure. This toughened formulation (with 25% thermoplastic) was selected for

DICYANATE OF BISPHENOL A:

250 ppm AlAcAc (catalyst)

2 pph NONYL PHENOL (cocatalyst)

+

25% REACTIVE THERMOPLASTIC TOUGHENER

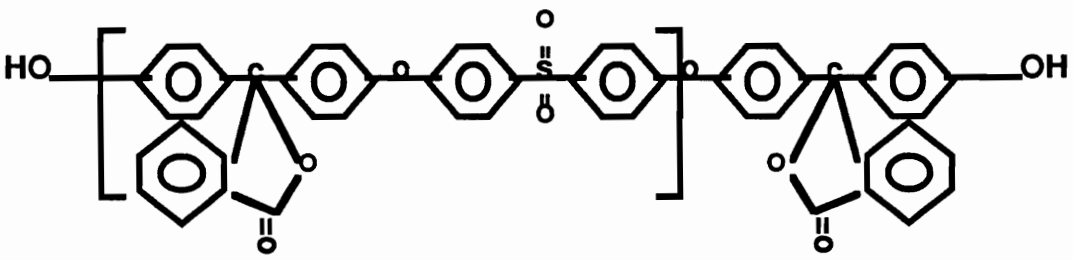

<Mn> = 15,000

Figure 2.10. Toughened Cyanate Formulation.

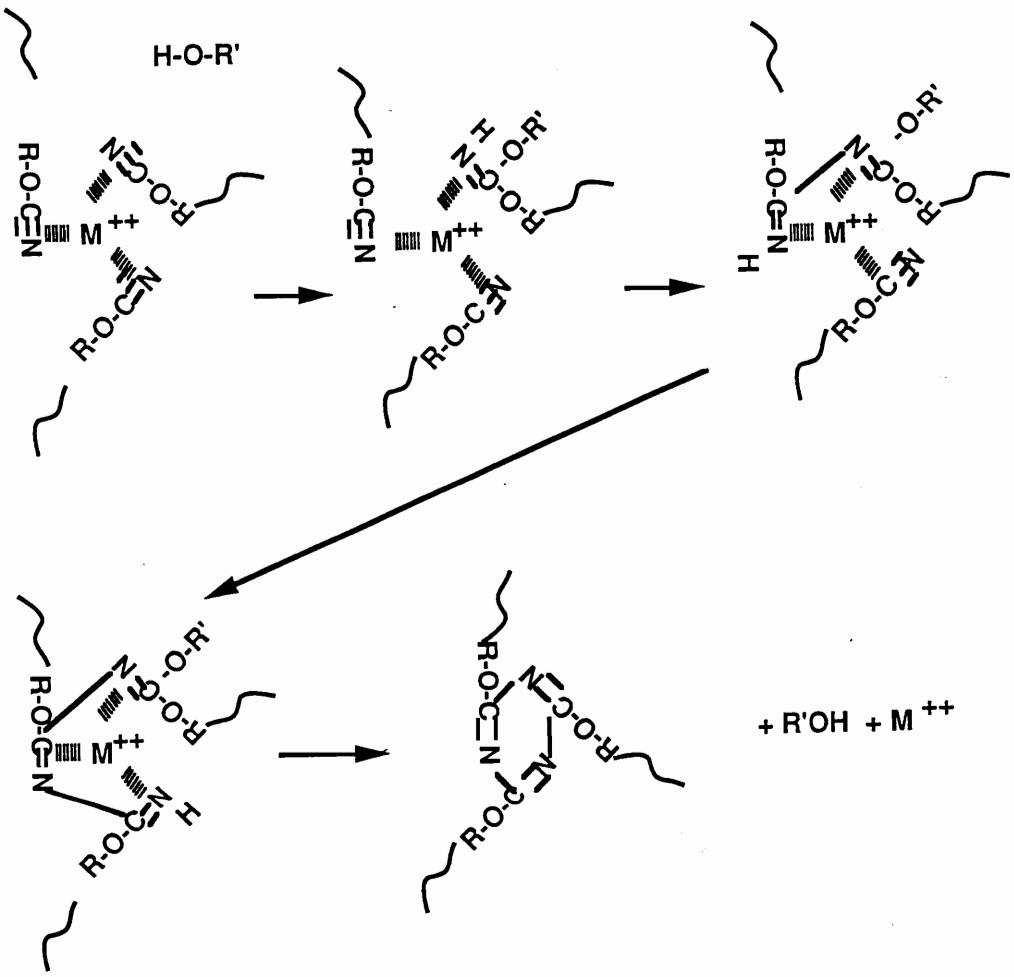

Figure 2.11. Cyanate Cure Mechanism after (2-59, 2-66).

further study with fiber optic (and other sensor) technology.

As shown in Figure 2.11, cyanate groups are the reactive groups in this system. The cyanate groups absorb between 2240 and 2280 cm^{-1} in the mid-infrared. A Ciba Geigy Technical brochure (2-64) recommended use of the cyanate peaks at these frequencies to monitor conversion in diffuse reflectance the mid-infrared. Use of these peaks was not recommended for bulk resin characterization due to extensive cyanate group interaction. The Ciba method monitored the cyanate peak height at 2270 cm^{-1} and ratiod this peak to the height of the CH peak at 2875 cm^{-1}

Snow, et al. (2-62 - 2-63, 2-91) have also used the triazine peak at 1580 cm^{-1} (referenced to the aromatic peak at 1490 cm^{-1}) to monitor the trimerization. Table 2.2 gives the important mid-IR peaks for cyanates, as well as their calculated overtones based on (2-38):

$$\nu = n\nu_0(1-nx)$$

ν = frequency

$x = 0.01$

$n = 2$ for first overtone

Based on this calculation, an overtone of the cyanate peak between 2240-2280 cm^{-1} would be expected to occur between 4390 and 4470 cm^{-1} and between 6515 and 6650 cm^{-1}. The region below 4500 cm^{-1} is both complex and quite near the "cut-off" region for the fiber optic sensor, making it hard to interpret information in the region. The absorbance chart in Colthrup (2-41) indicated a cyanate absorbance between 5200 and 5500 cm^{-1}. There was an extremely weak peak observed in this region of the spectra that decreased with cure as shown in Figure 2.12. The Nicolet white light source (with the fiber optic adapter) was not powerful enough to penetrate through the 4-5 mm path length needed to follow this peak. The calculated overtone between 6500 and 6650 cm^{-1} was not observed.

Figure 2.5-b is a NIR fiber optic spectra of the BADCy monomer at 104°C. There was no strong peak attributable to the

Table 2.2 Mid-Infrared Absorbances and Calculated Near-Infrared Overtones:

based on:
$\nu = n\nu_0(1-nx)$
First overtone is n = 2
x = .01

Identity	Peak (cm^{-1})	1st Overtone (cm^{-1})	2nd Overtone (cm^{-1})
Carbamate NH	3373	6611	9815
Cyanate	2280	4469	6645
Cyanate	2240	4390	6645
Carbamate C=O	1710	3352	4976
Intermediate	1672	3277	4866
C=N?	1640	3214	4772
Triazine Ring	1580	3097	4589
Aromatic C-C	1490	2920	4336
Triazine Ring	1380	2704	4016
+ - O-			
Sulfone Str	1351	2647	3931
C-O-C Str	1235	2420	3594
Sulfone Str	1176	2305	3422
Triazine Ring	815	1597	2372
C=O in phenyl-phthalein	1775	3479	5165

References: 2-37 - 42; 2-61 - 66.

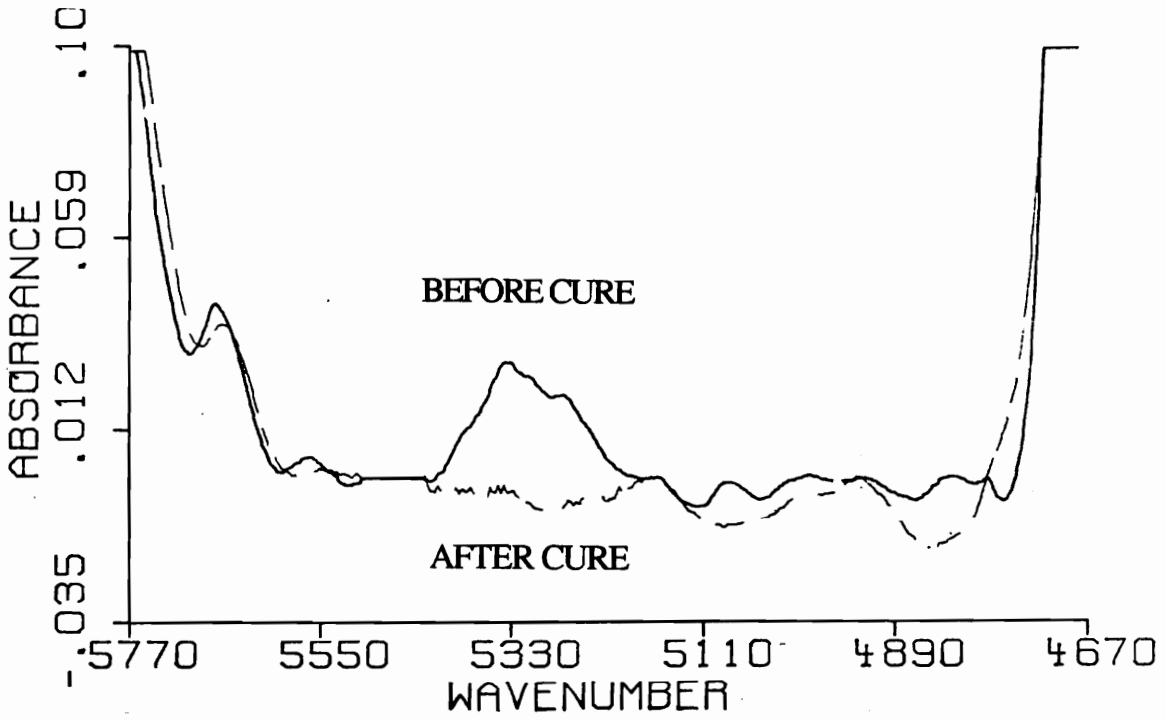

Figure 2.12. Weak Peak in (Literature) Reported Region for Cyanate (2-41) Disappears After Cure.

cyanate group. As mentioned in the preceding paragraph, there was a very weak peak between 5150 and 5400 cm^{-1} which may be the cyanate peak. This peak was not observed in the spectra of bisphenol A. In general, there was little change in the original peaks in the BADCy monomer upon curing, although shifts occur due to physical processes (see Chapter 3). Since little information was available from the monomer spectra, identification of all the peaks was not attempted. The peak at 4675 cm^{-1} was readily identifiable as a mixed aromatic ring deformation (2-37 - 2-40) and aromatic C-H stretch (2-37 - 2-40). This peak was used as a reference peak when normalizing the triazine absorbances.

Attempts were made to obtain spectra using a capillary tube as per George, et al. (2-20 - 2-25). The capillary tube, with an internal diameter just slightly larger than the outer diameter of the fiber optic, provided excellent optical alignment. Inserting the resin, especially the toughened resin, into the very small capillary tube was difficult. Some resin could be forced into the tube by capillary action by placing 1-2 cm lengths of capillary tube upright into a pool of liquid resin at 105-110°C. Upon removal from the oven, the resin rapidly solidified, making the insertion of the fiber optic ends almost impossible. Selective reheating of areas did allow the production of a few specimens. Hill (2-96) had recommended sealing the area between the end of the capillary tube and the outside of the fiber with clear fingernail polish. At the temperatures required for the cyanate study, the fingernail polish did not keep the capillary tube sealed and resin often ran out.

The specimen holder was redesigned based on a fiber optic splice. For a temporary splice, fiber optic ends are sometimes aligned in a groove in a piece of metal and coupled with a silicone fluid. This temporary splice concept was eventually modified to the configuration which was shown in detail in Figure 2.6. The metal plate based sensor may give slightly less energy throughput than the capillary tube. In exchange, the modified sensor allowed more control and reproducibility of path length. Most important, the open

configuration, when heated, allowed the resin to readily flow between the fiber ends. As was shown in Figure 2.5, there was no loss in spectral quality when the modified sensor was used. Not only did this design allow a much greater sample preparation success rate and a more rugged sensor, this change in configuration also allowed this fiber optic sensor to be used in a number of other applications (see Figure 2.7). The data used for chemical control of morphological changes in Chapter 4, was obtained using the aluminum mold modified to contain the fiber optic in the bottom of the mold. The geometry shown in Figure 2.7-b-d could be used to monitor processing of lap shear or double cantilever beam (DCB) specimens. A 90 degree geometry was also designed that could be used for scattering applications. The sensors shown in Figure 2.7 were all manufactured, although the lap shear configuration was never used to obtain cure data. Some other configurations that have been used for near-infrared fiber optic monitoring of water peak shifts as a function of temperature (2-44) with potential to be adapted for in-situ FTNIR fiber optic cure monitoring are shown in Figure 2.13.

There were slight differences in the spectra of the toughened resin at 104°C from that of the monomer, more in the peak ratios than in the number of peaks. The resin cures to form a triazine ring. This trimerization is apparently a fairly "clean" reaction, Gupta and Macosko (2-71 - 72) observed greater than 85% (usually > 90) conversion to the triazine crosslink with organometallic catalysts. Fyfe, et al. (2-88) have shown by C-13 NMR that for the uncatalyzed bulk-cured material there was very little side product and stated that the reaction was "remarkably efficient." They have also noted that the bulk reaction products were much "cleaner" than the solution products. To determine if the triazine crosslink could be monitored in the NIR, the toughened resin was spiked with 1,3,5-triazine (Figure 2.14) and exhibited a new peak at 4625 cm^{-1}. This is not far from the calculated overtone at 4600 cm^{-1} (based on the triazine ring stretch at 1560 cm^{-1}. Snow, et al. (2-61 -2-63, 2-91) found that this peak gave good conversion data when referenced to

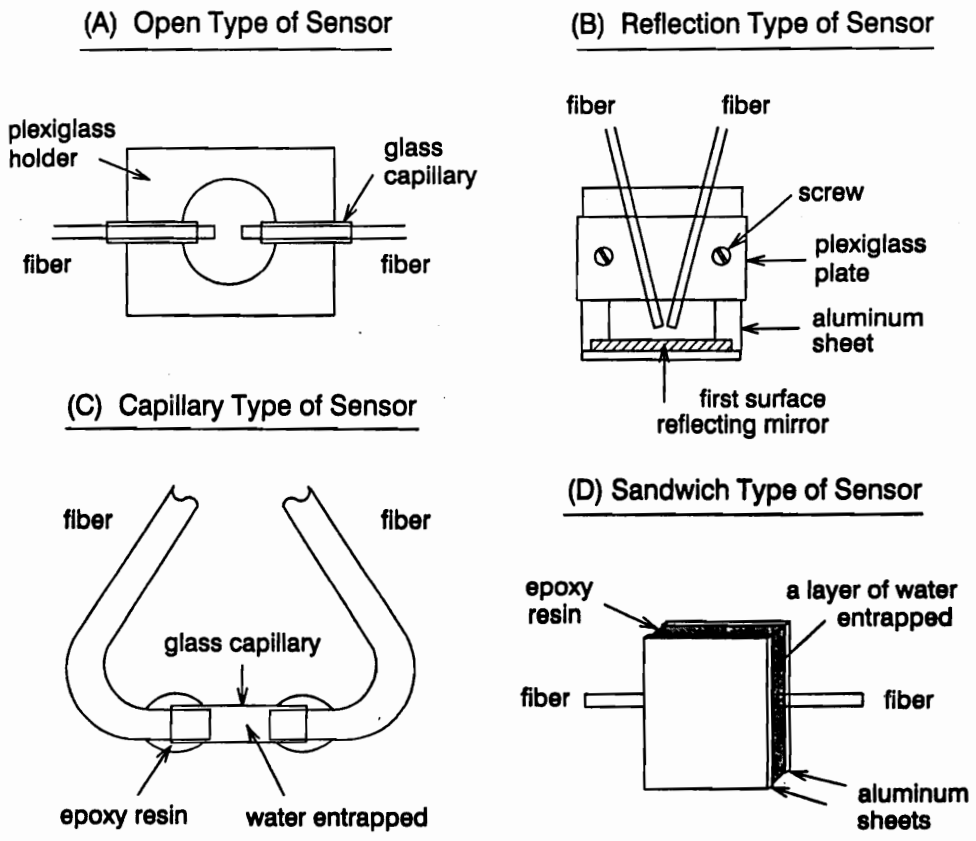

Figure 2.13. Other Geometries Used for FTNIR Fiber Optic Monitoring of Peak Shifts in Water (2-44) with Potential for FTNIR Fiber Optic Cure Monitoring.

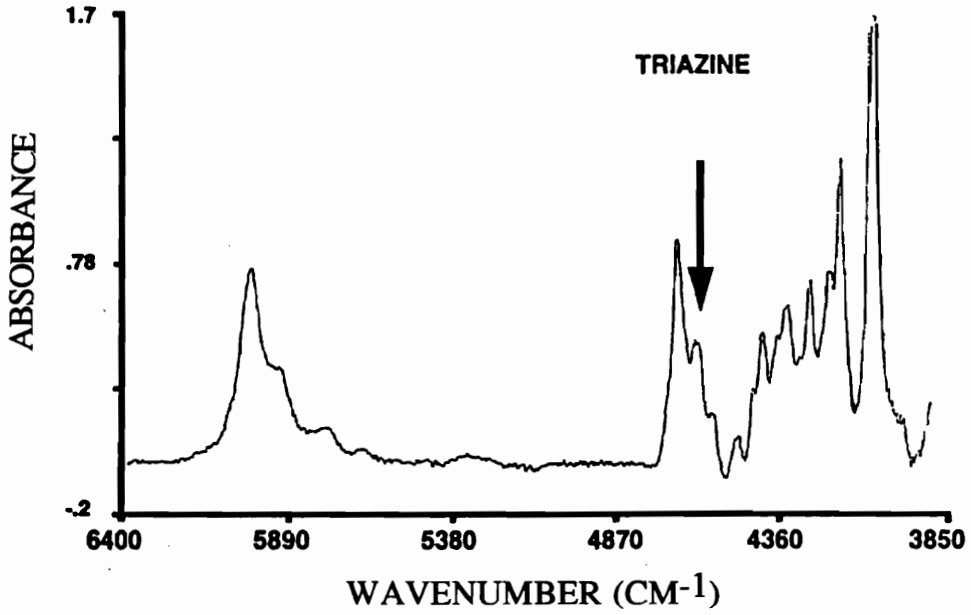

Figure 2.14. FTNIR Spectra of Toughened Cyanate Spiked with 1,3,5-Triazine.

the aromatic peak at 1490 cm^{-1} and felt that "the 1560 (cm^{-1}) cyanurate band was more sensitive and better suited for conversion measurements" than the 2250 cm^{-1} cyanate band. The regions at 4016 and 5300 cm^{-1} were calculated to have some input from the overtone of the triazine ring + O stretch at 1380 cm^{-1}, but this region is complex even in the NIR and extensive deconvolution would be required. There may also be some contribution from the triazine to the peak at 6000 cm^{-1} due to the calculated triazine ring stretch at 6070 cm^{-1} but most of the peak seems to be another aromatic ring overtone. The triazine peak at 4625 cm^{-1} was selected as the most appropriate peak in the NIR for following the cure reaction. Figure 2.15 shows growth of this peak when the resin was held at 149°C.

For the purpose of on-line determination of extent of cure, the following approach was used. The peak areas between 4790 and 4645 cm^{-1} (due to the aromatic ring stretch = A_B) and 4645 and 4580 cm^{-1} (triazine ring = A_T) were integrated by a software routine written in the Nicolet macro programming language. Since the aromatic absorbance was not expected to be affected by the reaction, the aromatic peak was used as a reference yielding a normalized value for the triazine ring. This was used in the macro to calculate a "relative degree of cure (α_r)" based on:

$$\alpha_r = \frac{\dfrac{A_{Tr,T,t}}{A_{B,T,t}} - \dfrac{A_{Tr,104,i}}{A_{B,104,i}}}{\dfrac{A_{Tr,270,f}}{A_{B,270,f}} - \dfrac{A_{Tr,104,i}}{A_{B,104,i}}}$$

α = degree of cure

A = integrated peak area

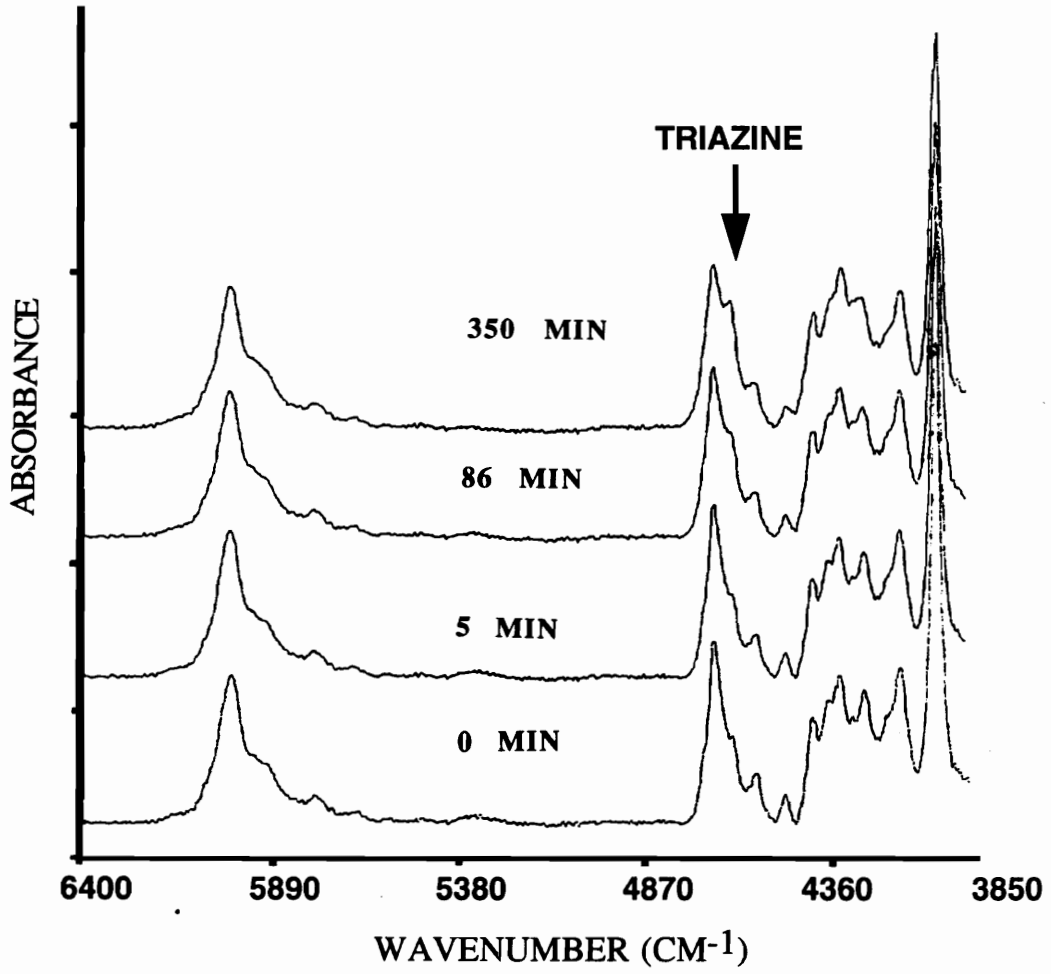

Figure 2.15. FTNIR Fiber Optic Spectra of Isothermal Cure of Toughened Resin at 149°C.

T = temperature

t = time

Tr = Triazine

B = Benzene

i = initial

f = final

Relative conversion = 100 * α_r

Values for α_r ranged from 0 to 1.0; relative conversion values from 0 to 100. Initial conditions were considered to be at 104°C where little reaction should have occurred; final at 270°C. The program for real-time calculation of relative degree of cure is shown in the Appendix. A more exact calibration (based on 1,3,5 triazine concentration) and the impact of the physical changes in the curing resin on the spectra are discussed in Chapter 3. The calibration used in Chapter 3 would require more sophisticated programming than provided by the Nicolet programming language. Deconvolution of the aromatic ring and triazine peaks was not used in the on-line calculation of relative conversion. The area of the aromatic ring shoulder was compensated for by the $A_{Tr,104,i}$ value. The Nicolet deconvolution program for the 800 Spectrometer required human intervention to determine when the peaks had been suitably deconvoluted. This sort of intervention would be too slow for on-line decision making.

Relative conversion data was obtained from the fiber optic sensor at 104, 125, 135, 149, 160, 177 and 200°C and in 1, 2, and 5°C/minute ramps. The isothermal data is shown in Figure 2.16 . A preliminary model could fit the isothermal data to apparent second order kinetics up to 60% conversion. In second order kinetics, the graph of $1/(1-\alpha)$ versus time should be linear (Figure 2.17) The rate

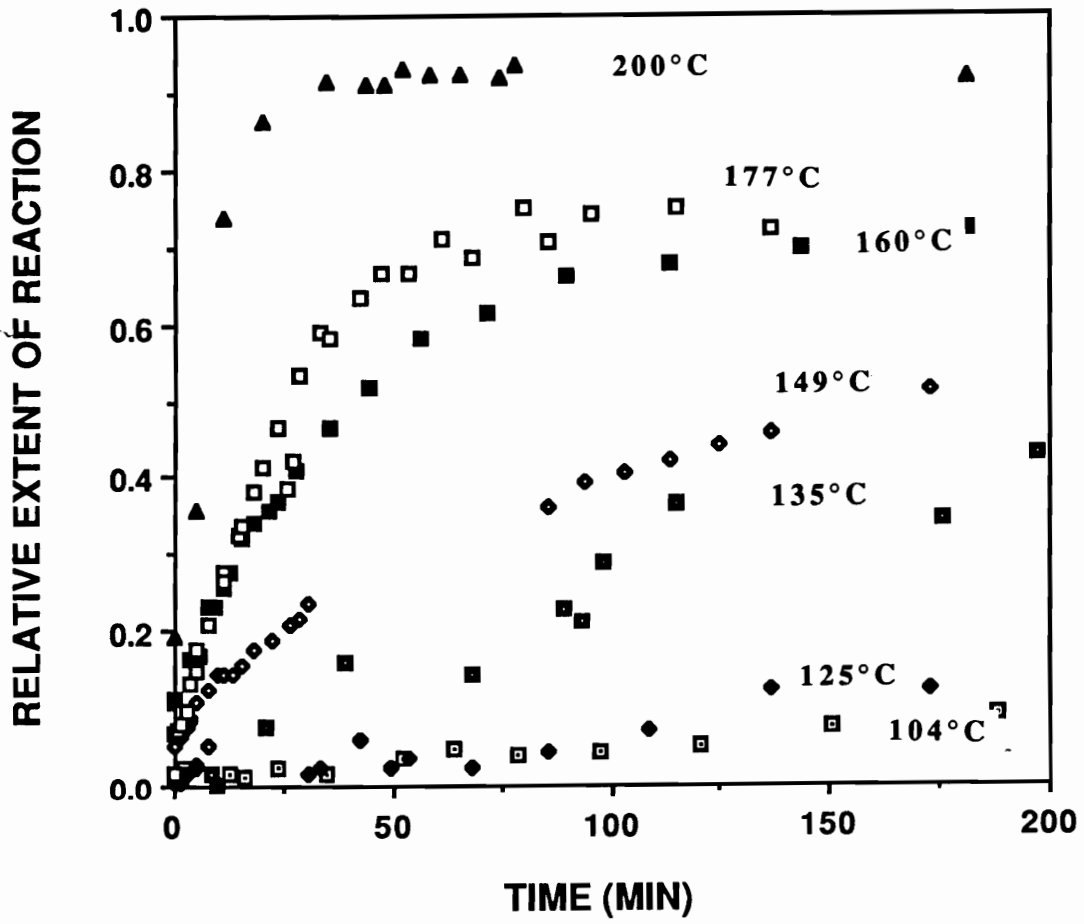

Figure 2.16. Relative Degree of Cure (α_r) at Various Temperatures as Determined with FTNIR Fiber Optic Sensor.

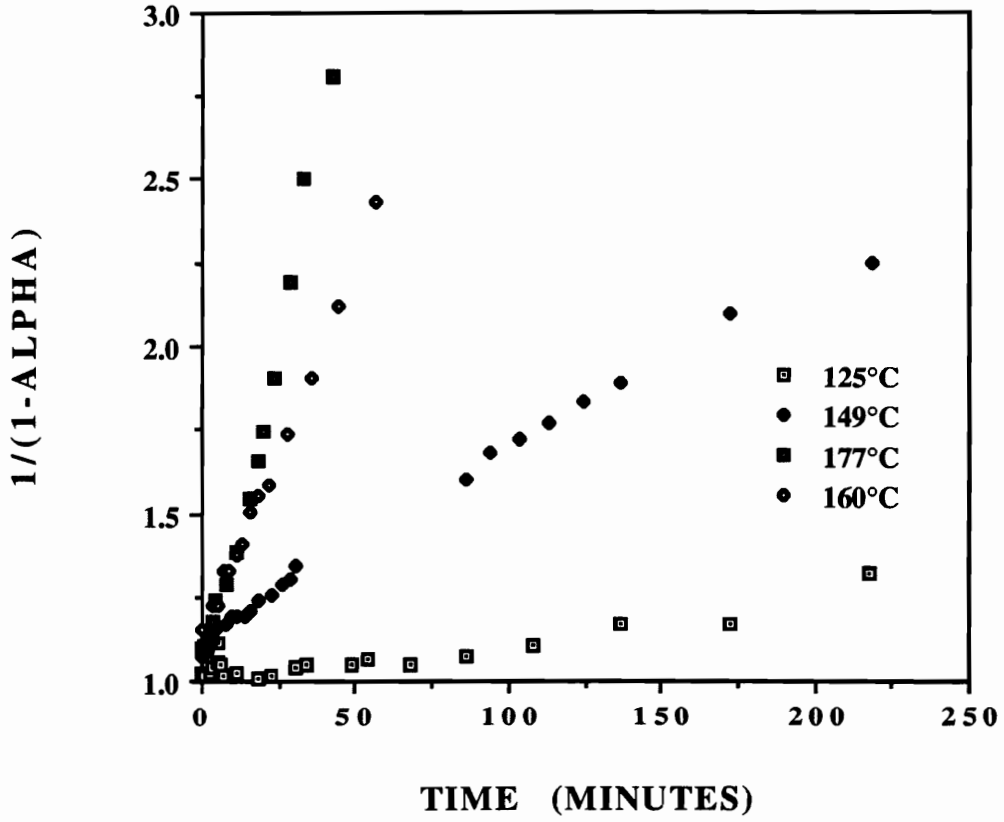

Figure 2.17. Second Order Fit for Relative Degree of Cure versus Time.

graph of $1/(1-\alpha)$ versus time should be linear (Figure 2.17) The rate form of this equation would be:

$$d\alpha/dt = k\ (1-\alpha)^n$$

$$n = 2 \text{ (second order)}$$

Second order kinetics have been reported in the literature for the organometallic catalyzed, untoughened dicyanate monomers (2-72 - 2-73). The natural log of the rate constants obtained versus reciprocal temperature are given in Figure 2.18. Up to approximately 60% conversion, the temperature dependence of the rate constant can be described by:

$$\ln k = 19.76 - (1.22 * 10^4) * 1/T.$$

This equation can be used with some reservations to predict apparent cure for the toughened resin. This preliminary model must be used with some discretion since it does not compensate for the physical effects on the spectra. Chen and Macosko (2-71) and Gupta and Macosko (2-72, 2-73) found with nth order kinetics that n = 2 prior to vitrification for catalyzed, untoughened dicyanate resins. Simon and Gillham (2-85, 2-86) reported a similar value of n=1.87. Gupta and Macosko (2-72, 2-73); Osei-Owusu, Martin, and Gothro (2-74, 2-75); and Bauer, Bauer, and Kuhn (2-79, 2-83 - 2-85) found that the uncatalyzed trimerization was autocatalytic. Osei-Owusu, Martin and Gothro found a first order dependence on catalyst concentration and a second order dependence on cyanate concentration for catalyzed systems. Rather surprisingly, Barton, Hamerton, and Jones (2-76) found first order behavior (with time) for the system.

Using nonlinear regression, Rau (2-101) has observed that the DSC data for the toughened cyanate used in this study follows mixed kinetics with a cure rate of:

$$d\alpha/dt = (k_1+k_2(\alpha m)) * (1-\alpha)^n$$

The nonlinear regression program would not converge for the relative degree of cure measurements from the fiber optic. This lack of convergence may be partly due to the noise in the fiber optic data, the fewer number of data points obtainable (200 spectra due to hard drive limitations versus 2000 data points in the DSC), but mostly due

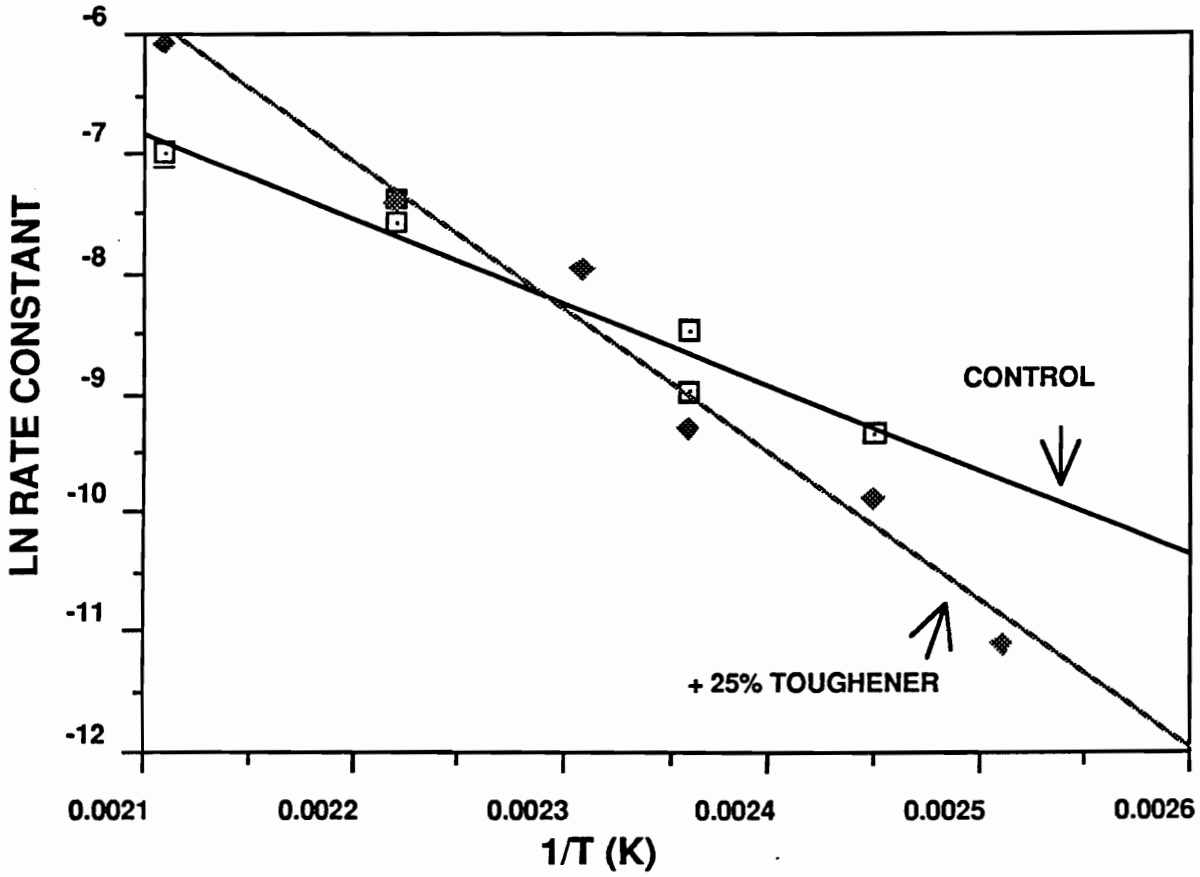

Figure 2.18. Arrhenius Relationship for Second Order Rate Constants.

reference. This phenomena will be discussed in depth in Chapter 3.

To determine the applicability of this technique to real processing situations, two material forms were evaluated: a commercial cyanate paste adhesive (Bryte EX-1529) and the model toughened cyanate combined with Hercules AS4 graphite fibers into a composite prepreg. Most adhesive formulations contain certain additives, including silica particles. Figure 2.19 shows the FTNIR spectra of the Bryte adhesive. There was a drop in light transmission and some loss in spectral quality when the formulated adhesive was used rather than the model system. This was probably somewhat exaggerated in this spectra since there were some difficulties with the intensity of the white light source at the time of the adhesive spectra was produced. Even so, the growth of the triazine ring could be readily monitored.

Since neither the Nicolet 800 FTIR spectrometer nor the press in the composite fabrication laboratory were portable (and located about 0.5 kilometers apart), the combination of spectrometer and press (or autoclave) was not demonstrated. With a stronger light source, it might be possible to link the spectrometer and press. The optical fibers used have reasonable retention (10-500 dB/km (2-97)) values, are strong and durable, and inexpensive. Several attempts were made to bring a more portable Nicolet spectrometer into the composite fabrication lab with little success. In lieu of press or autoclave, composite monitoring was performed in a forced air oven in the next room from the Nicolet 800 spectrometer. A 4-ply, 3.0 inch x 3.0 inch, $[0/90]_S$, AS4/model toughened cyanate layup was prepared. When this layup was placed in the preheated mold at 104°C, the resin did not flow into the groove of the mold. Even light contact pressure of a small steel plate on top of the mold did not result in resin flow into the groove. This had been observed on an earlier attempt with prepreg and the stand-alone sensor geometry. The mold was adapted from a composite mold from the composite processing lab. With the neat resin castings, placing the groove in the middle of the bottom plate worked well. Due to flow characteristics

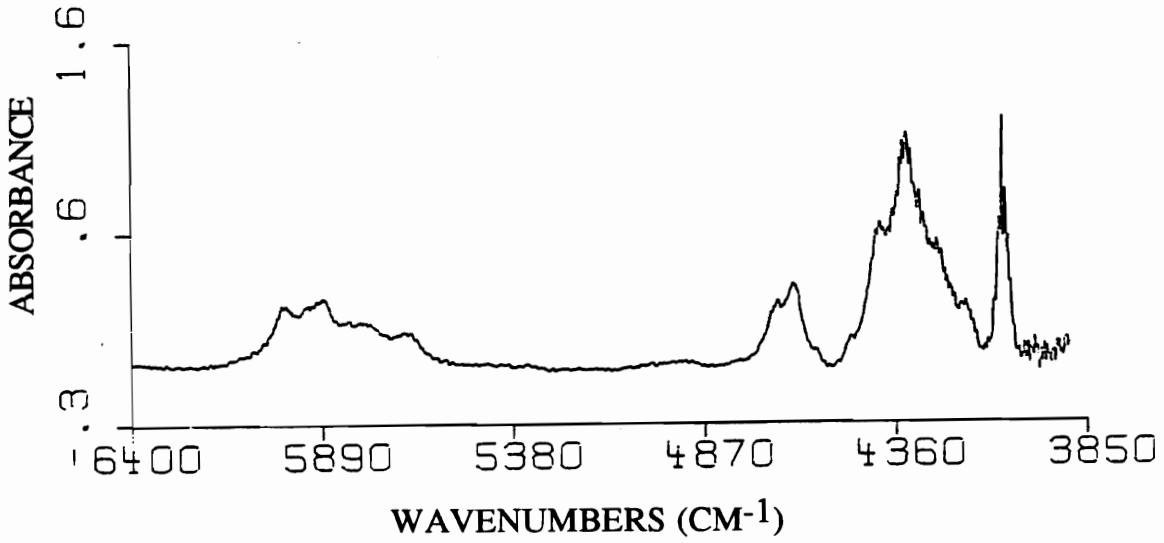

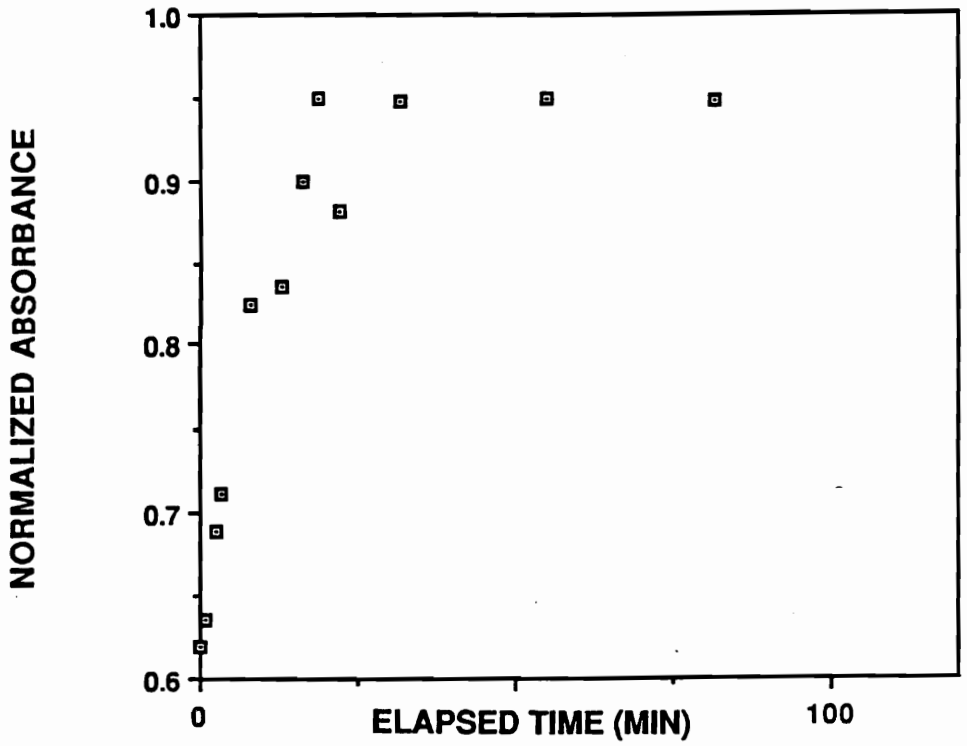

Figure 2.19. FTNIR Fiber Optic Monitoring of the Cure of Bryte Paste Adhesive.

of the continuous fiber reinforced composites, this is not a good location. Based on models (2-92 - 2-93) and observations, the resin will flow either down the fiber direction or up through the bleeder cloth at the top. To compensate for this, an alternate geometry such as shown in Figure 2.20-b would be recommended.

Since resin would not flow into the groove, resin enrichment in this region was attempted. Scraping of resin from the dry, boardy prepreg resulted in more fibers than resin being removed even upon heating. The fibers would have a detrimental effect on the light throughput. A small quantity of uncured model toughened cyanate resin was placed on the preheated mold and allowed to flow in between the fibers. Another [0/90]s layup was placed on top of the resin (see Figure 2.20-a). The fibers in the bottom ply were again aligned perpendicular to the groove (to try to keep the fibers from getting into the groove and obstructing the light). With contact pressure from the 2.0 inch x 3.0 inch metal plate, the fibers bridged the groove and did not obstruct the light path.

Initially, the resin enrichment worked well. Figure 2.21 shows the spectra for 114 and 135°C as the mold was heated. While not as ideal a situation as having the resin flow into a groove, placing a small amount of the same batch of resin in the groove is not an unreasonable solution for processing conditions and initially provided good spectra up to 140°C. At 140°C, as shown in Figure 2.21-b, the spectra was lost. This was not due to a blockage of the light path due to bending of the fibers into the groove. If there was something that transmitted in the light path, the interferagram would have "wings" on the side. A fairly clean (no wings) interferagram would be obtained in air. If the pathway were blocked, there would be no interferagram. A clean interferagram was observed above 135°C, indicating that there was nothing between the two fiber optic ends. The excess resin in the groove could have been sucked back into the prepreg by capillary action. Later microscopic evaluation of the bottom of the laminate showed that this was probably not the case. The resin appeared to have bubbled out of the

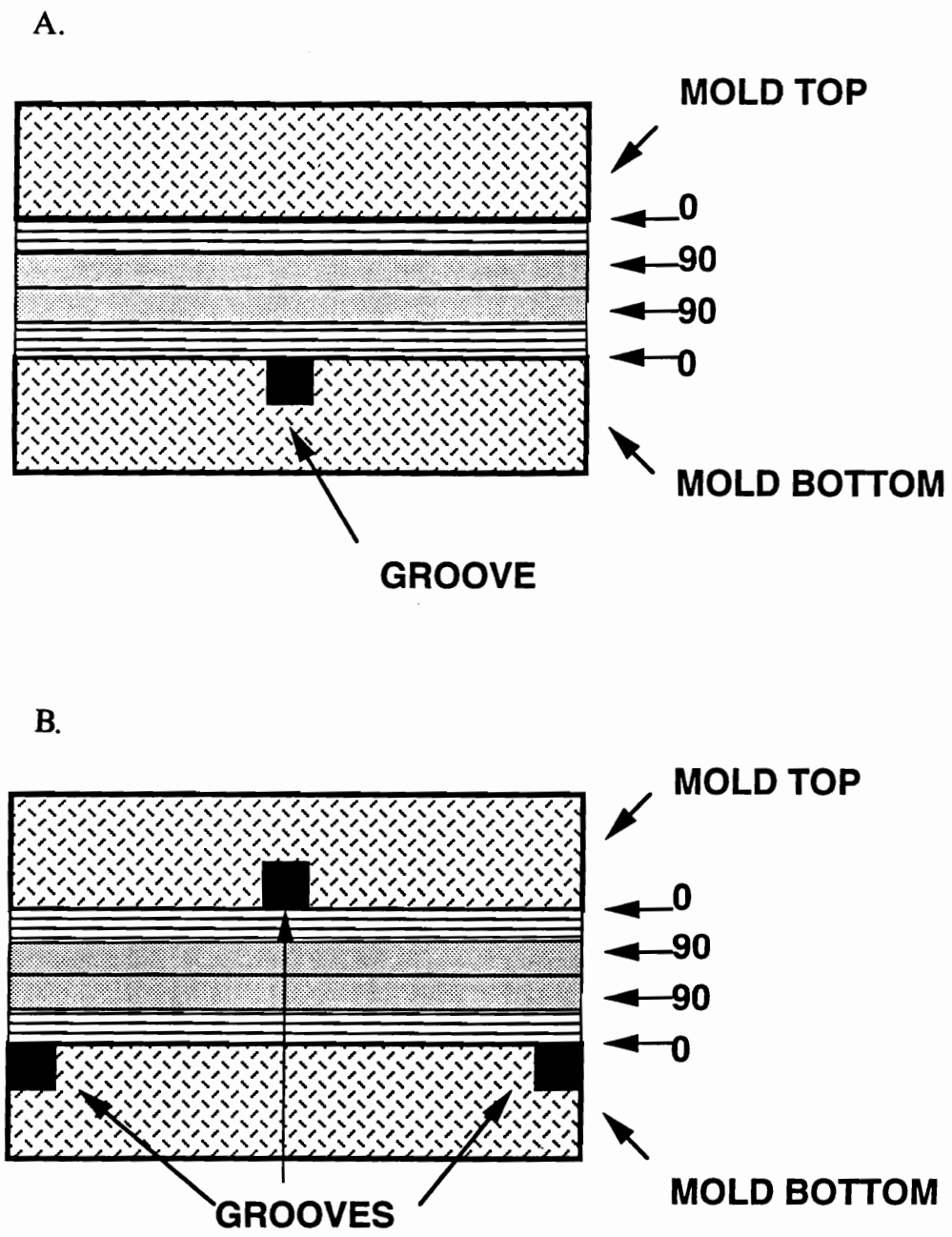

Figure 2.20. Composite Mold Design: A. Layup and Mold Used for Prepreg Cures and B. Recommended Mold Design for Composites.

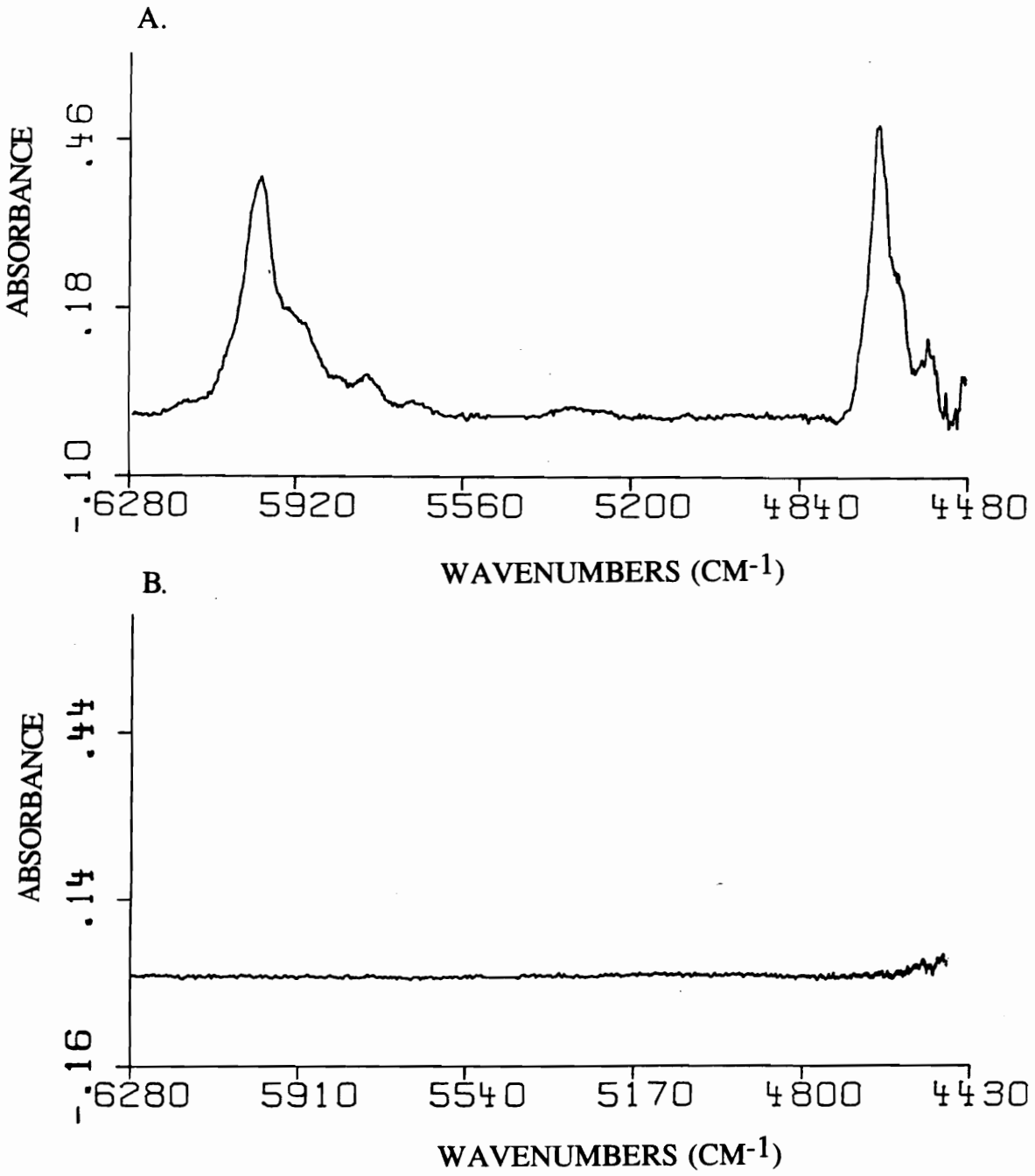

Figure 2.21 FTNIR Fiber Optic Spectra from Real-Time Processing of AS4/Toughened Cyanate in the Forced Air Oven: A. 114°C and B. 135°C.

groove. Either case would probably have been prevented in a press or autoclave.

2.5 CONCLUSIONS AND SUMMARY

A practical, durable, inexpensive FTNIR fiber optic technique was demonstrated. The design was suitable for many applications, including transmission and scattering in neat resin castings or adhesive joints. The cure of a model toughened cyanate was followed with this fiber optic sensor by the growth of the triazine at 4625 cm^{-1}. Preliminary modeling of the cure of the toughened system could be fit to (apparent) second order kinetic equations. It is expected that the kinetics will differ when an absolute rather than a relative calibration is used and corrections made for physical effects. The cure of a commercial cyanate paste material was successfully monitored. The mold design was not suitable for composite cure and a new design was proposed which relocated the sensor grooves to the side or top of the mold.

2.6 REFERENCES

2-1. J. Mijovic, J. M. Kenny, L. Nicolais, SAMPE Journal, Vol. 28, No. 5, Sept/October. 39-46 (1992).

2-2. D. A. Compton, S. Hill, N. A. Wright, M.A. Druy, J. Piche, W. A. Stevenson, and D. W. Vidrine, Applied Spectroscopy, Vol. 42, No. 6, 972-979 (1988).

2-3 M. A. Druy and L. Elandjian, SPIE Vol. 986 Fiber Optic Smart Structures and Skins, pp. 130-134 (1988).

2-4. P. R. Young, M. A. Druy, W. A. Stevenson, and D. A. C.. Compton, SAMPE Journal, Vol. 25, No. 2, 11-16 (1989).

2-5. M. A. Druy, P. J. Glatkowski, and W. A. Stevenson, SPIE Vol. 1437 Applied Spectroscopy in Materials Science, 66 (1991).

2-6. M. A. Druy, P. J. Glatowski, and W. A. Stevenson, SPIE, Vol. 1584 Fiber Optic and Laser Sensors IX, 48-52 (1991).

2-7. A. Ray Hilton, Sr., SPIE Vol. 1437 Applied Spectroscopy in Materials Science, 54-59 (1991).

2-8 X. H. Zhang, H. L. Ma, and J. Lucas, SPIE Vol. 1591 (Infrared Fiber Optics III), 43-48 (1991).

2-9. A. R. Kilton, Sr. SPIE Vol. 1591 (Infrared Fiber Optics III), 35-41 (1991).

2-10 S. J. Saggese, J. A. Harrington, G. H. Sigel, Jr. SPIE Vol. 1437, 44-53 (1991).

2-11. T. B. Colin, K-H. Yang, M. A. Arnold, G. W. Small and W. C. Stalley, Applied Spectroscopy, vol. 46, Number 7, 1129-1133 (1992).

2-12. R. D. Driver, J. N. Downing, and G. M. Leskowitz, SPIE Vol. 1591 Infrared Fiber Optics III, 168-179.

2-13. A. Bornstein, M. Katz, A. Baram, and D. Wolfman, SPIE Vol. 1591 Infrared Fiber Optics III, 256-262 (1991).

2-14. M. Rodrigues, G. H. Sigel, Jr., SPIE Vol. 1591, Infrared Fiber Optics III, 224-235 (1991).

2-15. R. J. Burger and P. J. Melling, SPIE Vol. 1591 Infrared Fiber Optics III, 246-255 (1991).

2-16. M. Katz, A. Bornstein, I. Schnitzer, and A. Katzir, SPIE Vol. 1591 Infrared Fiber Optics III, 236-245 (1991).

2-17. W. R. Moser, J. R. Berard, P. J. Melling, and R. J. Burger, Applied Spectroscopy, Vol. 46, No. 7, 1105 -1112 (1992).

2-18 M. Swajiro, K. J. Rothschild, B. Nappi, A. Lane, and H. Gold, SPIE, 1437 Applied Spectroscopy in Material Science 60-65 (1991).

2-19. M. A. Druy, P. J. Glatokowski, and W. A. Stevenson, SPIE, Vol. 1591, Infrared Fiber Optics III pp. 218-223 (1991).

2-20. G. A. George, P. Cole-Clarke, N. St. John, Materials Forum, 14, 203-209 (1990).

2-21. G. A. George, P. Cole Clarke, N. St. John, and G. Friend, Journal of Applied Polymer Science, Vol. 42, 643-657 (1991).

2-22. C. J. de Bakker, N. A. St. John, and G. A. George, Preprints of the 19th APS Conference, Perth, Feb. 1992 18-19.

2-23. N. St. John, and G. A. George, Polymer, Vol. 33, 2679-2688 (1992).

2-24. C. J. de Bakker, N. A. St. John, and G. A. George, Polymer, Vol. 34, Number 4, 716-725 (1993).

2-25 C. J. de Bakker, N. A. St. John, and G. A. George, ACS Polymer Preprints, Vol. 33, No. 1 (April 1992).

2-26. D. C. H. Chien and A. Penlidis, JMS- Rev. Makromol. Chem. Phys. C30(1), 1-42 (1990).

2-27. Chemical, Biochemical, and Medical Sensors by A. Harmer and A. Cheggi in Optical Fiber Sensors: Systems and Applications Vol. 2 (B. Culshaw and J. Dakin, ed)., pp. 599-651 (1989), Artech House, Inc., Norwood,MA.

2-28. W. C. Michie, G. Thursby, W. Johnstone, B. Culshaw, SPIE Vol. 1978 Fiber Optic Smart Structures and Skins 11-15 (1991).

2-29. M. A. Afromowitz and K.-Y. Lam, SPIE Vol. 986 (Fiber Optic Smart Structures and Skins), 135-139 (1988).

2-30. L. A. Cassis and R. A. Lodder, Anal. Chem., Vol.65, 1247-1256 (1993).

2-31. (K) W. D. Kingery, H. K. Bowen, D. R. Uhlmann, Introduction to Ceramics (2nd edition) , John Wiley and Sons, New York. 1976.

2-32. The Merck Index, 9th edition, Merck & Co., Inc, NJ, M. Windholz, Ed. (1976).

2-33. C. K. Mann, T. J. Vickers, W. M. Gulick, Instrumental Analysis, Harper and Row, New York,1974.

2-34. Handbook of Chemistry and Physics, 51st edition (1970-1971), the Chemical Rubber Co., Ohio. R. C. Weast, G. L. Tuve, S. M. Selby and I. Sunshine, ed.

2-35. J. Sinkankas, Gem Cutting, A Lapidary's Manual 2nd Edition, Van Nostrand Reinhold CO, NY 1962.

2-36. R. A. Flinn and P. K. Trojan, Engineering Materials and Their Applications, Fourth edition, Houghton Mifflin Co., Boston. 1990.

2-37. C. E. Miller, Near-infrared Spectroscopy of of Synthetic Polymers, Applied Spectroscopy Reviews, 26 (4), 277-339 (1991).

2-38. B. G. Osborne, T. Fearn, Near-infrared Spctroscopy in Food Analysis, John Wiley and Sons, New York, 1986.

2-39. Near-infrared Technology in the Agricultural and Food Industries, Ed. P. WIlliams and K. Norris, American Association of Cereal Chemists, Inc., 1987.

2-40. Handbook of Infrared Analysis, D. A. Burns, and E. W. Ciurczak, eds. Marcel Dekker, Inc. NY, 1992.

2-41. N. B. Colthrup, L. H. Daly, and S. E. Wiberley, Introduction to Infrared and Raman Spectroscopy,, Academic, New York, 1975.

2-42. R. M. Silverstein, G. C. Bassler, T. C. Morrill, Spectrographic Identification of Organic COmpoundsd, John Wiley and Sons, NY,1981.

2-43. J. Lin and C. W. Brown, Anal. Chem 1993, 65 287-292.

2-44. J. Lin and C. W. Brown Applied Spectroscopy, Vol. 47, No. 1, 1993. (Near IR Fiber Optic Temp Sensor).

2-45. Nicolet FT-IR Technical Note TN-9036.

2-46. D. O. Hummel, K.-U. Heinen, H. Stenzenberger and H. Siesler, Journal of applied Polymer Science, Vol. 18, pp 2015-2021 (1974).

2-47. J. J. King, M. Chaudari, S. Zahir, Proceedings of the 29th National SAMPE Conference, 1984 pp. 392-408.

2-48. M. Chaudhari, T. Calvin, J. King, 30th National SAMPE Symposium, March 19-21, 1985 pp. 735 -746.

2-49. S. Zahir, M.A. Chaudhari, J. King, Makromol. Chem., Macromol. Symp., 25, 141-154 (1989). p. 141-154.

2-50. H. Stenzenberger, "Chemistry and Properties of Addition Polyimides" in Green Polyimide book.

2-51. I. M. Brown and T. C. Sandreczki, Macromolecules 1990, 23, 94-100. (ESR of BMI).

2-52. S. Wilkinson, Ph.D. Dissertation, VA Tech, 1992.

2-53. R. J. Morgan, R. Jurek, D. E. Larive, C. M. Tung, and T. Donnelan "The Toughening of Bismaleimides," PMSE Preprints pp. 681-686.

2-54. J. Mijovic and B. Schafran SAMPE Journal, Vol. 26, no. 3, May/June 1990 pp 51-59.

2-55. F. Lee and M. A. Boyle 35th International Sampe Symposium April 2-5. 1990 162-175.

2-56. D. H. Wertz and D. Prevorsek, Plastics Engineering, April 1984 31-33.

2-57. G. Almen, P. MacKenzie, V. Malhottra and R. Maskell 35th International SAMPE Symposium April 2-5 1990 408-418.

2-58. Saul Patai, ed. The Chemistry of Cyanates and their Thio Derivatives. Part 1, John WIley and Sons, NY 1977.

2-59. D. A. Shimp, T. R. Christenson, S. J. Ising, 3rd International SAMPE Electronic Materials and Processing conference, Los Angeles,

CA, 1989.

2-60. P. C. Yand, D. M. Pickelman, and E. P. Woo 35th International SAMPE Symposium, 1131-1142 (1990).

2-61. J. Armistead and A. W. Snow, "Ether Linked Dicyanate Resin: Specific Volume Dependence on Conversion" ACS Polymer Preprints, Vol. 33, No. 1 p. 457-459 (1992).

2-62. A. W. Snow, R. F. Cozzens, W. H. Echols, J. P. Armistead, and D. A. Shimp, 33rd International SAMPE Symposium, 422-432 (1988).

2-63. R. F. Cozzens, P. Walter, and A. W. Snow, JAPS, Vol. 34, 601-616 (1987).

2-64. R-P Brochure: Quantitative Determination of Residual Cyanate in Cured Homopolymers via FTIR Analysis CET 105, Jan. 2, 1992.

2-65. R. B. Naik and P. P. Shah, European Polymer Journal, Vol. 25, No. 2, 193-195, (1989).

2-66. D. A. Shimp, J. R. Christenson, and S. J. Ising, "AroCy Cyanate Ester Resins, Chemistry, Properties and Applications," R-P Product brochure.

2-67. AroCy B-10 Cyanate Ester Monomer, R-P Product Borchure
R. B. Graver, "Cyanate Esters - High Performance Resins," Celanese Product Brochure.

2-68. R. B. Graver, Cyanate Ester Resins, in International Encyclopedia of composites, Vol. 2, S. Lee ed. (1990). VCH Pub. Inc. NY.

2-69. D. A. Shimp, presentation Virginia Tech August 1992.

2-70. D. A. Shimp and S. J. Ising ACS PMSE Preprints, April 1992, San Francisco.

2-71. Y-T Chen and C. W. Macosko 24th International SAMPE Technical Conference October 1992 Preprint.

2-72. A. M. Gupta and C. W. Macosko, Makromolecular Chem., Macromol Symp, 45, 105-115 (1991).

2-73. A. M. Gupta, and C. W. Macosko, Macromolecules, Vol. 26, 2455 (1993).

2-74. A. Osei-Owusu, G. C. Martin and J. T. Gothro, Poly. Eng. and Sci. Vol. 32, No 8, 535-541 (1992).

2-75. A. Osei-Owusu, G. C. Martin, and J. T. Gothro, , Poly. Eng. and Sci, Vol. 32, 535 (1992).

2-76. J. M. Barton, Hamerton, and J. R. Jones, Polymer International, 31, 95-106 (1993).

2-77. M. Bauer, J. Bauer, and B. Garske, Acta Polymerica, Vol. 37 Vol. 37, No. 10, (1986).

2-78. M. Bauer, J. Bauer, and G. Kuhn, Acta Polymerica, Vol 37, No. 4, 218-220 (1986).

2-79. M. Bauer, J. Bauer, and G. Kuhn, Acta Polymerica, Vol. 37 No 11/12 ,715-719 (1986).

2-80. M. Bauer, J. Bauer, and H. Much, Acta Polymerica 37, No. 4 (1986) 221-223.

2-81. M. Bauer, and R. P. Kruger Acta Polymerica, Vol. 37, No. 10, 6289-6301 (1986)

2-82. M. Bauer and G. Rodekirch, Acta Polymerica, No. 10, 653-655 (1986).

2-83. M. Bauer and J. Bauer Makromolecular Chemie, Macromol Symp. 30, 1-11 (1989).

2-84. M. Bauer, J. Bauer, S. Jahrig, Makromol. Chem., Macromol. Symp. 45, 97-103 (1991).

2-85. S. L Simon, J. K. Gillham, D. A. Shimp, ACS "Cure of a High-Tg Liquid Thermosetting Dicyanate Ester/Polycyanurate System. 96-101 (1992).

2-86. S. L. Simon and J. K. Gillham, ACS Polymer Preprints, Vol. 33, No. 1, 502-503 (1992).

2-87. R. H. Lin, J. H. Hong, and A. C. Su, ACS Polymer Preprints, Vol. 33, No. 1, "Kinetics of Polycyclotrimerization," (1992).

2-88. C. A. Fyfe, J. Niu, S. J. Rettig, N. E. Burlison, C. M. Reidsema, D. W. Wang, and M. Poliks Macromolecules, Vol.25, 6289-6301 (1992).

2-89. Y. T. Chen and C. W. Macosko, 24th International SAMPE Conference Proceedings, Ontario, Canada (1993).

2-90. S. L. Simon and J. K. Gillham, ACS PMSE Proceedings, Vol. 203, 231 (1992)

2-91. P. Armistead and A. Snow, ACS PMSE Proceedings, Vol. 203, 233 (1992).

2-92. A. Loos and G. Springer, Journal of Composite Materials, Vol. 17, March 1983.

2-93. A. Loos and S. Freeman, ASTM STP 873, 1985.

2-94. A. C. Loos, and P. H. Dara "Modeling the Curing Process of Thick-Section AutoClave Cured Composites" report to NASA Langley.

2-95. R. D. Driver, D. Brubaker, J. Downing, G. Leskowitz, and J. Stark SPIE , Vol. 1591 (Infrared FIber Optics III) 263-274 (1991).

2-96. D. Hill, Private communication.

2-97. Polymicro Technologies, Inc. Product List.

2-98. D. Shimp, private communication.

2-99. D. Rogers, E. Marand, D. Hill, to be published.

2-100 S. Srinivasan, Dissertation, VA Tech, 1994.

2-101 A. Rau, to be published.

2-102. M. A. Druy, L. Elandjian, and W. A. Stevenson, 35th Annual SAMPE Symposium, 1517 - 1521, (1990).

2-103. D. A. Shimp and S. J. Ising, ACS PMSE Preprints, April 1992, San Francisco.

2-104. S. A. Srinivasan and J. E. McGrath, High Perform. Polym., Vol. 5, 259-274 (1993).

2-105. F. Webster, Ph.D. Dissertation, VA Tech, 1993.

Chapter 3

CURE MODELING AND PHYSICAL ANOMALIES IN THE MID-INFRARED AND NEAR-INFRARED

3.1 INTRODUCTION

To most effectively use the fiber optic FTNIR data in an "intelligent processing" situation, a model is desirable. The near-infrared or infrared spectra should be suitable for such modeling because the spectra can measure the chemical changes. Many models are based on an indirect measurement of a physical change associated with the chemical changes instead of the reaction chemistry. The development of such a model based on the in-situ (chemical) reaction data is non-trivial due to a number of physical effects on the spectra. These physical effects, such as temperature dependent peak areas or peak locations, transitions from glass to rubber, or phase separation can significantly modify the observed spectra. Caution must be used when attempting to model based on in-situ infrared or near-infrared data. The physical changes can also provide added insight into the changes in the physical environments of the groups during the curing process.

Cure models based on conversion data, as obtained by differential scanning calorimetry (DSC), have been successfully developed for the processing of simple epoxy formulation to simulate changes occurring during the curing of graphite reinforced composites (3-1 - 3-6). One of the objections (3-5 - 3-8) to this approach has been that the DSC provides only an indirect measure of reaction. DSC often cannot distinguish multiple curing reactions and provides no information on the identity of the chemical changes. Many of the thermosetting resins have multiple cure reactions. Efforts have been made to tie the data from DSC to some measure of a real chemical reaction such as the change in concentration of a reaction product as measured by infrared spectroscopy. A recent elegant experiment by George, et al. (3-7 - 3-9) yielded simultaneous

DSC and infrared data. A "fundamental" modeling approach based on reaction mechanism and changes in the concentrations of chemical species rather than heat evolution in the DSC has been proposed by Chiao (3-5 - 3-6).

The modification of the fiber optic probe developed in Chapter 2 would appear ideal for following cure by monitoring the concentration of some chemical group in conjunction with a mechanistic based model. This portion of the research attempted to build that sort of model and to potentially substitute the data into the kinetic module of a computer cure model such as the Loos-Springer cure model (3-1 - 3-3). Two difficulties were encountered with the modeling. First, the data from the fiber optic spectra appeared to be slightly noisier than that from the bench top sample compartment. The noise problem was addressed by returning to the FTIR bench top sample compartment for the kinetic runs. Analysis of the data showed that the problem was not necessarily noise but sensitivity of the infrared spectra to physical changes. This second problem was not so easily remedied. Infrared spectroscopy is typically used to identify or monitor the changes in chemical species. In both the mid-infrared (MIR) and near-infrared (NIR), however, the spectra reflect a number of physical changes which complicate these measurements. Useful information can be obtained from the observed or apparent data. This approach was used in most of this study. For real information on the reaction chemistry, the physical and chemical changes have to be decoupled; this is much more difficult although it can be achieved with some knowledge of the chemical and physical changes in the curing resin and the resulting effects on the infrared spectra.

This chapter discusses the separation of the chemical and physical effects, the associated changes in the NIR spectra, attempts to model with the apparent data, differences in the kinetics when the physical effects were removed, and the potential for valuable processing information based on the spectral changes due to these physical effects.

3.2 BACKGROUND

3.2.1 Modeling

Processing decisions for the production of composite parts are often difficult. A series of actions must be taken based on information such as minimum viscosity of the resin, gelation, desired cure state, resin (or fiber) volume, volatile evolution, heat transfer, and equipment limitations. These decisions are typically based on some sort of desired performance value for the final part. Models have been proposed (3-1 - 3-6) to aid in these decisions by simulating the changes which occur during processing. These models typically predict the time, temperature, and location of events such as flow, compaction, degree of cure in the part, fiber volume, and residual stresses and can be used to optimize processing conditions.

One of the first of these models was developed by Loos and Springer (3-1 - 3-6). Based on information such as reaction kinetics, a viscosity model, initial ply thickness, initial resin content, heat transfer information, permeability, heat given off during the reaction, and density, the model predicts (as a function of location and time) the temperature, pressure, degree of cure, and the viscosity. Compaction, thickness and voids can be modeled as a function of time. Residual stress can also be calculated. This was successfully applied to an untoughened epoxy resin in the original work. Extent of reaction was typically modeled from the exotherm produced during cure as measured by a DSC. More recent models resemble the Loos-Springer model in concept, although they may differ in detail. Of interest in this study is whether this type of model can be applied to chemical reaction data as obtained at temperature with a Fourier transform infrared spectrometer and how the model would have to be modified to account for a toughened resin.

Pragmatically, whether the approach is theoretical or empirical, and whether the predictor is a chemist or an engineer, what is needed is a confirmable way of predicting the reaction rate (generally referred to as a "kinetic model"). Many of the physical changes, such as increases in viscosity, can be empirically tied to this

kinetic model. If one is dealing with a simple processing problem, a model based on an associated physical change may be as much as one needs or wishes to know. In many cases, high performance resins are very complex with multiple path dependent reactions, changes from liquid to rubber to glass, possible phase separation of a toughening phase, and/or evolution of volatiles. In such complex systems, more information is often desired.

Chiou and Letton (3-46) attempted to circumvent the issue of multiple reaction in the cure of an epoxy by isothermally aging the epoxy at low temperatures to allow the lower temperature reactions to occur, then to analyze the higher temperature major reaction by DSC. The higher temperature, major peak was analyzed as an nth order reaction in dynamic scans. Data was analyzed in terms of the shifts in the maximum heat evolution peak temperature (T_p). The smaller, lower temperature peaks were then fit to Guassian curves to analyze their peak temperatures. The authors proposed three nth order reactions and the total evolved heat should be considered as the weighted sum of the individual reactions.

Chiao (3-5) and Chiao and Lyon (3-6) proposed a more "fundamental" or "mechanistic" approach based on the reaction chemistry rather than the indirect physical changes used in models based on DSC data. The proposed advantages to this approach were the "flexibility" to handle resin formulation alterations as well as more insight into the topology (they refer to it as "morphology") of the cured resin. They proposed a model and calculated degree of cure based on the epoxy cure mechanism.

A very interesting series of articles (as discussed in Chapter 2) by George, et al. (2-22 - 2-25) have begun to tie the heat evolution, as observed in the DSC, to the actual chemical changes by simultaneous DSC-FTNIR. The light beam was removed from the benchtop and through a series of mirrors, introduced into the DSC pan. Changes in chemical species were followed along with the changes in heat evolved.

One of the advantages of modeling based on DSC data is the

simplicity of the information compared to that of a chemical mechanism. Chemical reaction mechanisms are often complex and may have steps which are not readily measurable (requiring certain assumptions), are possibly reversible, and may not always lead to the desired end product. A mechanistic approach must also consider such aspects as path dependent reactions and steric effects. If the reaction is measured in-situ, non-chemical changes, such as the physical contributions covered later in this Chapter must be considered.

The various kinetics proposed for the cure of cyanates will not be discussed here. Cyanates cure to form a six-membered triazine ring crosslink. As explained in Chapter 2, whether this occurs by nth order, autocatalytic or mixed kinetics is still in question. Cure data have been fit to all of the above kinetics and rationalized (3-10 - 3-18). The majority opinion is that the untoughened, uncatalyzed reaction should be autocatalytic. With organometallic catalysts (3-10 - 3-18), nth (probably second) order is most likely. The infrared data for the cure of this toughened, catalyzed cyanate system did not clarify the mechanism. Data based on normalized triazine peak areas could be fit to apparent second order kinetics. As will be discussed later, this data was not strictly chemical information but included certain physical effects. Data obtained later for the toughened, catalyzed resin based on triazine concentration measurements (a chemical measurement), did not fit second order kinetics. Since the differences in spectra with and without physical corrections provide no real input to the controversy, the mechanisms and rationales will not be discussed here. One is referred to the above references as well as Rau's discussion (3-44) of the isothermal DSC data for this toughened system.

3.2.2 Physical Effects

The FTIR spectrometer is typically used to obtain chemical information. The spectra, however, contain a wealth of physical information about polymers. Physical changes such as temperature effects, secondary bonding effects, densification, phase

transformations, phase separation, rotational effects and mechanical stress can be reflected in the spectra by peak shifts, broadening or sharpening of peaks, and/or changes in intensity of some but not all peaks. These changes must be considered when using mid-infrared or near-infrared for in-situ monitoring. The information obtained may not be strictly chemical, which was the case for the toughened cyanate resin used for this study.

In 1968 (3-19 - 3-22), it was observed that infrared peaks shifted and intensities changed as a function of temperature for certain thermoplastic polymers. Studies in the 1970's observed spectral changes in poly(methyl methacrylate) (PMMA) (3-23), poly(vinyl chloride)(PVC) (3-24 - 3-25), poly(ethylene terephthalate) (PET) (3-26), and poly(acrylonitrile) (PAN) (3-27). More recent studies have followed further changes in poly(ethylene terephthalate) (3-28), poly(vinyl chloride) (3-29), polystyrene and (PS) (3-33 - 3-24). Most recently, Webster (3-35) observed irreversible changes upon heating and cooling a semicrystalline polysulfide in contact with copper.

Hravilak and Roman (3-19) observed temperature sensitive changes in peaks between 1050 and 1300 cm^{-1} in poly(methyl methacrylate) (PMMA) and a PMMA-polystyrene (PMMA-PS) copolymer. The ester oxygen absorbance in this region was split into five absorbances due to intramolecular and intermolecular interactions. The peak splitting was attributed to intramolecular interactions. The ratio of the first peak to the second was followed as a function of temperature. The authors believed that if the two peaks were due to two different conformations, then the total integrated area of both peaks should be constant as a function of temperature. The percentage of the area due to each conformation should vary. The combined area of the first two peaks was found to be independent of temperature. The ratio of the two peaks was found to be independent of temperature below T_g but temperature dependent above T_g. The third and fourth peaks behaved similarly. The authors concluded that the rotation in the solid was only possible above T_g.

Dilute solutions of the polymer showed temperature dependence extending down below T_g. The authors proposed that the ester sees two distinct environments and two possible conformations for each environment and that below T_g the conformations must be locked in by intermolecular forces.

Anton (3-20) postulated that above T_g there should be a reduction in the integrated area as interactions are reduced and the groups are allowed to "relax". He also cited still earlier observances of the effect of T_g on spectra by Fukawa; Martin, et al.; Nichols; Sutherland and Jones; Nikitin; Volchek; and Silibia and Patterson. Most interesting is the work by Fukawa relating the changes in peak absorbances with temperature to changes in refractive index (which can be connected to changes in the dielectric constant and hence the dipole moment). Anton proposed designating the temperature at which this decrease in integrated area occurred as the glass transition, but also saw several different transition regions by observing different peaks. Anton suggested determining the T_g of the material by scanning a single peak if the sample "does not change thickness or become tacky." If the material softened upon heating, using a temperature insensitive thickness peak as a reference was recommended in case the sample changed dimensions.

Polyethylene terephthalate (PET) samples were air quenched from melt then heated, unconstrained, from 17 to 150°C at 1°C/minute. A peak at 970 cm^{-1} was shown to decrease until 58°C, then to increase between 58-85°C, the peak area being fairly constant at the higher temperatures. This was accompanied by a 10% change in thickness. An annealed film showed a constant peak area until 60°C with a slight decrease between 60 and 80°C. The glass transition (T_g) was determined to be 56°C and a small crystallization was observed at 82°C by thermal analysis. Monitoring of a peak at 920 cm^{-1} in commercial poly(vinyl acetate) showed a T_g of 30°C. Figure 3.1 shows integrated peak area decreasing with increasing temperature as the T_g is passed. The peak at 940 cm^{-1} yielded a T_g of 70°C for PS (literature value is 85°C). Nylon 6, 66, and 610 showed

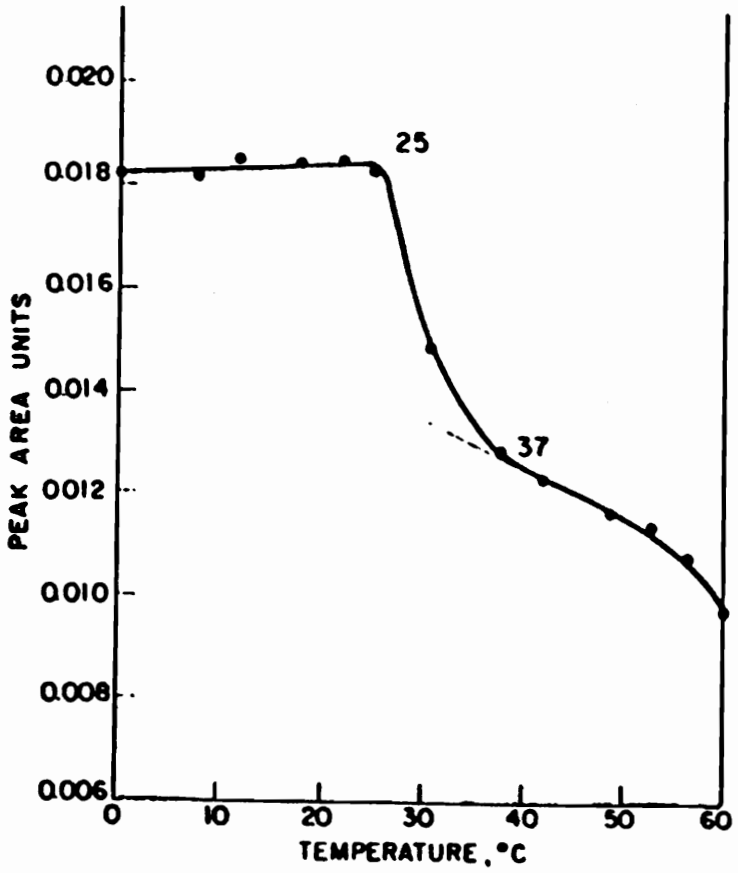

Figure 3.1. Changes in Peak Area upon Passing through the Glass Transition Temperature (3-20).

a change in slope (again, downward) upon heating between 35-50°C, although the data was more complex for Nylon 610. The T_g was also observed upon cooling for the nylons. Upon cooling, the integrated absorbance increased as the temperature was lowered, becoming much less temperature sensitive after T_g.

At about the same time, Hannon and Koenig (3-21) conducted a more in-depth study of the effects of temperature on the spectra of PET and showed that a T_g as well as a two component beta transition could be observed. More interesting is Hannon and Koenig's explanation for the observance of transitions via infrared spectroscopy. Earlier work by Ovander predicted a simple linear relationship between the integrated intensity (peak area) and absolute temperature of the form:

$$I = I_0 + aT$$

where I is the integrated intensity; T is the absolute temperature; and a is a constant (typically negative). In other words, peak area would be expected to decrease with increasing temperature. This relationship had been experimentally observed earlier for low molecular weight materials and some polymers and was explained by Lisitsa as being due to temperature increasing the distance between molecules (thermal expansion) and decreasing the interaction between them (resulting in a reduced induced dipole moment and a reduced absorbance). Hannon and Koenig explained that an "abrupt change in thermal expansion occurs at T_g" and that one would expect to see these transitions as "changes in slope of the absorbance in the infrared spectra as a function of temperature." Changes in frequency might be expected (with enough intermolecular interaction) but the authors expected the changes in absorbance to be more sensitive and dramatic.

Experimentally, the authors used PET films which had had various heat treatments and then looked at the absorbances of different groups which might be located in the amorphous, crystalline, or fold region. Of interest in this study is the unusual behavior of the aromatic ring deformation at 1380 cm^{-1} due to the

aromatic ring in the crystalline region. This peak was not even observed in the amorphous, uniaxially drawn, or biaxially drawn sample but became evident upon the annealing of the commercial Mylar. The presence of this peak did not reflect a chemical change, strictly a physical one. Hannon and Koenig also related the slope of the temperature dependence to the local "thermal expansion coefficient in the vicinity of..." the group and "the order of magnitude change in the environment of the group as one goes through the transition."

Brockmeier (3-22) looked at the frequency shifts of six $-CH_2$ infrared peaks upon cooling polyethylene and ethylene-propylene co-polymer and observed that thermal contraction (or changes in density) explained "most" of the changes. Three shifted to higher wavenumbers; three to lower. The shifts to higher wavenumbers upon cooling were expected; the lower were not. The author proposed that the cooling may have produced a slight increase in secondary bonding (primarily London dispersive forces), or changes in crystalline interaction. Shifts were relatively small, less than four wavenumbers.

Later works extended the effects of temperature on other polymers. Schmidt, et al. (3-23) studied PMMA and proposed changes with temperature to be due to rotation around the oxygen-methyl bond. Augury (3-24) investigated several absorbances of poly(vinyl chloride) and found that the intensity of some peaks changed with temperature and had discontinuities at T_g, some did not. Joss, Bretzlaff, and Wool (3-25) also studied the shift in frequencies of PVC and by deconvolution and subtraction observed physical aging effects. Huang and Koenig (3-26) extended earlier work on the changes in PET upon cooling and began to study styrene. In 1983, Lin and Koenig (3-28) revisited PET. Changes in intensities with heating for some aromatic ring vibrations (1507 and 1580 cm^{-1}) were as high as 30-48%. In this case, these peaks were typically part of the crystalline structure. (Overtones of these aromatic ring deformations were used as a reference in much of this study but

later found to show significant temperature dependence, decreasing 13-20% in the cured polymer below Tg. This is addressed in a later section). Lin and Koenig found the frequency shifts to be less than 5 wavenumbers. Many of the changes in the various peaks were found to be thermally reversible, but some were shown to be thermally irreversible.

Joss, Bretzlaff and Wool (3-29) studied heating and cooling of PVC and PS. They observed a "slope discontinuity" in the wavenumber versus temperature graph at Tg, a change in peak location when the polymers were annealed below Tg, and developed a theoretical treatment for the change in slope based on intermolecular forces, intramolecular forces, and stress. For polystyrene, they observed that changes in the peak due to the pendant phenyl ring should reflect the "intermolecular environment." Figure 3.2 shows the effect of heating and cooling on the frequency of the aromatic ring peak at 1452 cm^{-1}. The authors concluded that different groups, in different locations (for example backbone versus pendant) would respond differently to changes in the local environment. Magonov, Shen, and Qian (3-30) also studied the effects of temperature on PS.

3.2.2 Blends and Hydrogen Bonding

In blends, phase separation may also result in changes in the infrared spectra. Coleman and Painter (3-36) have published an excellent review of (mid) infrared spectroscopy of blends. Interactions in compatible blends may result in peak shifts and/or peak broadening. Many differences were very small. Coleman and Painter admit that they made "a big deal out of frequency shifts that would be as little as 1 or 2 cm^{-1}" and resorted to computerized routines such as spectral addition and subtraction, curve resolving, derivatives, and least squares spectral fitting. The spectra of a blend consisting of large well-separated polymer particles with a very small interfacial region should be the sum of the individual polymers and should be able to be resolved into the spectra of the one polymer by properly subtracting the other. If there was a single phase, the

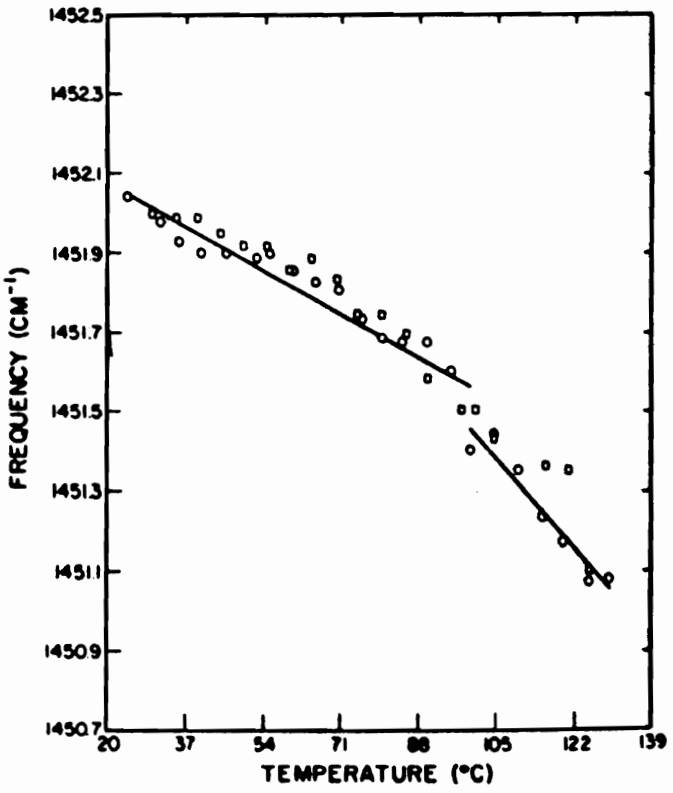

Figure 3.2. Effects of Temperature on a Pendant Aromatic Ring in Polystyrene (3-29).

spectra would not be the sum of the components due to interactions and changes in conformation resulting in "frequency shifts, band broadening and changes in the relative intensities of infrared bands."

In compatible blends, where one or more of the polymers contained a carbonyl group, there were a number of reported carbonyl shifts due to intermolecular interactions, often hydrogen bonding. Typically, the carbonyl absorbance would shift to lower wavenumbers and display asymmetric peak broadening. In blends of phenoxy polymers with poly(e-caprolactone) (PCL), a new carbonyl peak was produced due to H-bonding. The extreme case was poly(vinyl phenol) and PCL. Two distinct carbonyl groups 25 cm^{-1} apart were produced. The hydroxyl group was also affected. In pure phenoxy polymers, the hydroxyl groups were highly hydrogen bonded with a few free hydroxyls at higher wavenumbers. Heating of the pure phenoxy yielded two peaks: one H-bonded (lower wavenumber) and one due to free (at higher wavenumbers) hydroxyl groups as the kinetic energy overcame the hydrogen bonding. When mixed with PCL, free, self-associated, and interacting (with the carbonyl) hydroxyls were produced. The overall result was a peak shift to higher wavenumbers than for the pure compound. In polyethylene oxide-phenoxy blends, the -OH shifted instead to lower wavenumbers.

In the event of a lower critical solution temperature (heat polymers up; they phase separate), raising the temperature should change the spectra. Many polymers degrade below the lower critical solution temperature (LCST). Blends of ethyl vinyl acetate (EVA) and polyvinyl chloride (PVC) or chlorinated polyethylene (CPE) had a reasonable phase separation temperature, around 130°C. At room temperature, the carbonyl peak was broadened and shifted about 4 wavenumbers (from pure EVA). At 130°C, the carbonyl peak looked like pure EVA. When a EVA-CPE blend was heated from room temperature to 150°C, the phase separation was evident. As the blend was heated, the carbonyl peak shifted to higher frequencies. An "S-shaped" curve (Figure 3.3) was produced with the non-

linearity occurring as the materials phase separated. The heating (and separation) resulted in a 5-6 cm^{-1} shift.

Changes in hydrogen bonding result in the more dramatic spectral changes. Not all compatibilization is due to hydrogen bonding. Spectral shifts may or may not be apparent with the more subtle interactions. Polystyrene and poly(2,6-dimethyl-1,4-phenylene oxide) (PPO) or poly(vinyl methyl ether) (PVME) were compatible but have neither carbonyl nor hydroxyl groups. Nuclear magnetic resonance data indicated that the compatibilization interaction was through a "pi hydrogen bond" between the PPO methyl group and the aromatic ring in PS. This sort of interaction would most likely not be visible with FTIR spectroscopy. The authors concluded, "infrared spectroscopy will thus be limited in compatibility studies to systems involving significant and detectable interactions between the two individual polymers."

A very interesting recent article by Bhagwagar, et al. (3-38) extended FTIR spectroscopic studies of blends to mapping the phase diagram of a poly(meta-phenylene adipamide) (MPDn) - poly(ethylene oxide) (PEO) bend. Different compositions of MPDn-PEO blend were heated at 1°C/minute to 150°C in a heated sample holder. On heating, the blend separated into polyamide rich and polyamide poor phases. Free and H-bonded carbonyl peak contributions were observed. Separation temperature (defined as the temperature at which there were "significant changes" in the area of the free carbonyl peak) versus the area of the hydrogen bonded carbonyl with temperature was graphed as a function of composition.

Many of the effects seen in the mid-infrared are also present in the near-infrared (NIR). H-bonding can have a significant effect on the spectra in the NIR. Lin and Brown observed (3-37) a 162 cm^{-1} shift in the -OH peak in water over a 65°C range. They used this peak shift to their advantage to produce a temperature sensor. George, et al. (2-20 - 2-25) were plagued by the presence of both free and hydrogen bonded hydroxyls when trying to measure the concentration of the hydroxyl reaction product. In a review of NIR

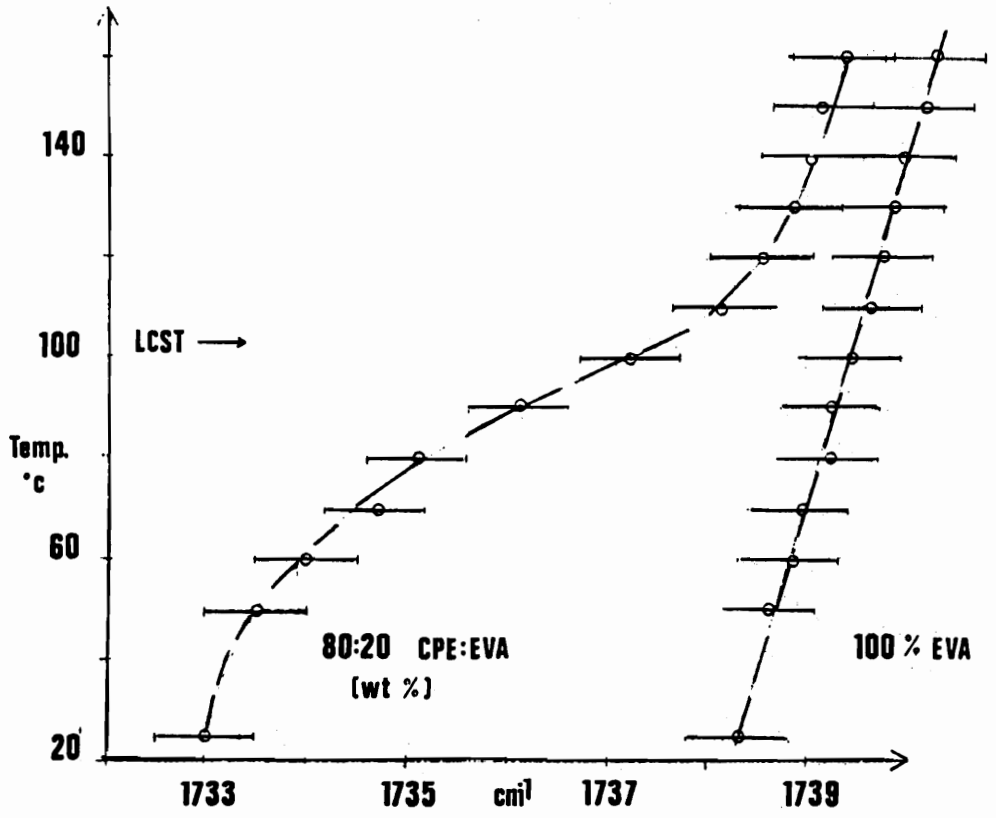

Figure 3.3. Carbonyl Peak Shifts as an EVA-CPE Blend is Heated through Phase Separation (3-36).

Spectroscopy of Polymers, Miller said (3-39) that the "sharp contrasts between free and hydrogen-bonded NH and OH groups...enable accurate analyses of surface interactions and other structural properties that depend on hydrogen bonding." Phase separation in urethanes block copolymers has been followed in the NIR by watching the shifts of the carbonyl overtone peaks as well as a free NH band. More subtle interactions can also be observed in the NIR. In a blend of polystyrene and polybutadiene, the 6112 cm^{-1} peak from the $=CH_2$ in butadiene changed with styrene concentration. More significant differences were seen in the $-CH_2-$ backbone peak at 4255 cm^{-1}

3.3 EXPERIMENTAL

Infrared sampling techniques, instrumentation parameters and heating instrumentation were as described in Chapter 2. In all instances, the salt cell or sensor was preheated to either 104°C (for ramps) or the isothermal dwell temperature for isothermal cycles. Integration of the peaks was previously described (Chapter 2). Peak locations were determined by the Nicolet peak pick routine. Calibrations were obtained by doping the toughened resin with 1,3,5-triazine (Aldrich T4,605-1).

Data analysis used either a fit to an integrated rate equation as described by Prime (3-40) or the nonlinear regression.

3.4 RESULTS AND DISCUSSION

When analyzing infrared spectra of reacting systems, it is common to chose a reference peak (3-43 - 3-45, 2-21, 2-64), one that doesn't take part in the reaction, to compensate for changes in film thickness and other physical differences. An NIR overtone at 4675 cm^{-1} of the aromatic ring stretch at 1490-1500 cm^{-1} (2-61 - 2-64, 2-66) was selected as a reference peak. The phenyl ring should not take part in the cyanate trimerization to a triazine ring. The integrated triazine peak was "normalized" by dividing it by the integrated aromatic reference peak at 4675 cm^{-1}. Normalization is common practice in evaluating the cure of thermosetting systems, typically, after cooling to room temperature.

There are, however, a number of physical changes that have to be considered at temperatures other than ambient in the mid-infrared and near-infrared. Spectra do not strictly reflect chemical changes. Physical changes more subtle than changes in thickness can alter the spectra. Physical changes (not just chemical ones) can result in changes in peak height, peak area, and peak location. In this study, this first became apparent upon trying to fit the normalized triazine peak to kinetic models. The initial decrease in the aromatic peak as the sample was rapidly heated on a preheated stage to the isothermal cure temperature made the triazine peak appear to increase more than it actually should at the beginning of the isothermal cycles. This was due to the more negative slope of the temperature dependence of the area of the aromatic reference peak and the very small temperature dependence of the triazine peak.

Most of the rest of this study uses data obtained as a "relative conversion" resulting from the normalized peak areas. This is a reasonable approach based on historical precedence and general acceptance of the use of a reference peak (3-43 - 3-45, 2-21, 2-64). This calculation is given in Chapter 2. The relative conversion data could be fit to a second order ($1/(1-\alpha)$ vs. time should be linear) kinetics up to 50-60% conversion. This is one of the more commonly proposed kinetics (3-10 - 3-12, 3-17 - 3-18) in the literature for organometallic catalyzed cyanate systems. First order (3-15), autocatalytic (without the organometallic catalyst) (3-16, 3-43), and mixed kinetics (3-17 - 3-18) have also been reported.

More powerful curve fitting techniques such as nonlinear regression software would not converge for the relative conversion data set (3-47). Initially, it was thought that this might be due to noise in the fiber optic spectra. More likely, it was due to the use of the normalized values for conversion affecting the values early in the cure cycle. This may explain why the autocatalytic kinetics observed by Rau (3-47) using nonlinear regression of DSC conversion data was not observed for the FTNIR analysis of the normalized data.

From a processing standpoint, the apparent kinetics based on

relative conversion may be acceptable. A more quantitative evaluation of the chemical and physical changes, fitting the data to a meaningful model, and setting a basis for further use of on-line FTIR or FTNIR sensors require that a more rigorous analysis be attempted. This involved analyzing the temperature dependence of the triazine and aromatic peaks and other physical changes in the system as reflected in the NIR spectra. To obtain this data and further information on the cure, slightly thicker samples were made and placed in the heated cell in the more isolated FTIR sample chamber. Temperature dependent data was obtained isothermally at 120, 130, 150, 160, 170, and 200°C and during a 2°C/minute ramp. Above 200°C, the co-catalyst volatilized upon placement upon the preheated cell.

As detailed in Section 3.2, a number of physical changes can occur in these spectra (3-19 - 3-39). Upon heating the frequency (or wavenumber) and integrated absorbance should decrease based on density. Conversely, upon cooling the frequency (or wavenumber) and integrated area increase. There should be a change in slope of the integrated absorbance versus temperature graph for some groups at the T_g. The slopes of the curves should reflect the environment of the group. Aromatic ring intensities seem particularly sensitive to changes. Differences in the effect of temperature on peak shift may reflect differences in environment such as a pendant group instead of a backbone group. Physical aging may induce frequency shifts. In compatible blends, H-bonding or dipole-dipole interactions may result in a shift in peak locations compared with the pure compounds. This is most obvious in the carbonyl peak or the hydroxyl peak (assuming one has a carbonyl or hydroxyl peak). Typically, the carbonyl absorbance in a compatible blend is at lower wavenumbers and broader than that of the pure compound. In extremes, a new peak, due to H-bonded carbonyl may show up at lower wavenumbers. The -OH peak may move to either way depending on whether the blend has stronger or weaker H-bonding than in the self associated pure compounds. The shift in a

compatible blend should reverse as the blend separates into two phases. Hydrogen bonding may move peaks either way depending on whether the hydrogen bonding in the blend is stronger or weaker than in the pure material.

Of the physical effects, the most obvious would be interaction between two components or phases. Mid-infrared and near-infrared has been used extensively (3-36 - 3-39) to study such hydrogen bonding in blends. There is little evidence of hydrogen bonding between the thermoplastic and the cyanate in this resin system (see Figure 3.4) based on the mid-infrared spectra. Neither the carbonyl peak at 1235 cm^{-1} nor the sulfone peaks at 1351 and 1176 cm^{-1} (2-42) cm^{-1} shift when the thermoplastic is combined with the cyanate monomer. The cyanate peak location in the monomer did not appear altered by the presence of 25% thermoplastic. Subtler interactions were not readily apparent in the mid-infrared.

What was apparent was a rather unusual behavior exhibited by the aromatic absorbance at 4675 cm^{-1}. There was some evidence of unusual behavior in the aromatic peak at 1490 cm^{-1} (in the mid-infrared) but it was hard to quantify. It is possible that the aromatic ring is interacting with another group. Another explanation is that this aromatic absorbance is temperature/environment sensitive. As explained in Section 3.2, changes due to temperature on the coefficient of thermal expansion should result in a linear relationship with a negative slope between integrated absorbance and temperature. Figure 3.5 curves 2,3, and 4 show the changes in the area of the aromatic absorbance at 4675 cm^{-1} as the cured resin is cycled from the postcure temperature to room temperature (cycle 2) and then heated again (cycle 3). It can be seen that the aromatic integrated absorbance was quite sensitive to temperature even after the resin was cured. The cured resin showed the expected negative slope temperature dependence.

During the cure (cycle 1), the behavior was somewhat more complex. The integrated absorbance varied linearly (with a negative slope) with increasing temperature from 120 to 170°C and again

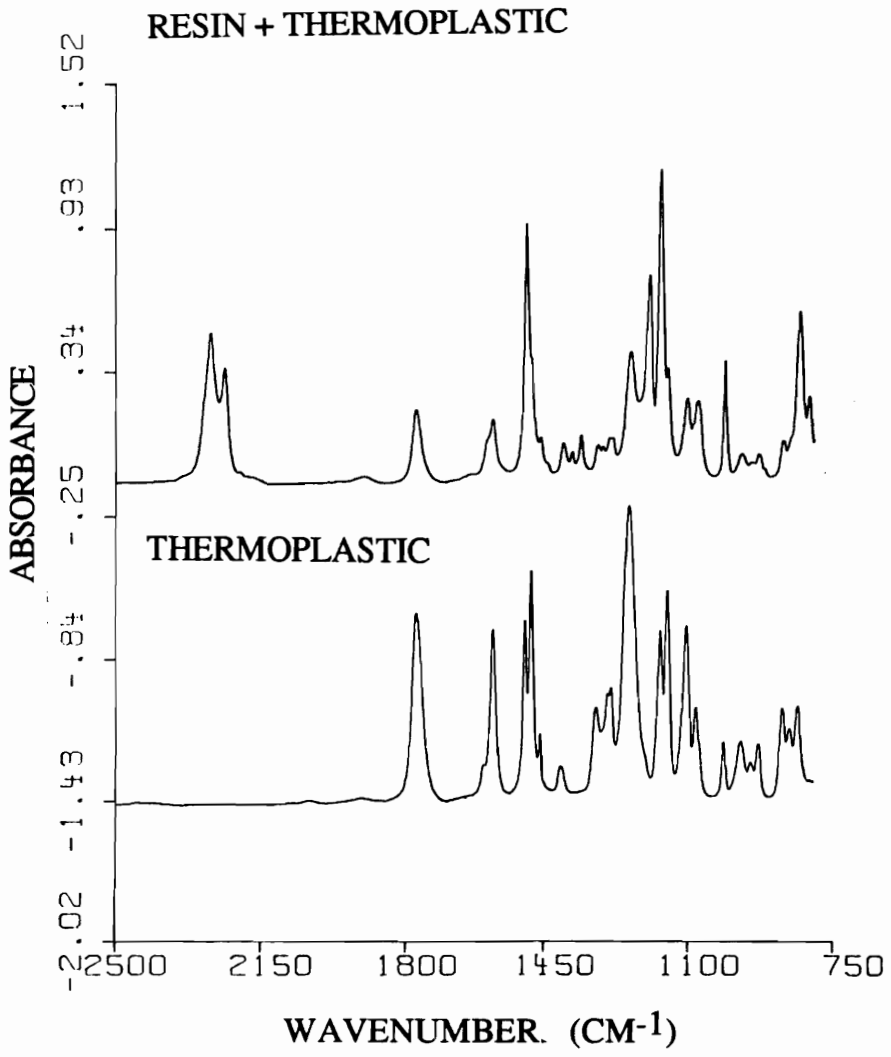

Figure 3.4. Peak Shifts due to Hydrogen Bonding were Not Seen in the Mid-infrared.

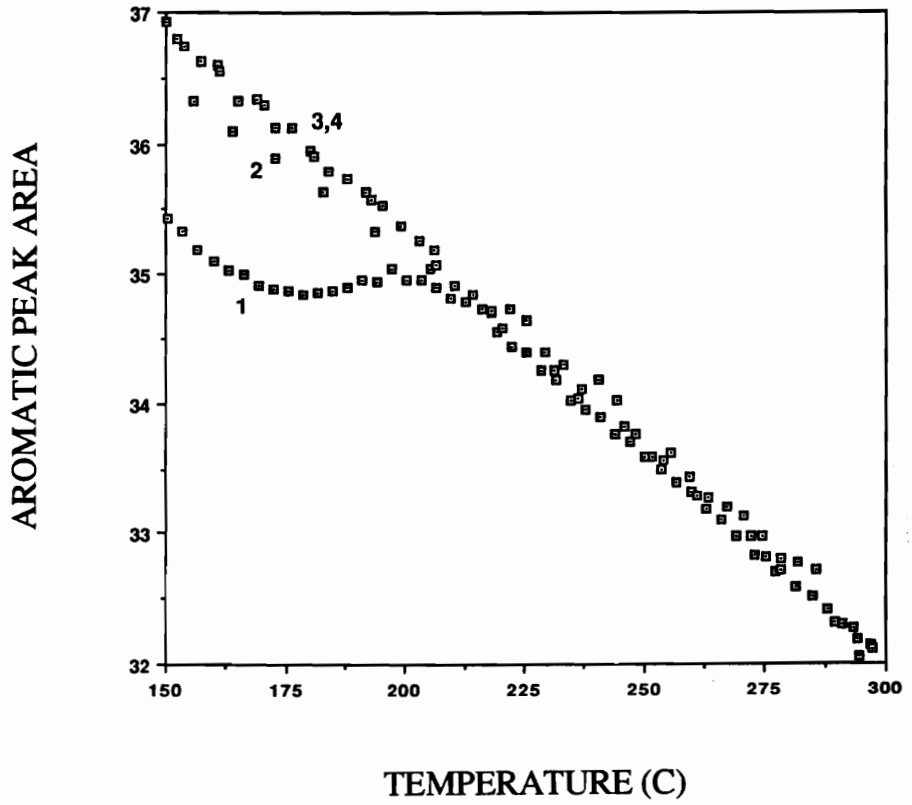

Figure 3.5. Changes in the Area of the Aromatic Peak at 4675 cm^{-1} upon Thermal Cycling at 2°C/minute: 1. Initial Cure, 2. First Cool, 3. Second Heat, and 4. Second Cool.

above 210°C. The temperature dependence above 200°C was retained on all subsequent cycles. The peak became relatively independent of temperature between 170 and 210°C during the cure. Several things happened between 150 and 200°C. The crosslinking reaction became significant at these temperatures. Since the triazine peak did overlap the aromatic peak, there might be some influence of the triazine peak on the aromatic peak. The peaks were not deconvoluted since the deconvolution program could not be used for real-time data analysis. Also occurring in this temperature range was phase separation as observed in the permittivity of the dielectric response (Chapter 5), by decreases in visible light transmission (Chapter 5), and scanning transmission electron microscopy (Chapter 4). Distinct (in terms of concentration gradient) 0.5 - 1.0 micron particles occurred between 170 and 200°C. The non-linearity observed may be reflecting the change in environment during the phase separation. There was a lot of intriguing information in the aromatic peak. Unfortunately, this also meant that the aromatic stretch was not the optimum choice for a reference peak, even although it was not expected to take part in the reaction and there were very few other peaks in the spectra to use as an internal reference peak.

The triazine peak behaved as would be expected from a reaction product. As shown in Figure 3.6 (cycle 1), the triazine peak area did not change from 100 to 125°C. Once the reaction began, the triazine peak area rapidly increased (rather than decreased as shown by the aromatic peak and predicted for unreactive groups) up to 200°C - 220°C. Afterwards, a slower increase was observed. The slower increase might be due to trapping of reactive groups, to the reaction becoming diffusion controlled or due to changes in the physical environment. Once the resin was cured, the triazine absorbance peak area showed little or no temperature dependence with subsequent cycling (Figure 3.6, curves 2,3, and 4).

Although shifts in peak location due to hydrogen bonding were not seen in the carbonyl or sulfone in the mid-IR, the peak locations of the aromatic peaks used for reference were evaluated since there

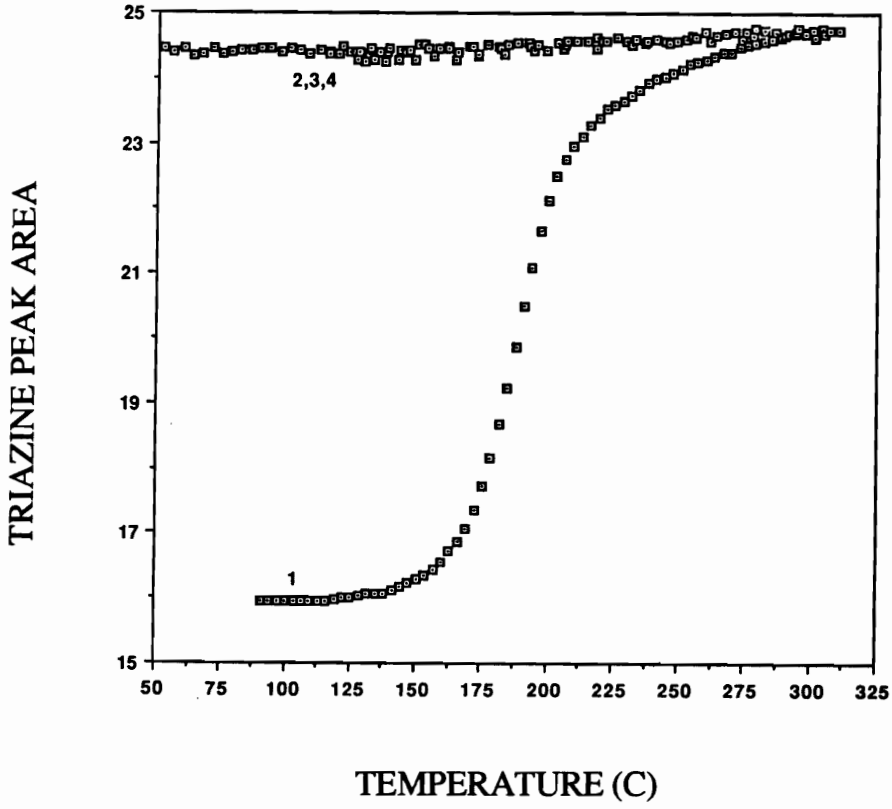

Figure 3.6. Changes in the Area of the Triazine Peak at 4625 cm^{-1} upon Thermal Cycling at 2°C/minute: 1. Initial Cure, 2. First Cool, 3. Second Heat, and 4. Second Cool.

appeared to be some shifting occurring. The NIR, as explained in Chapter 2, is a region of overtones and mixed peaks. The peak (nominally) at 4675 cm^{-1} (designated "Benzene 1 or B1" for the sake of brevity) is referred to in this study as a aromatic peak, but most likely it resulted from a mixture of an aromatic ring deformation (2-37 - 2-41) and an aromatic C-H stretch (2-37 -2-41). There is another peak 5995 cm^{-1} (designated "Benzene 2 or B2") of a similar nature but not as well documented and perhaps of a more mixed nature. These two "aromatic" peaks, along with the triazine ring peak make up the most noticeable absorbance in the NIR spectra of this resin system between about 4500 and 6500 cm^{-1}.

The effect of the temperature and conversion on the peak locations of two aromatic peaks were observed. Peak locations for B1 in isothermal cures do not show any clear trend as far as the effect of temperature on peak location. Over the isothermal temperature range from 135 to 180°C, only a change of 3-4 wavenumbers was observed (Figure 3.7). Any further effects (due to vitrification) were lost in the noise. A 2°C/minute temperature ramp from 120°C to 300°C allowed access to more information. The location of B1 (nominally at 4675 cm^{-1}) had a very definite, negatively sloped, linear relationship with increasing temperature, moving about 10 cm^{-1} from 4677 to 4667 cm^{-1} (as one would expect based on density changes). It was rather interesting that the area B1 peak, as explained earlier, was dependent upon cure state while the location of this peak had no dependence on cure state (as shown in Figure 3.8 for both the initial cure (heating) ramp and the subsequent cooling ramp). Shifts in the water peak at 6900 cm^{-1} in the NIR have been used to calibrate temperature (3-37). The aromatic peak seems to show a similar dependence and could operate as an internal temperature reference.

The aromatic peak B2 at (nominally) 5995 cm^{-1} behaved quite differently from the aromatic peak at 4675 cm^{-1}. This peak should contain an aromatic ring deformation combined with an aromatic C-H stretch contribution (2-37 - 2-41) as did the peak B1. Since the

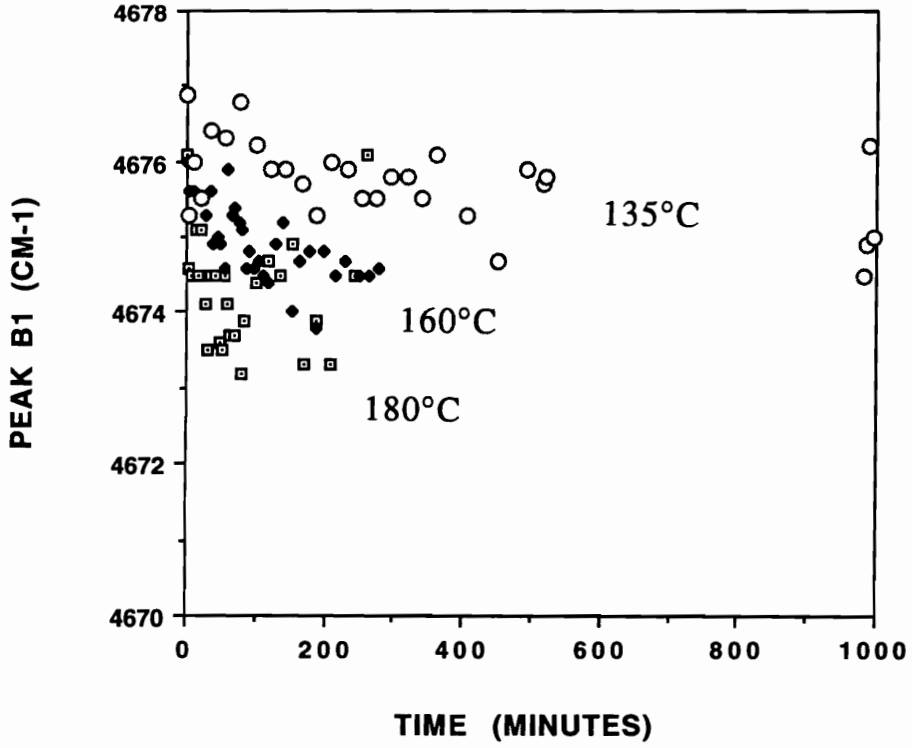

Figure 3.7. Shifts in the Aromatic Peak (B1) Location during Isothermal Cures.

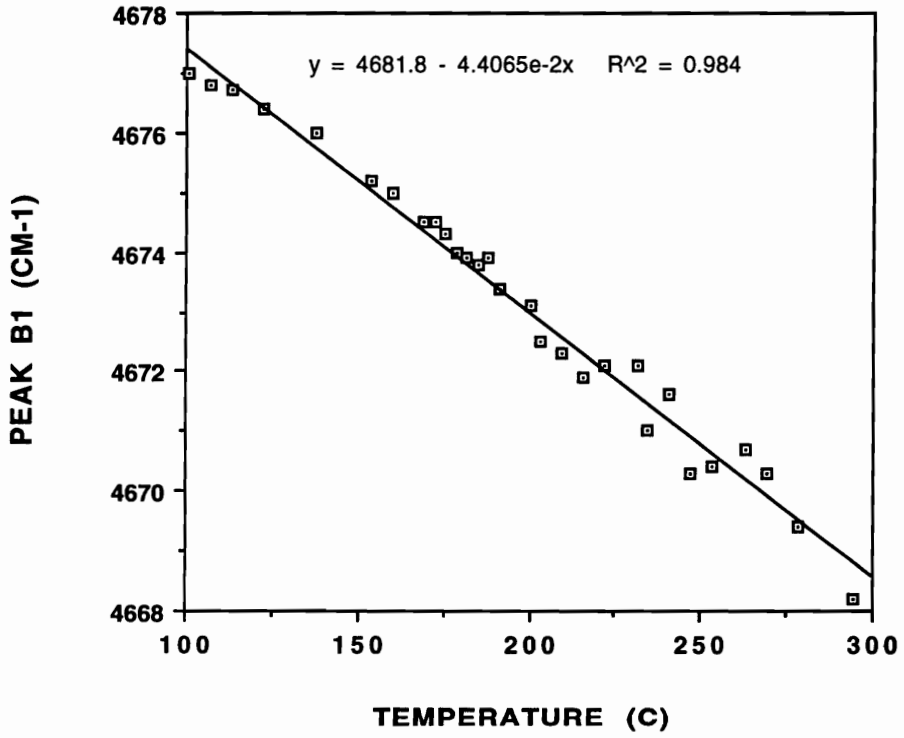

Figure 3.8. Shifts in the Aromatic Peak (B1) Location at 4675 cm-1 during a 2°C/minute Cure Ramp and Subsequent Cooling.

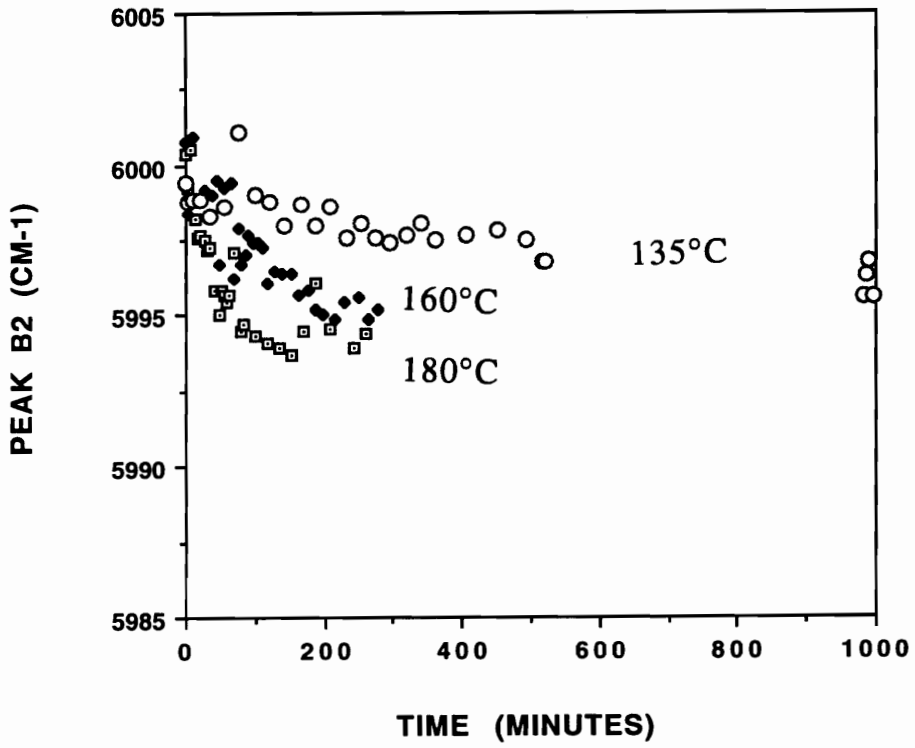

Figure 3.9. Changes in the Aromatic Peak (B2) Location during Isothermal Cures.

buildup of the triazine peak on the shoulder of B1 does not seem to move the peak location of B1, one would not expect the even weaker shoulder calculated to be 6970 cm^{-1} to affect the peak location in B2. There appears to be another, unidentified effect (or absorbance) in B2. When held isothermally at 135, 160 or 180°C, there was a 3-7 wavenumber shift to lower wavenumbers during the dwell (Figure 3.9). This might be due to changes in mobility or due to slow, subtle secondary bonding or interaction altering as the concentration gradients are increased in spinodal decomposition. The 2°C/minute ramp displayed some more intriguing behavior. Unlike B1, which had a cure state independent, negatively sloped, linear relationship between temperature and peak location, there were three distinct frequency regions for B2 during the cure ramp (Figure 3.10). The negatively sloped linear relationship was exhibited for all temperatures, only by the cured material. There were two regions of similar (negative) slopes in the cure ramp, from 100°C to 160°C and 200°C to 280°C. Between 160 and 200°C, there was a discontinuity. Such discontinuities could be associated with a T_g or a phase separation. Morphological studies (Chapter 4), dielectric permittivity (Chapter 5) and visible light transmission (Chapter 5) have shown that phase separation occurs between 150 and 200°C during the 2°C/minute cure ramp.

These changes were subtle and were obtained in the insulated, well controlled FTIR benchtop specimen holder. Note the small shift in the B2 peak in Figure 3.11, as well as the flattening of the B1 peak as well as the slight shift to lower wavenumbers. With a short (1-3 meters each) fibers and the Spectratech heated cell, these subtle changes can still be observed as shown in Figures 3.12. Although one can say qualitatively that the changes should be occurring in the oven with the longer fibers, the spectra are noisy enough that it is difficult to detect small peak shifts.

Despite the interesting information in the aromatic peaks, these effects made them somewhat unsuitable as references peaks and required a calibration. Eliminating the temperature dependent

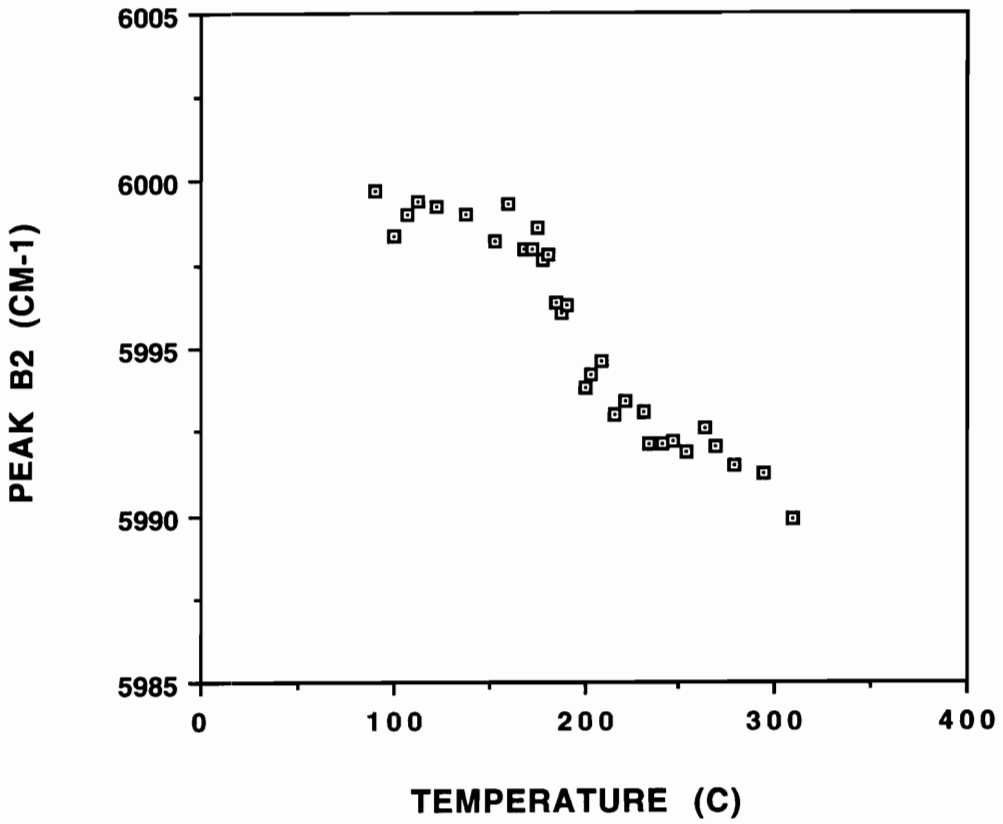

Figure 3.10. Changes in the Aromatic Peak (B2) Location during 2°C/minute Cure Ramps.

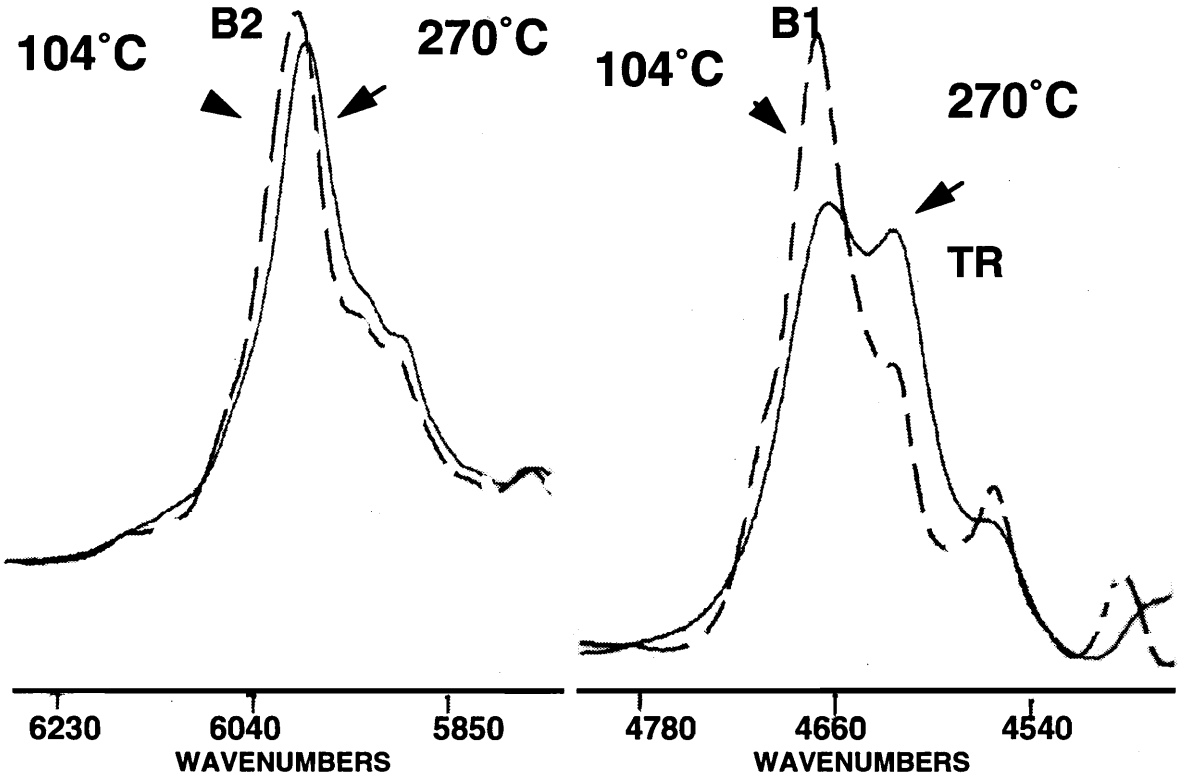

Figure 3.11. Temperature Effects on NIR Spectra.

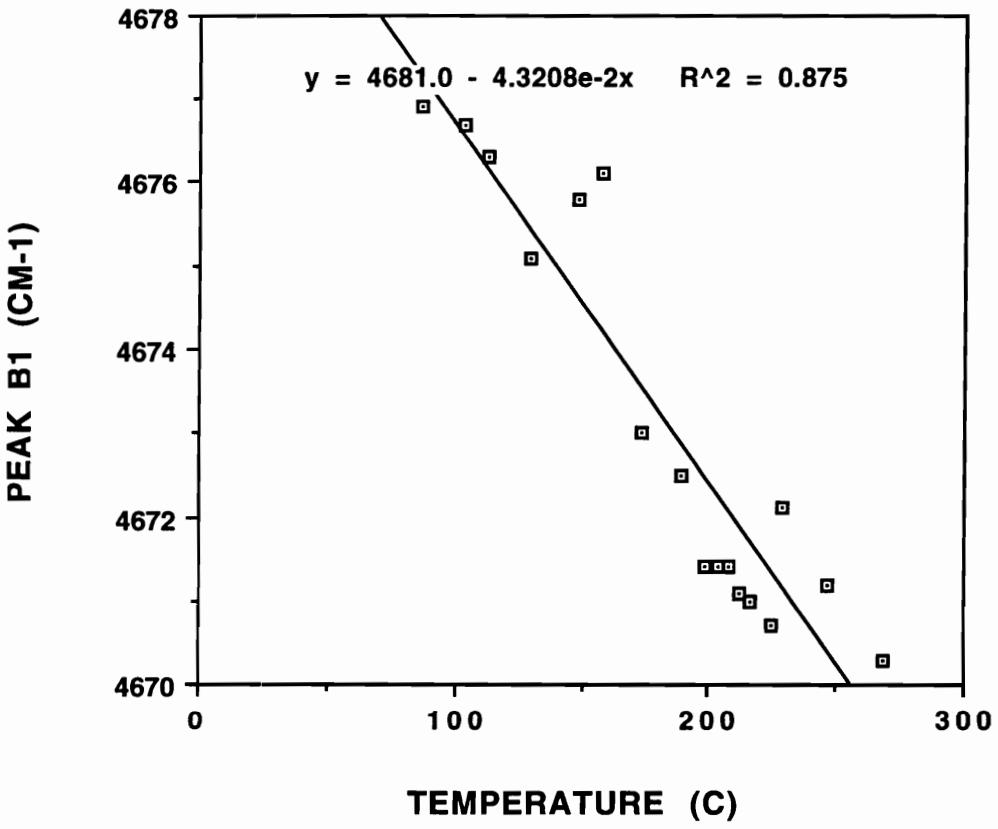

Figure 3.12. Peak Shifts with Short Fiber Optics.

effects of the normalization based on the aromatic ring stretch required a calibration of triazine concentration and measurement of the path length. Resin samples were heated to 104°C to insure proper mixing of the resin sample. The BADCy monomer melts around 84°C as does the 1,3,5-triazine additive. The incorporation of 25% of 15 K number average molecular weight thermoplastic with a T_g around 260°C made the resin very viscous. Resins had to be kept above 104°C for mixing and pouring. Weights of 1,3,5-triazine were added to the higher concentration standards, then dilutions were attempted for the lower concentrations. The standards were then heated to 110°C for 5-10 minutes to insure good mixing. The standards were placed on the preheated 104°C stand-alone fiber optic sensor. FTNIR spectra of these samples showed little or no triazine in the spectra. The higher concentration of triazine did show a peak, which rapidly declined to that of a 5% concentration. The triazine appeared to be either disappearing or degrading. The melting point for 1,3,5-triazine was 84°C with a boiling point was of 114°C (2-34). Standards were made again limiting the temperature to 104°C and the time at this temperature and making each standard individually. This seemed to work for values up to 10 weight percent of triazine. Above that value, the triazine was rapidly lost.

Beers law was assumed and seemed to be appropriate when the standards did not boil off:

$A = a * b * c$

A = Absorbance

a = absorbtivity

b = path length (cm)

c = concentration (g/L).

Concentration was calculated using a "rule of mixtures" density estimate of 1.25 for the uncured resin with 25 weight percent of thermoplastic (density for uncured cyanate = 1.21 (3-49) and density of polyethersulfone as 1.37 (3-48)). The absorbtivity (not the molar absorbtivity) was calculated by linear regression based on a 0.159 cm path length. This gave an absorbtivity of 0.127 g-cm/L and the

relationship

$$\text{Absorbance} = A_i + 0.127 * b * c$$

A_i = integrated area of the initial shoulder

The initial area of the shoulder was not zero. In the case of b = .159 cm, A_i was 17.5. Since the calibration could not experimentally be extended above 10%, Beer's law was assumed to continue to hold for the higher concentrations.

Fixed path lengths were used for calibration runs, the earlier tests had path lengths which varied from 1 - 2 mm with most of them being around 1.5 mm. Since the normalization was supposed to compensate for this difference, the exact path length was not measured prior to most fiber optic tests. A calibration based on the aromatic peak area temperature and path length could potentially be derived (Figure 3.13) from known path lengths and temperatures. This relationship could be used to calibrate path length. In reality, the experimental A_i for the known path length calibration standards were used. Cured samples from the sample salt cells, rather than the fiber optic cell were removed by dissolving the KBr salt cells in water and path lengths were measured. These calculations allowed the corrections to be made shown in Figure 3.14 and 3.15 for α versus time at various temperatures. A second order kinetic fit ($1/(1-\alpha)$ versus time) of the conversion data, corrected for triazine concentration rather than normalized triazine peak area is shown in Figure 3.16 for 130, 150, 160 and 170°C. A second order reaction would show a linear relationship of $1/(1-\alpha)$ with time. For the corrected values based on triazine concentration rather than relative triazine peak height, this is obviously not the case. There appears to be an initial time lag at the start of the reaction. The salt cells for this test were preheated to the reaction temperature. However, it cannot be said unequivocally that the reaction temperature was reached instantaneously. It is, therefore, difficult to say with absolute certainty that this is due to an autocatalytic reaction.

Admittedly, not all of the physical effects are eliminated by the triazine calibration. There will be some slight changes in density as

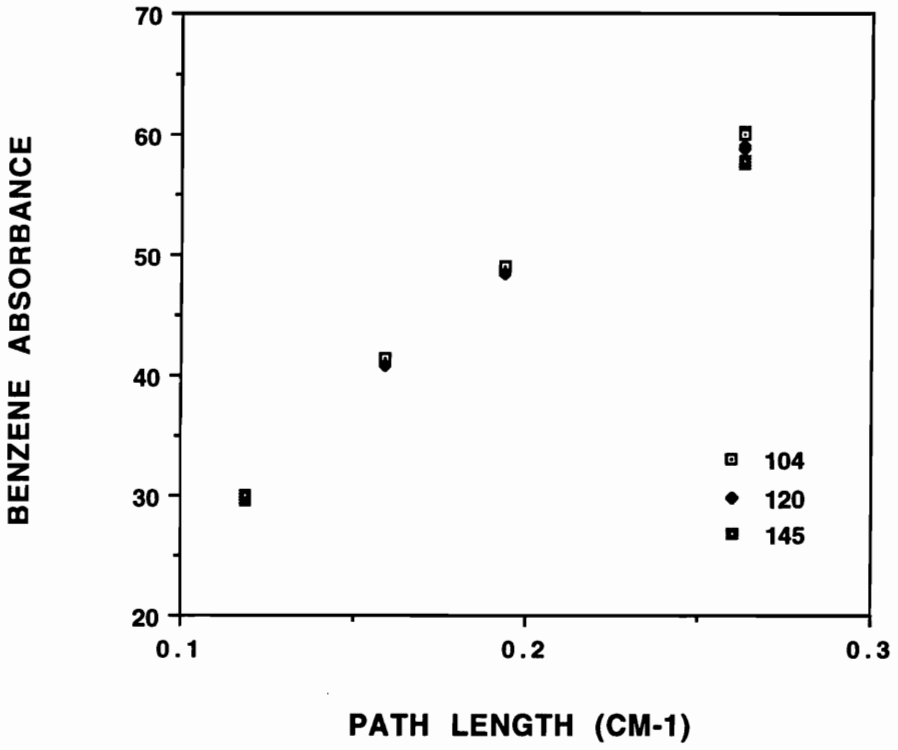

Figure 3.13. Effect of Path Length and Temperature on Aromatic Peak (B1).

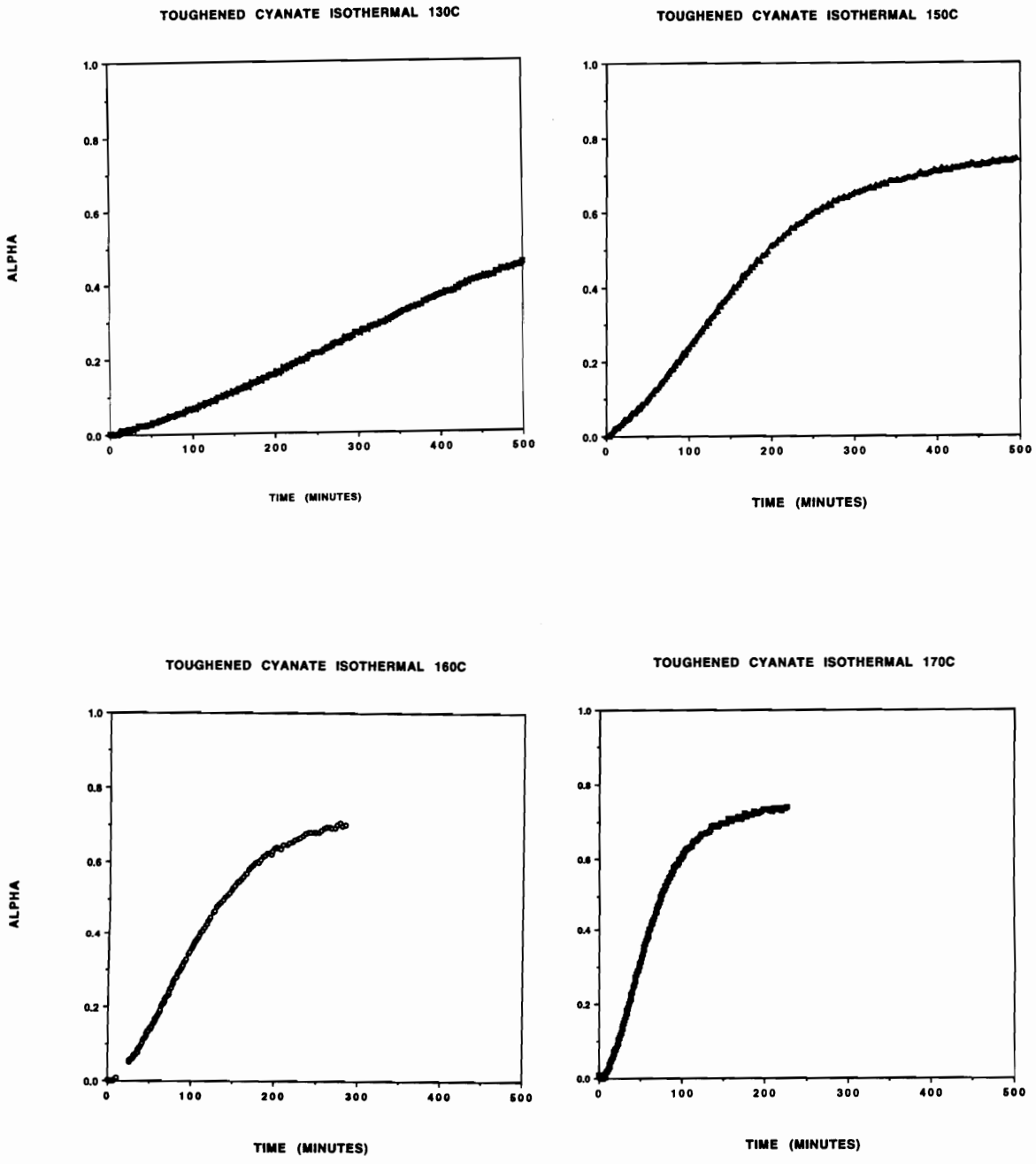

Figure 3.14. Degree of Reaction (α) based on Triazine Concentration.

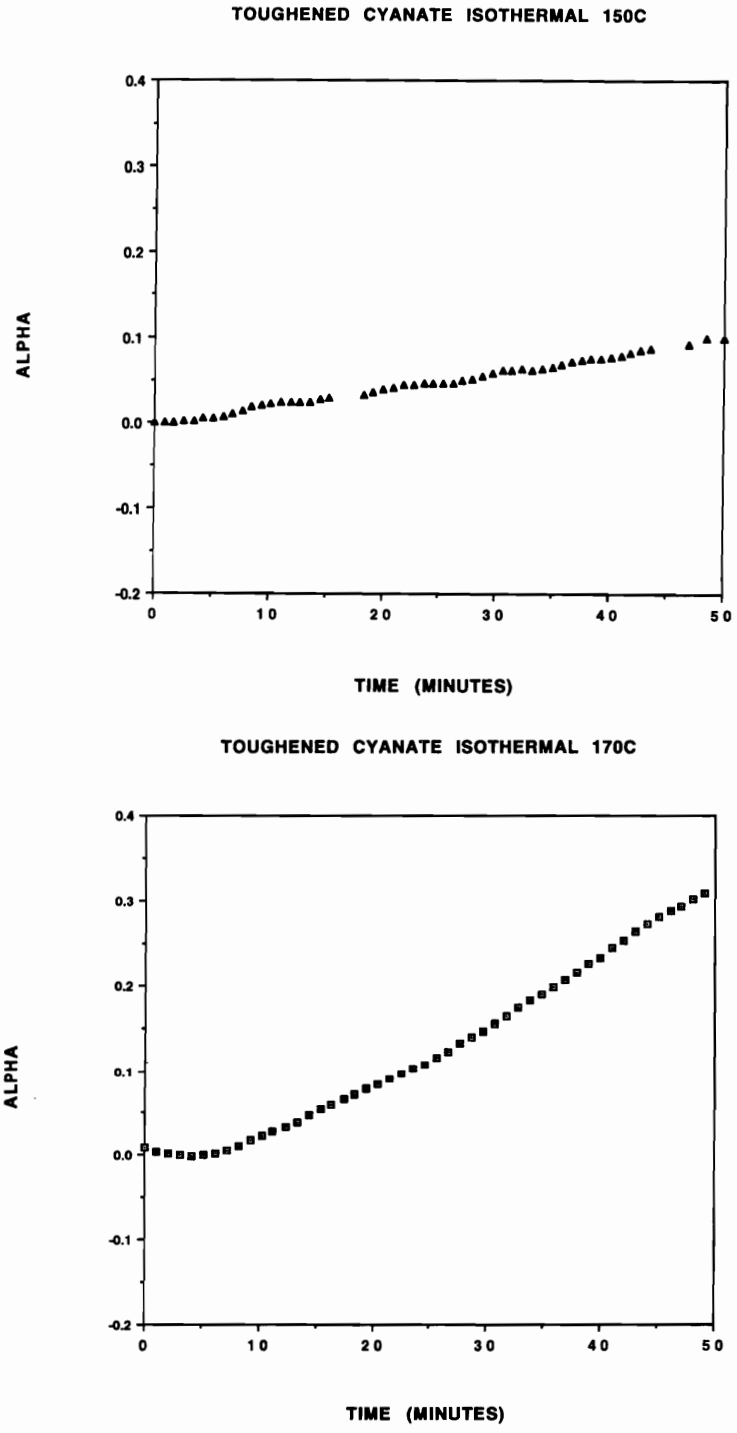

Figure 3.15. Degree of Reaction (α) based on Triazine Concentration (expanded).

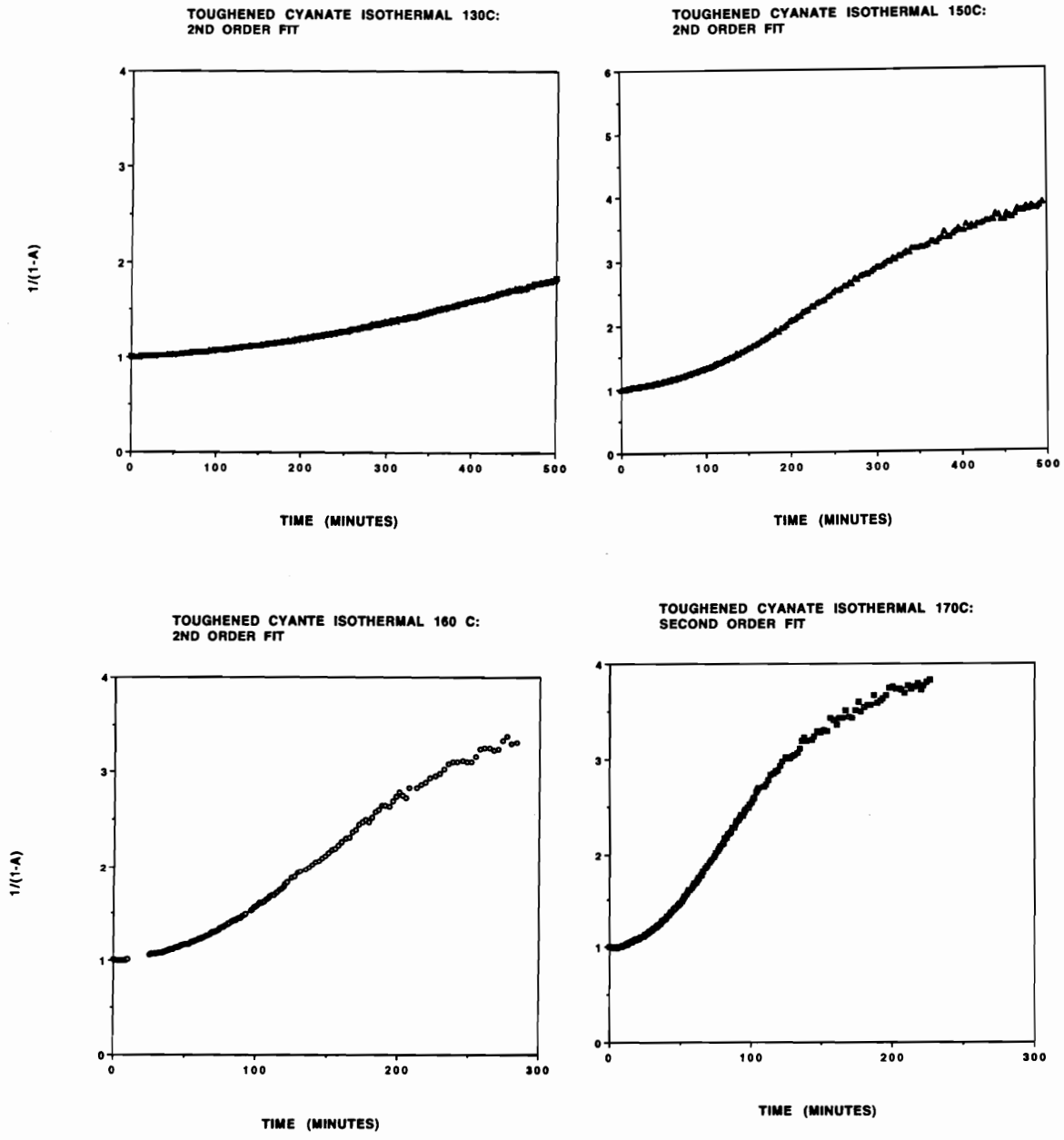

Figure 3.16. Attempted Second Order Fit based on Triazine Concentration.

the material is heated and cures that were not compensated for in the triazine calibration. When compared to the aromatic ring stretch, the triazine ring stretch peak area seems relatively insensitive to environment and temperature. The triazine concentration values could possibly be corrected a bit by incorporating a density correction term. This last correction was not attempted in this study.

3.5 CONCLUSIONS AND SUMMARY

The normalized peak or relative conversion approach to degree of cure has historical basis and was used successfully in most of this study. It may be inadequate for some modeling purposes but the alternative (considering both the chemical and physical and temperature dependent nature of the peaks) may be too complex for real-time control. Although the triazine absorbance was fairly temperature and environment insensitive, the aromatic peaks were not. The location of the aromatic peak at 4675 cm^{-1} exhibited a negatively sloped, linear dependence with increasing temperature and might find use as an internal temperature or density standard. The area of the aromatic peak at 4675 cm^{-1} peak 1 and the location of the aromatic peak at 5995 cm^{-1} appear to reflect the phase separation behavior of the resin. Up to 60% conversion, relative or normalized conversion could be described by second order kinetics. The real conversion data (based on the triazine calibration) fit did not fit second order kinetics.

3.6 REFERENCES:

3-1. A. Loos and G. Springer, Journal of Composite Materials, Vol. 17, p. 135-169 (1983).

3-2. A. Loos and Freeman, ASTM Vol. 873, p. 119 - 130 (1985).

3-3. A. C. Loos and P. H. Dara, "Modeling the Curing Process of Thick Section Autoclave Cured Composites" report to NASA Langley (1987).

3-4. J. Mijovic and S. Wang, SAMPE Journal, p. 42-55 (March/April 1988).

3-5. L. Chiao, SAMPE Journal, p. 27 - 35 (Jan/Feb. 1990).

3-6. L. Chiao and R. E. Lyon, J. Composite Materials, Vol. 24, p. 739 - 752 (1990).

3-7. N. St. John, and G. A. George, Polymer, Vol. 33, 1992 p. 2679-2688.

3-8. C. J. Bakker, N. A. St. John, and G. A. George, ACS Polymer Preprints (San Francisco) Vol. 33, No. 1 (1992).

3-9. G. A. George, P. Cole-Clarke, N. St. John, and G. Friend, Journal of Applied Polymer Science, Vol. 42, 643-657 (1991).

3-10. Y-T. Chen and C. W. Macosko, 24th International SAMPE Technical Conference Preprint, (October 1992).

3-11. A. M. Gupta and C. W. Macosko, Makromolecular Chem., Macromol. Symp., Vol. 45, 105-115 (1991).

3-12. A. M. Gupta and C. W. Macosko, Macromolecules, Vol. 26, 2455 (1993).

3-13. A. Osei-Owusu, G. C. Martin and J. T. Gothro, Poly. Eng. and SCI., April 1992, Vol. 32, No. 8, 535-541.

3-14. A. Osei-Owusu, G. C. Martin, and J. T. Gothro, Poly. Eng. and Sci., Vol. 32, 535 (1992).

3-15. J. M. Barton, Hamerton, and J. R. Jones, Polymer International, Vol. 31, No. 193, p. 95-106 (1993).

3-16. M. Bauer, J. Bauer, and G. Kuhn, Acta Polymerica, Vol. 37, No. 4, p. 221-223 (1986).

3-17. S. L. Simon, J. K. Gillham, and D. A. Shimp, ACS PMSE Preprints, Vol. 62, 96-101 (1990).

3-18. S. L. Simon and J. K. Gillham, ACS PMSE Proceedings, Vol. 67, 231 (1992).

3-19. S. Havriliak, Jr. and N. Roman, ACS Polymer Preprints, 1966, Vol. 7, p. 253 (1966).

3-20. A. Anton, Journal of Applied Polymer Science, Vol. 12, pp. 2117-2128 (1968).

3-21. M. J. Hannon and J. L. Koenig, Journal of Polymer Science: Part A-2, Vol. 7, 1085-1099 (1969).

3-22. N. F. Brockmeier, Journal of Applied Polymer Science, Vol. 12, p. 2129-2140 (1968).

3-23. P. Scmidt, B. Schneider, S. Dirilikov, and M. Mihailov, European Polymer Journal, Vol. 11, pp. 229 - 232 (1975).

3-24. K. Augury, British Polymer Journal, Vol. 7, 221-223 (1975).

3-25. B. L. Joss, R. S. Bretzlaff, and R. P. Wool, J. Appl. Physics, Vol. 54 , No. 10, p. 5515-5524 (Oct. 1983).

3-26. Y. S. Huang and J. L. Koenig, Journal of Appl. Polymer Science, Vol. 15, p. 1237-1245 (1971).

3-27. K. Augury, S. Kawamura, H. Sobue, Macromolecules, Vol. 4, No. 1, January - February 1971 PP. 79-81.

3-28. S.-B. Lin and J. L. Koenig, Journal of Polymer Science, Polymer Physics edition, Vol. 21, 2067-2083 (1983).

3-29. B. L. Joss, R. S. Bretzlaff, and R. P. Wool, Polymer Engineering and Science, Vol. 24, No. 14, 1130-1137 (1984).

3-30. S. N. Maganov, D. Shen, and R. Qian, Macromol. Chem., 190, 2565-2570 (1989).

3-31. D. J. Skrovanek, S. E. Howe, P. C. Painter, and M. M. Coleman,

Macromolecules, Vol. 18, 1676-1683 (1985).

3-32. M. M. Coleman, K. H. Lee, D. J. Skrovanek, and P.C. Painter, Macromolecules, Vol. 19, 2149-2157 (1986).

3-33. H. Hageman, R. G. Snyder, A. J. Peacock, and L. Mandelkern, Macromolecules 1989, 22, 3600-3606.

3-34. J. A. King, Jr. and P. J. Codella, Macromolecules, Vol. 23, 345-348 (1990).

3-35. F. Webster, Ph.D. Dissertation, VA Tech 1993.

3-36. M. M. Coleman and P. C. Painter, Applied Spectroscopy Reviews, 20 (3&4) 255-346 (1984).

3-37. J. Lin and C. W. Brown, Applied Spectroscopy, Vol.. 47, No. 1, (1993).

3-38. D. E. Bhagwagar, P. C. Painter, M. M. Coleman, and T. D. Krizan, Journal of Polymer Science,: Part B: Polymer Physics, Vol. 29, 1547-1558 (1991).

3-39. Charles E. Miller, Applied Spectroscopy Reviews, 26(4), 277-339 (1991).

3-40. B. Prime, in "Thermosets" in Thermal Characterization of Polymeric Materials, E. A. Turi, ed. Academic Press, New York, p. 435 - 520 (1981).

3-41. M. Bauer and J. Bauer Makromolecular Chemie, Macromol. Symp. 45, 97-103, (1991).

3-42. S. L. Simon and J. K. Gillham, ACS PMSE Proceedings, Vol. 67, p. 502-503 (1992).

3-43. R. W. Snyder, B. Thomson, B. Bartges, D. Czerniawski, and P. C. Painter, Macromolecules, Vol. 22, p. 4166-4172 (1989).

3-44. Pryde, J. of Polymer Science, Part A: Polymer Chemistry, Vol.

31, p. 1045-1052 (1993).

3-45. M. Zumbrum, Dissertation, Virginia Tech, 1990.

3-46. P. Chiou and A. Letton, Polymer, Vol. 33 (1992).

3-47. A. Rau, private communication.

3-48. Modern Plastics Encyclopedia, McGraw Hill, USA, 1985.

3-49. Rhone Poulenc product brochure.

CHAPTER 4
DEVELOPMENT OF CONTROLLED NETWORKS AND MORPHOLOGIES IN TOUGHENED THERMOSETTING RESINS USING A FTNIR FIBER OPTIC PROBE

4.1 INTRODUCTION

High performance thermosetting resin systems are often multi-component formulations requiring a number of complex physical and chemical changes to occur in the proper sequence to produce the appropriate mechanical properties. Depending on the chemistry of the system, what seems a simple issue of processing may involve four or five potentially competing or sequential reactions, phase separation, and the transformation of the liquid low molecular weight material to a glassy network. Changing the cure profile of such a thermosetting resin can drastically alter the properties through changes in the network and/or the morphology. There is evidence (4-1 - 4-2) that the time-temperature pathways affect the properties of the untoughened systems even when eventually taken to the same level of conversion. The effect is much more dramatic for toughened systems where toughening phases separate as the initially homogeneous resin cures. As shown by Butta, et al. (4-2) and Montarnal, et al (4-3) and others (4-15 - 4-33), for rubber-toughened epoxies, a 0-50% change in mechanical properties, such as K_{IC} and impact strength, can result strictly from the introduction of an isothermal dwell. Researchers have produced changes in morphology, dynamic mechanical behavior, Young's modulus, elongation, t-peel strength, yielding behavior, lap shear strength, failure mode, and damping behavior of toughened epoxies by changing the cure cycle (4-1 - 4-3, 4-15 - 4-33, 4-37 - 4-42). Microwave curing has been used at Virginia Tech (4-37 - 4-38, 4-44) to trap novel morphologies by accelerating the chemical reactions. Yamanaka and co-workers (4-26 - 4-27) suggested that a "controlled" morphology with novel properties could be obtained

thermally through the proper balance of chemical and physical changes.

These network and morphological changes are not considered in conventional processing. Resins typically undergo a thermal processing cycle which is optimized to produce certain macroscopic mechanical (toughness, modulus) or thermal properties (such as T_g), ignoring to some extent the chemical and morphological changes that contribute to these properties. Not all of the changes in the time-temperature pathway are intentional. In 1983, Loos and Springer (3-1 - 3-2) demonstrated that the temperature inside of a thick graphite-reinforced composite panel was significantly different from the intended autoclave cycle due to heat transfer from the outside and the exothermic nature of most thermosetting reactions. For thick panels and a rapid heating rate, the center of the panel would first lag behind the outer plies by about 70°C then overshoot the desired cure temperature by 20-30 degrees due to the exotherm. The latter processing example is obviously an unsatisfactory extreme, resulting in severely thermally degraded resin, gradient conversions, and poor mechanical properties. It is not unreasonable, based on the above, to suppose that there may be a 10-30 degree differential across a composite panel or an adhesive joint at some time during the cure cycle or that a processing dictated isothermal dwell might be introduced to allow flow and/or compaction resulting in unexpected chemical and morphological changes.

Reliably producing such "controlled" networks, morphologies, and novel properties or maintaining the ones originally designed into the system requires the use of appropriate techniques for monitoring chemical and physical changes in-situ. The FTNIR fiber optic technique developed in Chapter 2 was selected to provide chemical conversion data. Real-time monitoring of crosslink formation allowed trapping a series of novel morphologies in a "model" reactive thermoplastic toughened cyanate by either by gelation (i. e. network formation) or vitrification. This process is described qualitatively by Manzione and coworkers (4-15 -4-16); Verchere (4-22 - 4-25), et al.;

Hsich (4-29 - 4-33), and Yamanaka, Takagi, and Inoue (4-26 - 4-27) for toughened epoxies. Extremes in morphology were produced in resin castings within reasonable cure cycle variations such as might be introduced during processing. Resulting resins were evaluated microscopically, thermally, environmentally, and for differences in durability and damage tolerance. The morphology changes shown in the neat resin castings were shown to occur in graphite reinforced composite panels during a processing dictated dwell, potentially changing the desired morphology and resulting mechanical properties.

4.2 BACKGROUND

4.2.1 Toughening

Modification of a brittle matrix by the inclusion of a particulate morphology has been used to toughen a number of thermoplastics and thermosets. Historically, the toughener was a rubber as used in rubber-modified high impact polystyrene (HIPS) (4-10) or rubber-toughened epoxy (4-11). More recently, high performance thermoplastics have been incorporated into higher temperature thermosets to achieve moderate levels of toughness without sacrificing higher temperature performance (4-41 - 4-44). In a review of rubber-toughened polymers, Echte (4-10) summarized a number of chemical and physical factors that contribute to the desirable properties in HIPS. Among these variables were the type of rubber used, the phase volume (ratio) of toughener, the toughener particle size, the particle size distribution, the particle "structure" (balls, cells, rods, etc.), the molecular weight of the matrix, and the degree of grafting or crosslinking. In the same review, Kinloch (4-11) listed some of the factors which could potentially contribute to the toughness of a rubber-toughened epoxy. These included matrix crosslink density and T_g, rubbery phase volume fraction, particle size, size distribution, morphology, and T_g, as well as the interphase between the particles. As explained by Echte (4-10), many of the HIPS variables are affected or even preferentially induced by

processing. A number of other researchers have shown that the same can be said of rubber modified epoxies (4-15 - 4-33). Recent efforts show that this is also true for thermoplastic toughened epoxies (4-26, 4-37 - 4-38, 4-43 - 4-44).

4.2.2 Two Phase Blends

An in-depth thermodynamic discussion will not be included in this review. There are a number of papers and books available which cover that topic (see 4-4, 4-5, 4-7, and 4-9). What will be addressed are some of the phase separation behaviors, how these phenomena relate to the processing of thermosetting materials, how the phase diagrams change with respect to changes in temperature and molecular weight, and the resulting morphologies. As explained by Paul (4-9), simple phase behavior in terms of temperature and volume fraction of a two component system can be thought of as relating to two basic diagrams shown in Figure 4.1 The curve labeled "B" is the binodal. The "S" curve is the spinodal. Phi refers to the volume fraction of one phase and increases from left to right. The first case would be the phase diagram for a system exhibiting upper critical solution temperature (UCST). Above some critical temperature, the blend exists as one phase. Heat the blend up, it becomes miscible. The second diagram is lower critical solution behavior (LCST). Below some critical temperature, there is a one phase region. Combinations of these two behaviors can exist. Blends of lower molecular weight materials often exhibit UCST behavior. Blends of high polymers, often separate when heated, showing a LCST behavior. Toughened thermosets, can show either behavior (4-26 - 4-27).

Figure 4.2 (from Ryan (4-34)), is a phase diagram in terms of temperature, molecular weight, interaction parameter, and volume fraction for a UCST. On suddenly cooling or quenching the blend (a temperature jump), certain things would happen. Beginning at point A (in the one phase region) and proceeding from A to B (a lower temperature), nothing happens. A one phase system still exists. A binodal phase separation would result from a jump from C (in the

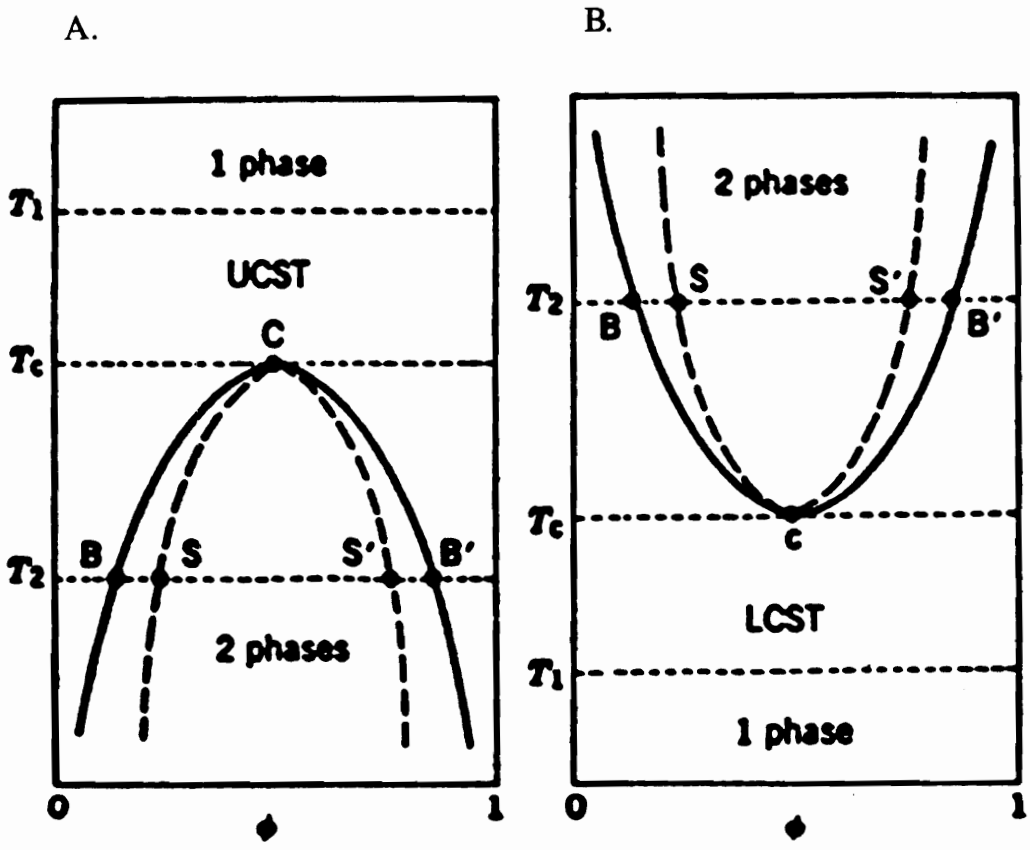

Figure 4.1. Simple Phase Diagrams Showing (A) Upper Critical Solution Behavior or (B) Lower Critical Solution Behavior (4-9).

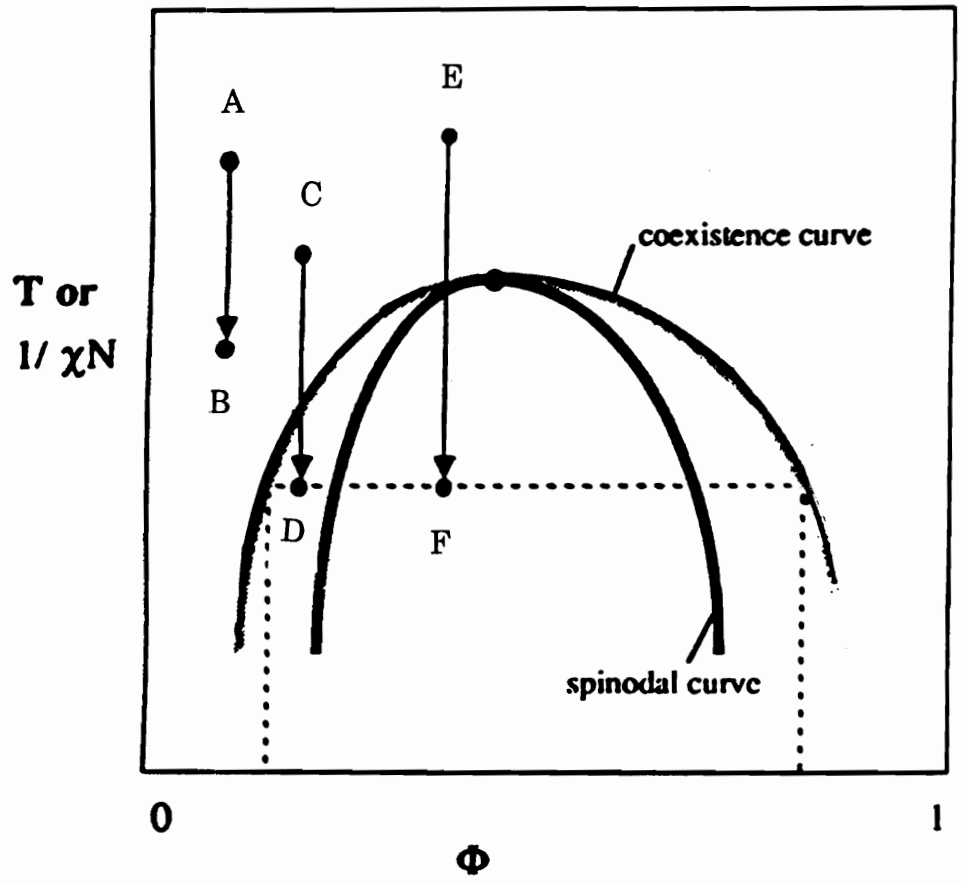

Figure 4.2. Phase Diagrams in Terms of Temperature, Number of Repeat Units, and Interaction Parameter (4-34). A->B. No Phase Separation, C->D. Binodal Decomposition, and E->F. Spinodal Decomposition.

one phase region) to D (in the metastable region). In the metastable region, there is an energy barrier to nucleation. Once this barrier is overcome, binodals initially have a strong concentration gradient and get larger by growth and, later, by ripening. In the quiescent state, resulting particles are typically spherical. Binodal decompositions have been suggested for rubber-toughened epoxies, although recent data from Yamanaka, Takagi, and Inoue (4-27) proposed that the morphology could result from spinodal decomposition. A spinodal decomposition would result from cooling from E to F, entering the unstable region. In this region, phase separation is "continuous and spontaneous" (4-34). This is usually said to occur rapidly, although this may only be in comparison to nucleation and growth. There is no activation energy for the spinodal decomposition. There are small initial fluctuations in concentration over a distance or "wavelength". This fluctuation will grow until the two phases given in Figure 4.3 result. At the early stages of spinodal decomposition, an interlocked structure results. This particular morphology has been said to produce certain desirable mechanical properties (4-26 - 4-27). Later, the concentration gradients will become more pronounced, and possibly still later, "coarsen" into globules due to surface tension effects. This "coarsening" process has been argued by Yamanaka and coworkers (4-27) as possibly producing a morphology which appears to have been a result from a binodal decomposition. The phase diagram in terms of molecular weight, as also explained by Ryan (4-24) would give the drawing in Figure 4.2, with the molecular weight increasing down the y-axis. Molecular weight jumps (or increases), analogous to the temperature jumps previously discussed would produce the following changes: A to B (increasing the molecular weight) would still result in the one phase, C to D results in the metastable region, and E to F in the unstable region where the separation goes by spinodal decomposition. Changes in molecular weight or interaction parameter may occur during the processing of reactive systems.

4.2.3 Effects of Processing on Reactive Systems such as Toughened

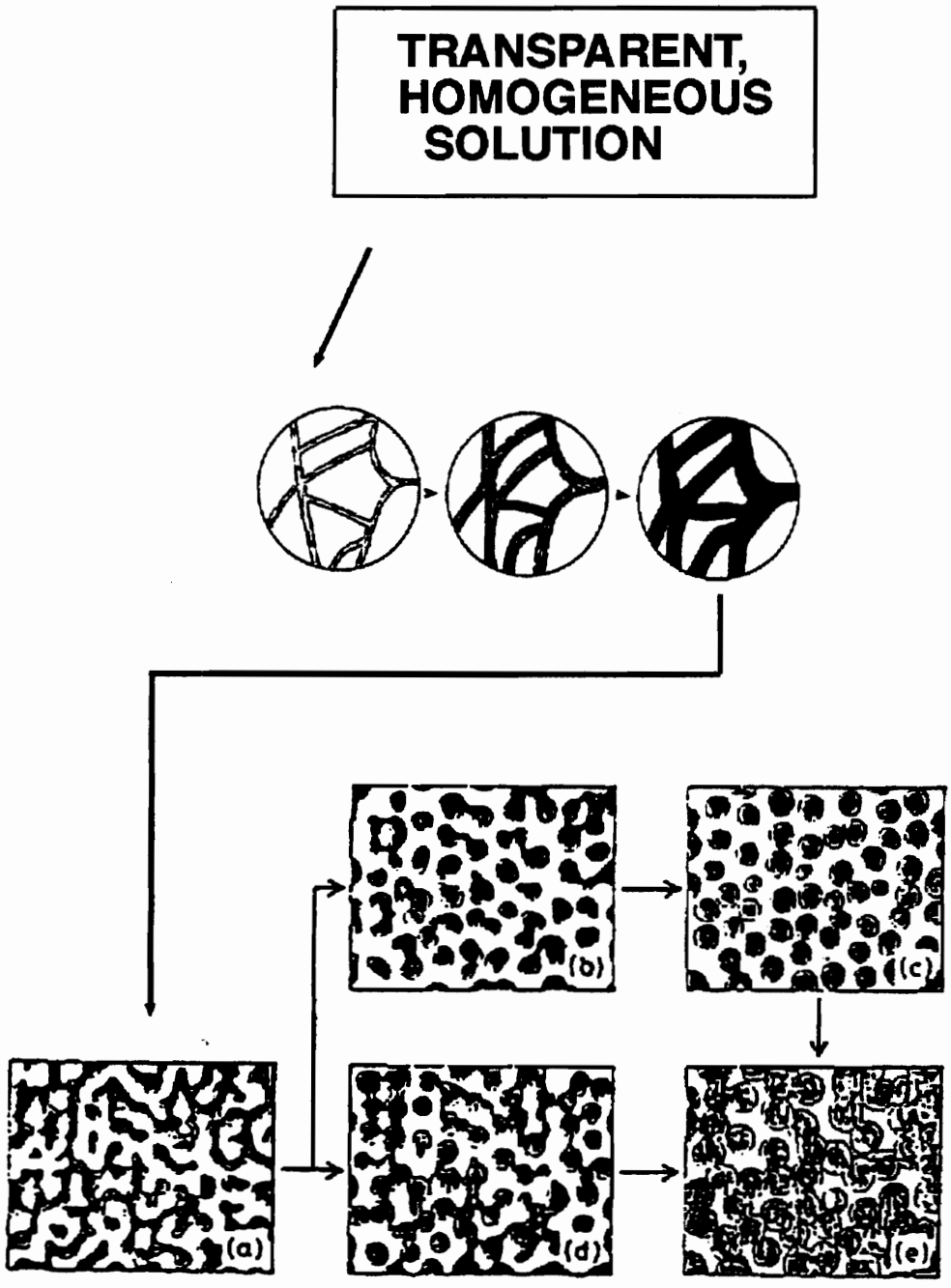

Figure 4.3. Morphologies Resulting from Spinodal Decomposition (4-4, 4-26 - 4-27).

Epoxies

Alternately, the point can be taken as stationary and the binodal or spinodal curve thought of as moving up or down with temperature or molecular weight. This approach was further explained by Yamanaka, Takagi, and Inoue (4-26 - 4-27) for a reacting system. In a reacting system, not only is there a molecular weight change, but also a change in the glass transition. Beginning in the homogeneous region in Figure 4.4, as the reaction occurs, the molecular weight increases moving the phase separation curve downward and plunging the resin into a two phase region. Since a reaction is occurring, this separation may be halted at a non-equilibrium morphology due to the approach of the gelation or the glass transition temperature. This approach has been used by Manzione, Gillham and MacPherson (4-15 - 4-16), Hsich (4-29 - 4-33), Montarnal (4-3), Yamanaka, Takagi, and Inoue (4-26 - 4-27), Williams, et al. (4-19 - 4-25), Hedrick (4-37), and Liptak (4-38) to produce nonequilibrium morphologies.

In 1981, Manzione, Gillham, and MacPherson (4-15 - 4-16) looked at the effect of processing on rubber-toughened epoxies. Working with a 10 percent carboxyl terminated butadiene nitrile rubber (CTBN) toughened diglycidyl ether of bisphenol A (DGEBA) epoxy and a piperidine curing agent, the authors subjected the resins to different curing temperatures and characterized the resulting resin by scanning electron micrographs, T_g's, and mechanical properties. For a given rubber-toughened epoxy system, they found that:

> A variety of different morphologies, and therefore material properties, can be obtained from a single rubber-modified epoxy formulation. The volume fraction, domain size, and number of particles of phase-separated rubber are determined by the competing effects of incompatibility, rate of nucleation and domain growth, and the quenching of morphological development by gelation.

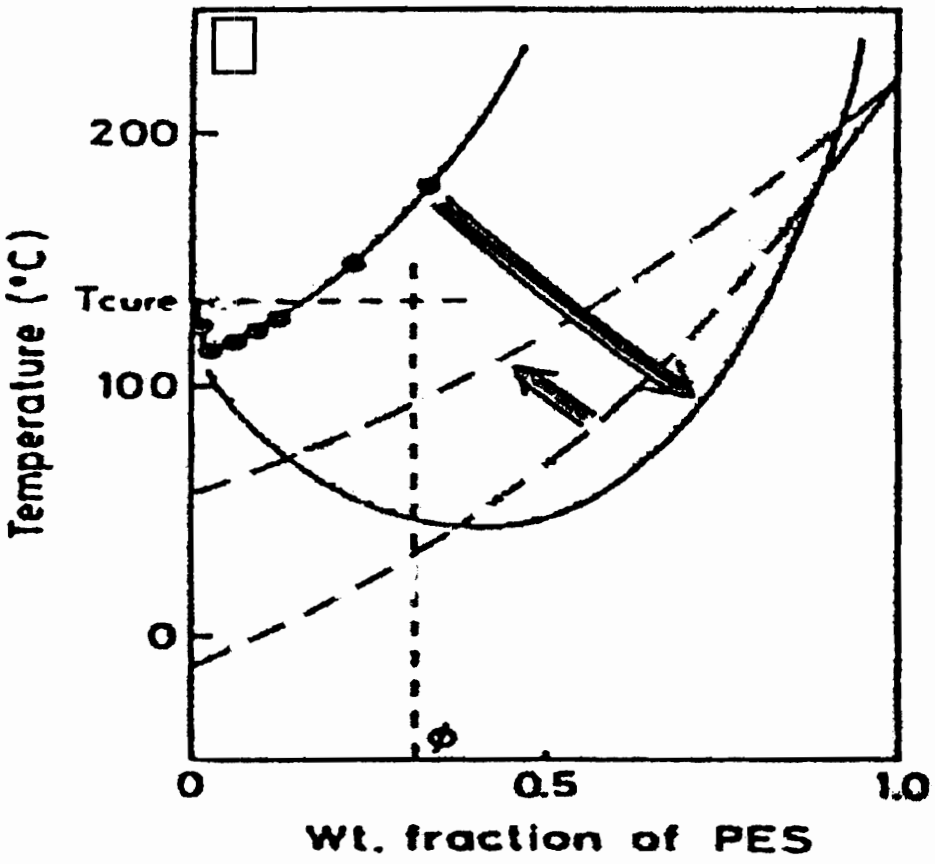

Figure 4.4. Changes in Phase Diagram with Cure (4-26 - 4-27).

In other words, in the processing of these toughened systems, the chemical and physical changes occurring during cure could determine the morphology and mechanical properties of the system.

The authors proposed that phase separation occurred prior to gelation and that a certain time was required for phase separation. This time was related to the diffusivity of the rubber. The diffusivity was inversely proportional to the viscosity. Higher temperature cures would initially provide a lower viscosity environment. Higher temperatures would also provide a higher reaction rate, resulting in an increasing viscosity. As the viscosity increased, the ability of the rubber to diffuse into a separate phase would decrease. If there was insufficient time for the rubber to separate due to this decrease in mobility (gelation or vitrification), the morphology would be "kinetically" controlled. Consequently "the temperature of gelation therefore determines the morphology." Eventually, a phase separation region was added to the TTT diagram as shown in Figure 4.5.

For the mechanical property study, DGEBA was formulated with a prereacted CTBN rubber, dicyandiamide (dicy) as a curing agent and Monuron. Data for tensile, notched Izod impact test, and toughness (as area under stress train curve) were obtained. Morphology was evaluated by SEM and TEM. T_g was determined by torsional braid analysis. Only one of the CTBN formulations was better than the unmodified formulation. Izod impact strength was obtained as a function of cure temperature. If the morphology was not phase separated, the impact strength was the same as the unmodified specimens. Generally, if the resin was phase separated, the impact strength was better. At higher temperatures, some changes in the finer morphology within the rubbery domains may have lead to lower values than expected. The authors concluded that there was a "correct combination of phase separated and dissolved rubber" to give "optimum properties"

Several years later, Chan, Gillham, Kinloch and Shaw (4-17 -4-18), looked at the effects of a lower temperature dwell plus a

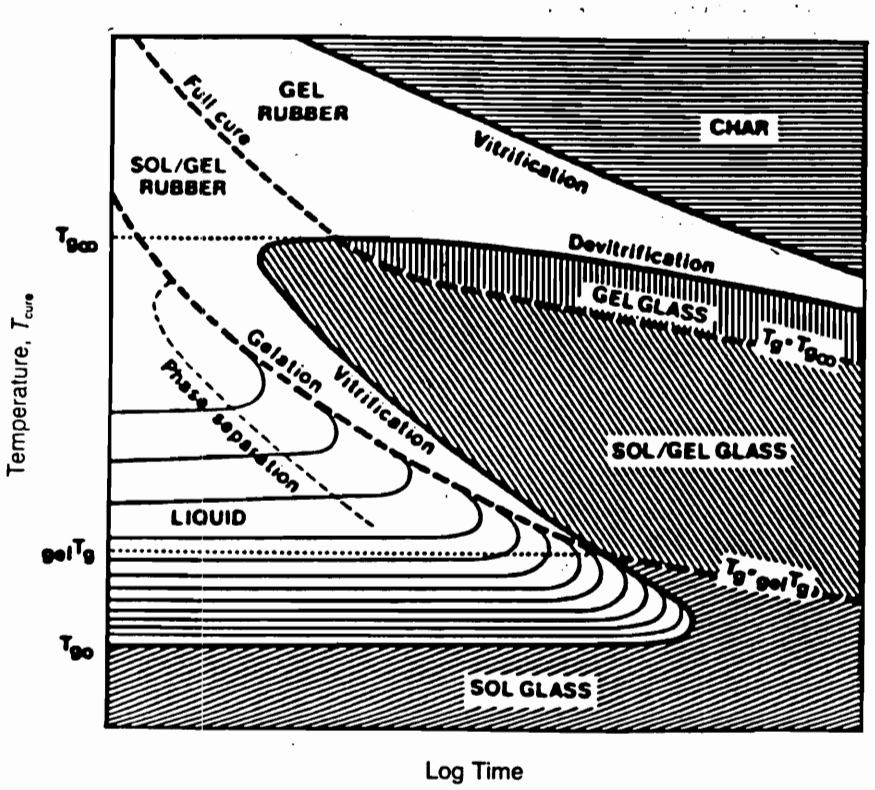

Figure 4.5. TTT Diagram with Phase Separation (4-40).

final postcure above T_g infinity on a DGEBA epoxy cured with an aromatic diamine and toughened with 15% of either an prereaccted epoxy terminated CTBN rubber (ETBN) or diamine terminated rubber (ATBN). In the case of the ETBN, only the morphology was affected by the cure cycle changes. In the ATBN-toughened system, both the morphology and the network were affected. The ATBN rubber was expected to compete with the curing agent. Instead, the addition of the ATBN catalyzed the homopolymerization of the epoxy at certain temperatures. The ETBN rubber made little difference in the TTT diagram. Gelation occurred at approximately the same times and temperatures as the untoughened system. Vitrification occurred slightly earlier under some condition. Phase separation occurred before gelation with most of the structure forming quickly. There were some changes occurring after gelation (but prior to vitrification). The volume fraction of the rubbery phase was not affected by cure cycle for the ETBN resin, but the particle size distribution was changed. It was felt that the lower cure temperatures with higher viscosity produced more numerous, smaller particles due to high nucleation but slow growth. At higher temperatures, there were fewer, larger particles probably due to lower nucleation with faster growth.

The ATBN toughener had a significant effect on the TTT diagram, causing the resin to gel earlier at lower temperatures. At higher temperatures, there was little difference. The vitrification curve was also changed. Phase separation behavior was similar to the ETBN system. The volume fraction and size of the rubbery phase as well as the glass transition of the epoxy phase varied with processing. In general, the ATBN systems had higher rubbery phase volume fractions than the ETBN modified resins. The T_g of the epoxy phase (especially with a low temperature isothermal dwell) was depressed. This was first thought to be due to the rubber in solution in the epoxy phase, but later the researchers decided that the depression was due to be due to an amine catalyzed homopolymerization.

Mechanical testing determined that the modulus above the rubber T_g was lower when the epoxy was toughened with the ATBN, probably due to the lower T_g of the epoxy phase with the ATBN. Compression stress at yield was less than the unmodified formulation for the rubber-toughened specimens. Values were not a function of the low temperature dwell for the ETBN toughened resins. They were for the ATBN toughened systems. Compression strain at yield was higher for the ETBN toughened; lower for the ATBN toughened. The low temperature dwell for the ATBN not only produced the highest rubber volumes, but the epoxy homopolymerization produced a more ductile matrix resulting in the highest G_{IC} values. It was noticed that "the yield behavior of the matrix is controlled by the details of the molecular structure of the matrix" (4-18).

In the mid 1980's Williams and coworkers (4-19 - 4-25) at the Institute of Materials Science and Technology in Mar del Playa, Argentina began evaluating the effects of processing cycles in rubber-toughened epoxies and predicting phase separation behavior. This effort continued and most recently has been performed in conjunction with researchers such as Verchere, Pascault, and Sautereau at the Laboratoir des Materiaux Macromoleculaires in Cedex, France. In 1983, Williams, et al. (4-19) proposed a model to predict particle size, volume fraction, and composition of the rubbery phase resulting from the binodal decomposition during the cure of in rubber-toughened epoxies. The diffusion coefficient for phase separation was assumed to be directly proportional to temperature and inversely proportional to viscosity. Since viscosity was a function of temperature and conversion, the nucleation rate could be expressed in terms of conversion. High polymerization rates (faster than the nucleation) at high temperatures were predicted to decrease the "concentration of dispersed phase." At low temperatures, the volume of the dispersed phase was fairly constant. Coalescence, growth rate, mean particle size, volume fraction, and composition were predicted.

In 1987, Williams, et al. (4-20) extended the phase separation

model to predict size distribution and compared the model with experimental data for a DGEBA, 4,4'-diaminodiphenylsulfone (DDS), and ETBN resin system. Predictions and morphological data were compared. "Reasonable agreement" was found between the predictions and reality. The authors found that the most important factor was the difference between the conversion at which phase separation occurred and the conversion at which gelation occurred. Extremely low or extremely high values were not desirable. If the conversions at the cloud point and at the gel were extremely close, high viscosities and low diffusion did not allow phase separation. If too far apart, excessive coalescence might occur. There was an optimum region for desired properties. Within this region, a slight increase in the time between the cloud point and the gel point would increase the concentration of rubbery particles, the volume fraction of the rubber phase, the number of small particles and decrease the amount of rubber dissolved in the epoxy phase, and the concentration of rubber in the rubbery phase. The interaction parameter and surface tension (below a critical value) did not have a large effect.

Moschiar, Riccardi, and Williams in Argentina began a joint project with Verchere, Sautereau and Pascault in France to determine the variables that affect the morphology in rubber-toughened epoxies (4-22 - 4-25). The effects of rubber content and cure cycle on morphology were experimentally evaluated, compared with a model, and mechanical properties were determined for a DGEBA epoxy with ETBN rubber and a cycloaliphatic diamine (3DCM). The physical characterization and modeling was relatively successful. The results of the mechanical characterization was somewhat inconclusive because the diamine used produced very small rubbery domains (under 0.5 microns) which were not very successful in toughening the epoxy.

Montarnal, Pascault, and Sautereau (4-3) in 1989 worked with an epoxy, a CTBN Rubber, and a sterically hindered (low reactivity) diamine. The rubber phase separated before gelation and

vitrification. They felt that the size was determined by the viscosity at the cloud point. An intermediate temperature cure yielded bigger particles and a tougher material. The volume fraction of rubber was the same but the particles were fewer and larger. In this case, the addition of the rubber delayed gelation. A 15% CTBN loading resulted in about a 50% increase in Charpy impact strength with the intermediate temperature dwell over the room temperature dwell. No clear tensile or compression trends were observed except that low cure gave low tensile strain.

Hsich also emphasized "by properly manipulating the kinetics of cure and phase separation, desirable properties can be obtained" (4-29 - 4-33) and proposed control of morphology in polymer alloys by proper use of phase diagrams, type of phase separation and growth processes, and cure. He found little temperature effect for some diamines and felt that best ways of controlling the morphology in some rubber-toughened epoxies was to change the curing agent, add a catalyst, or "pregel" the rubber.

Yamanaka and Inoue (4-26), working with a polyethersulfone toughened epoxy which phase separated by spinodal decomposition, produced a novel two phase morphology. LCST behavior has been reported for a bisphenol A based polyhydroxy ether known as "phenoxy" and polyethersulfone (PES). The authors expected this sort of phase separation for epoxy with PES. Figure 4.4 shows a phase diagram for LCST behavior. Starting in the homogeneous region and heating the resin should result in phase separation. Beginning at a point in the one phase region, in a reactive system, the curve of the LCST would move downward as the reaction proceeds. Eventually, the phase separation curve would pass below the point and phase separation would be induced. The T_g of resin, shown by the dashed line, would increase as the reaction proceeds, trapping a morphology as the Tg of the reacting system reached the cure temperature of the resin. The scattering angle as measured by light scattering was observed to decrease with time (and the periodic distance increase and eventually level off), indicative of spinodal decomposition frozen

in by crosslinking. Examination of fracture surfaces showed "interconnected globules" resulting from spinodal decomposition followed by ripening. These morphologies resulted in increases in peel and shear strength over the untoughened epoxies. No values were reported for the more conventionally (spherical) toughened morphologies. The authors felt that the co-continuous structure due to spinodal decomposition would give a high initial modulus, high strain, and good strain recovery.

Various ramps and isothermal dwells were evaluated. Slower temperature increases produced smaller domain sizes (or periodic distances) as shown in Figure 4.6. The sizes were also reduced by lower temperature isothermal dwells. To obtain this sort of morphology in a resin undergoing spinodal decomposition, the authors recommended that, "coarsening of the phase-structure should be suppressed by network formation in the early stages of spinodal decomposition" by curing as close to T_g as possible. Near T_g, the reaction rate should be much faster than the phase separation rate.

Yamanaka, Takagi, and Inoue (4-27) looked at various concentrations of either CTBN or ATBN rubber with either the polyamide Versamid, a rapid curing agent, or piperidine, a slower curing agent. They proposed that the spherical structure often observed with rubber-toughened epoxies could be generated from a spinodal decomposition. A combination of a rapid curing agent, low temperature cure, and an ATBN rubber, produced a co-continuous morphology indicative of gelation during the early stages of a spinodal decomposition. This morphology yielded interesting peel strength and damping properties. Rather interestingly, the rubber-toughened epoxy showed the reverse of the trend for the PES toughened epoxy as far as domain size dependence on temperature. Higher temperatures gave smaller domain sizes for the rubber-toughened epoxy, especially with the Versamid curing agent. The rubber-toughened epoxy also had a UCST rather than a LCST.

Untoughened systems can be changed by cure cycles as

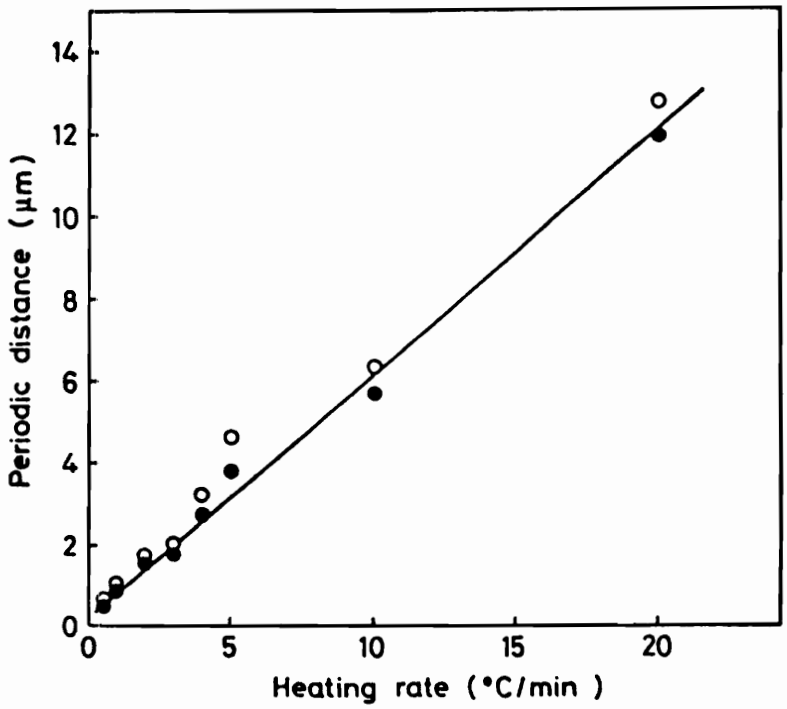

Figure 4.6. Changes in Domain Size with Heating Rate for PES Toughened Epoxy (4-26).

demonstrated by Brett (4-1) for an untoughened diamine cured epoxy. After subjecting the resin to various cure cycles (ramps and/or dwells), he found that isocure states did not necessarily yield the same lap shear strength values. He attributed these differences to a preferential selection of one of the many curing reactions. This problem may exist for many systems since a number of resins have multiple curing reactions. In this study, the cyanates have been selected to reduce the possibility of competitive reactions. The cyanate reaction is not perfect, but has at least 85% (often better than 95%) conversion to triazine crosslink (2-72, 2-88).

4.3 EXPERIMENTAL

Approximately 20-25 g of the toughened cyanate resin described in Chapter 3 (composed of the dicyanate of bisphenol A (BADCy) with 250 ppm aluminum acetyl acetonate (AlAcAc) and 2 pph nonyl phenol with or without 25% of a reactive thermoplastic, 15 K PPES-OH) was mixed at 104°C and then subjected to various time/temperature profiles. These cure cycles consisted of a 2°C/minute ramp to a 250°C and a 2.25 hour postcure with or without intermediate dwells at 135, 150, 180 or 200°C. The specimens were held at these temperatures to a relative conversion of either 30% or 60% then ramped to the postcure.

A thermocouple was attached to the aluminum mold in a Fisher Isotemp Model 800 programmable oven to measure mold temperature rather than oven air temperature. There were only slight differences between mold temperature and resin temperature but significant differences were observed between the oven air temperature and the mold temperature. All temperature measurements were for mold temperature. The oven program was modified to insure that the mold would heat up at 2°C/minute to the first dwell temperature. The specimens were held at the dwell temperature until a "relative conversion" of either 30% or 60% (or degree of cure = 0.3 or 0.6) was obtained then allowed to ramp at a nominal 2°C/minute to the postcure at 250°C. A limited number of

steps in the microprocessor did not allow such precise control on the second ramp. Samples were then cooled with a nominal 1°C/minute cooling rate and stored in a desiccator until testing.

Conversion in the NIR was monitored-situ during the specimen cure by a Nicolet Model 800 FTIR spectrometer equipped with a fiber optic adapter and Polymicro Technologies' low hydroxyl silica fiber optics. A special aluminum mold with a 0.38 mm wide by 0.5 mm deep groove in the bottom and small openings in the side was machined (see Figure 4.7) to allow the insertion of the fiber optic sensor for monitoring the triazine peak at 4625 cm-1.

With many catalysts, the reaction of the dicyanate to the triazine was expected to yield greater than 85% trimerization (2-72, 2-88). No side reaction were observed in the near infrared for this system. Using the aromatic ring stretch as a reference, a relative alpha or conversion was calculated as described in Chapter 2 based on a normalized triazine peak. Initial (104°C) and final (270°C) values had been previously obtained from a 2°C/minute ramp to 300°C.

A software program (see Appendix) allowed real-time collection of spectra, baseline correction, integration of aromatic ring and triazine ring stretches, ratioing of peaks, and real-time calculation of a relative degree of conversion. This real-time information made it possible to produce a series of novel morphologies based strictly on chemical (conversion) control. Using a 2°C/minute ramp to 250°C with a 2.25 hour postcure at 250°C as a control processing ramp, interactive dwells were introduced at 135C, 150C, 180C and 200°C. The specimens were held at these temperatures until either a relative conversion of 30% or 60 % was obtained then the ramp continued to the 250°C/2.25 hour postcure.

Scanning transmission electron micrographs were obtained by first microtoming thin samples of the specimens from the castings. These specimens were vapor stained with ruthenium tetroxide (2-100), and photographed in a Phillips 420T scanning transmission electron microscope (STEM) using nominal magnifications of 12,500 X and 25,000 X. Srinivasan (2-100) had earlier used the ruthenium

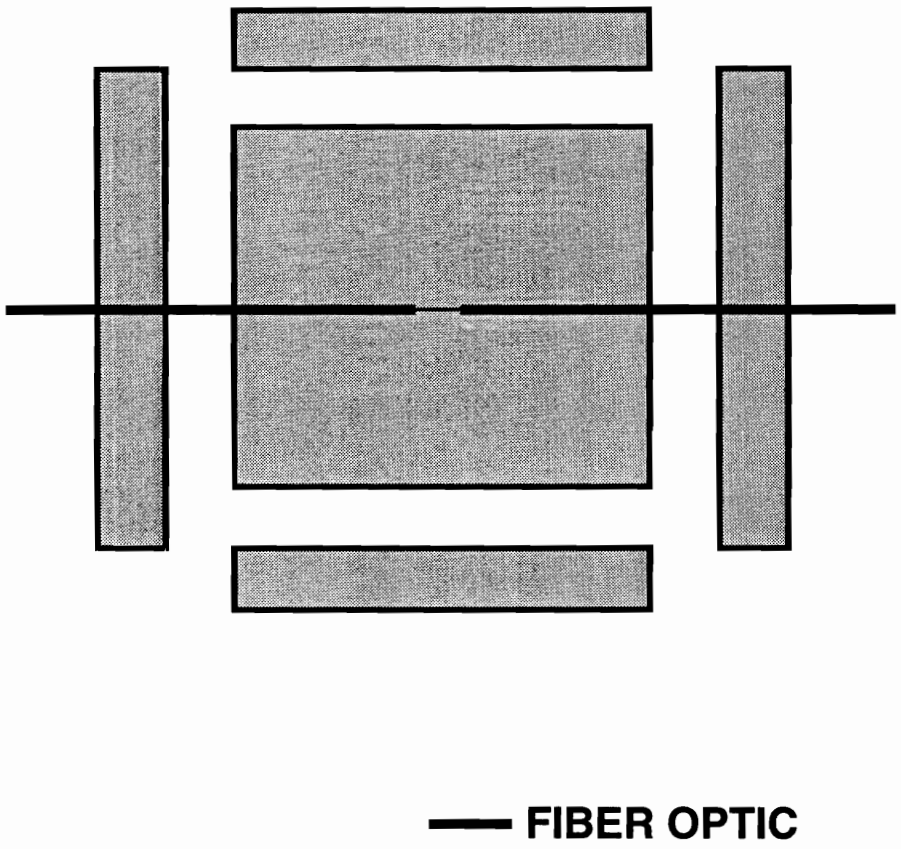

Figure 4.7. Resin Casting Mold Adapted for Fiber Optics.

tetroxide to preferentially stain the thermoplastic phase.

Dynamic mechanical specimens of the unreinforced resin were machined and tested at multiple frequencies on either Polymer Laboratories Dynamic Mechanical Analyzer on a Dupont Dynamic Mechanical Analyzer or a Polymer Laboratories DMTA. DSC and TGA (in air) were obtained using a heating rate of 10°C/minute on Dupont DSC.

With the sensors included, the 20-25 g samples did not yield very many test specimens. Additional uninstrumented specimens were made for the control and the 150°C dwell to 60% conversion cycles.

4.4 RESULTS AND DISCUSSION

The resin chosen as a model resin for characterization in Chapter 2 had been shown by Srinivasan (2-100) to produce a 0.5 -1.0 micron, interlocked thermoset-rich and thermoplastic-rich morphology typical of that resulting from spinodal decomposition when subjected to his chosen cure cycle of a heated ramp to 200°C, a two hour dwell at 200°C, and a two hour postcure at 250°C. The purpose of this study was to see if this morphology could be intelligently modified using processing variations and information on chemical conversion from the FTNIR fiber optic sensor. To change the morphology of the resin, two conditions needed to be satisfied (4-15 - 4-18). The resin needed to be heated to a fairly low temperature to keep the mobility low (and the viscosity high) and then held until gelation. Figure 4.8 shows a TTT diagram with four pathways designated A, B, C and D. Pathway A cuts diagonally across the TTT diagram from a low temperature to a high temperature. This would be the 2°C/minute control ramp and yield a heterogeneous morphology. At some temperature T_A, phase separation would begin and end at T_A'. Pathway B would be a ramp to a low temperature hold at a very low temperature, low enough that phase separation does not occur prior to gelation. The resulting morphology would be homogeneous. Path C would be typical of most of the cure cycles used

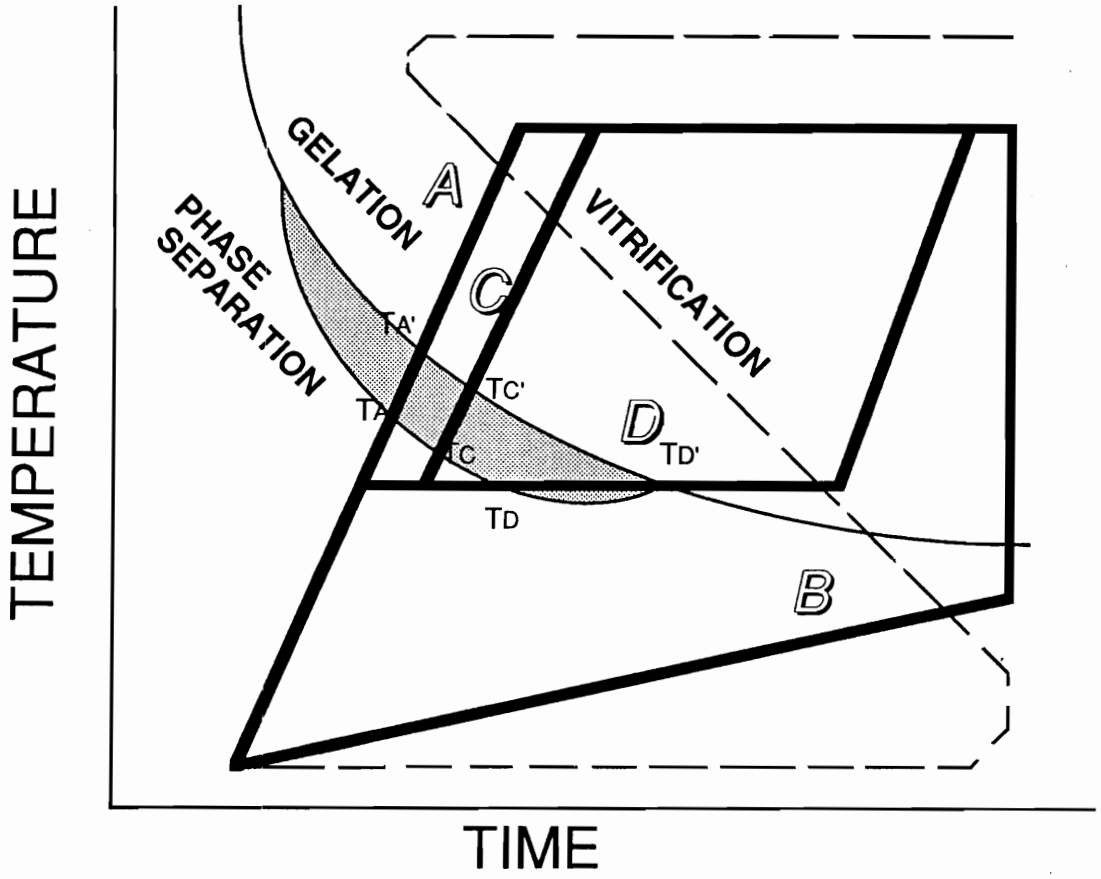

Figure 4.8. Basic TTT Diagram for Toughened Resins with Superimposed Processing cycles.

in this study. The resin would be ramped to a temperature between path A and path B. In cycle C, a very short dwell at this temperature would not be sufficient to induce phase separation. Phase separation would begin at temperature T_C in the second ramp. The fourth cycle, path D should result in a very different morphology. In this cycle, again, the intermediate temperatures would be used but the dwell would be held to gelation or vitrification of the resin. Gelation or vitrification of the resin should effectively trap the morphology that has been formed at this temperature. Subsequent temperature ramps should not provide sufficient mobility to change the morphology.

Cyanate resins have been empirically observed to gel at 60-65% conversion (2-71 -2-73). An isothermal cure at a low temperature to 60-65% conversion should effectively trap the different morphologies by network formation. A processing cycle of 2°C/minute to 250°C and 2.25 hours at 250°C was selected as a control cycle. Isothermal dwells were introduced at 135, 150, 180, or 200°C; interactively held to a predetermined level of conversion (30 or 60%) based on the real-time conversion data from the FTNIR fiber optic sensor in the mold; and then allowed to finish the cure cycle. These cycles were shown schematically in Figure 4.9. Real-time relative conversion (or alpha = conversion/100) data is shown in Figure 4.10 for two of the cure cycles.

Scanning transmission electron photomicrographs of the morphologies for the (2°C/minute) control cycle are shown in Figure 4.11-b. In the photo, the black was the (stained) thermoplastic-rich areas, the white the thermoset-rich regions. The black line to the side of the photo indicates 0.5 microns. The particles were irregular, approximately 0.5-1.0 microns in size, well phase separated, and highly interlocked, with no one phase appearing to be continuous. The morphology could be altered between 135 and 180°C. The morphologies resulting from the dwells are shown in Figures 4.11-c to i. The lower levels of conversion (30%), like path C on the TTT diagram, had little effect on the morphology for the low temperature

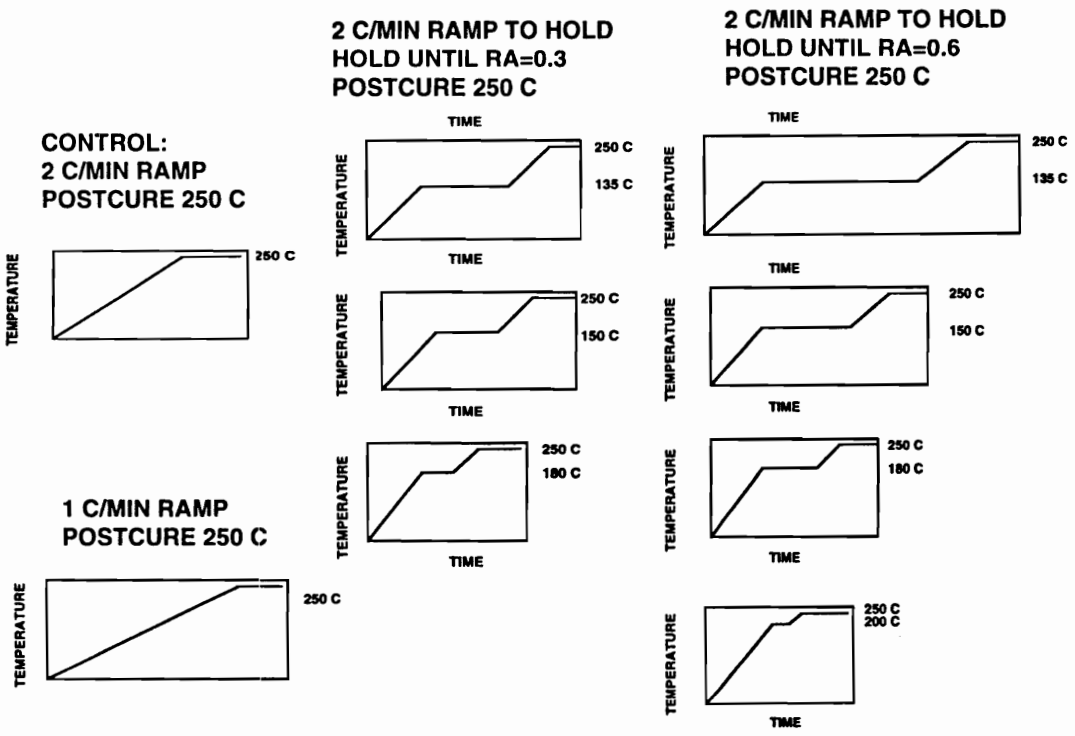

Figure 4.9. Cure Cycle Variations.

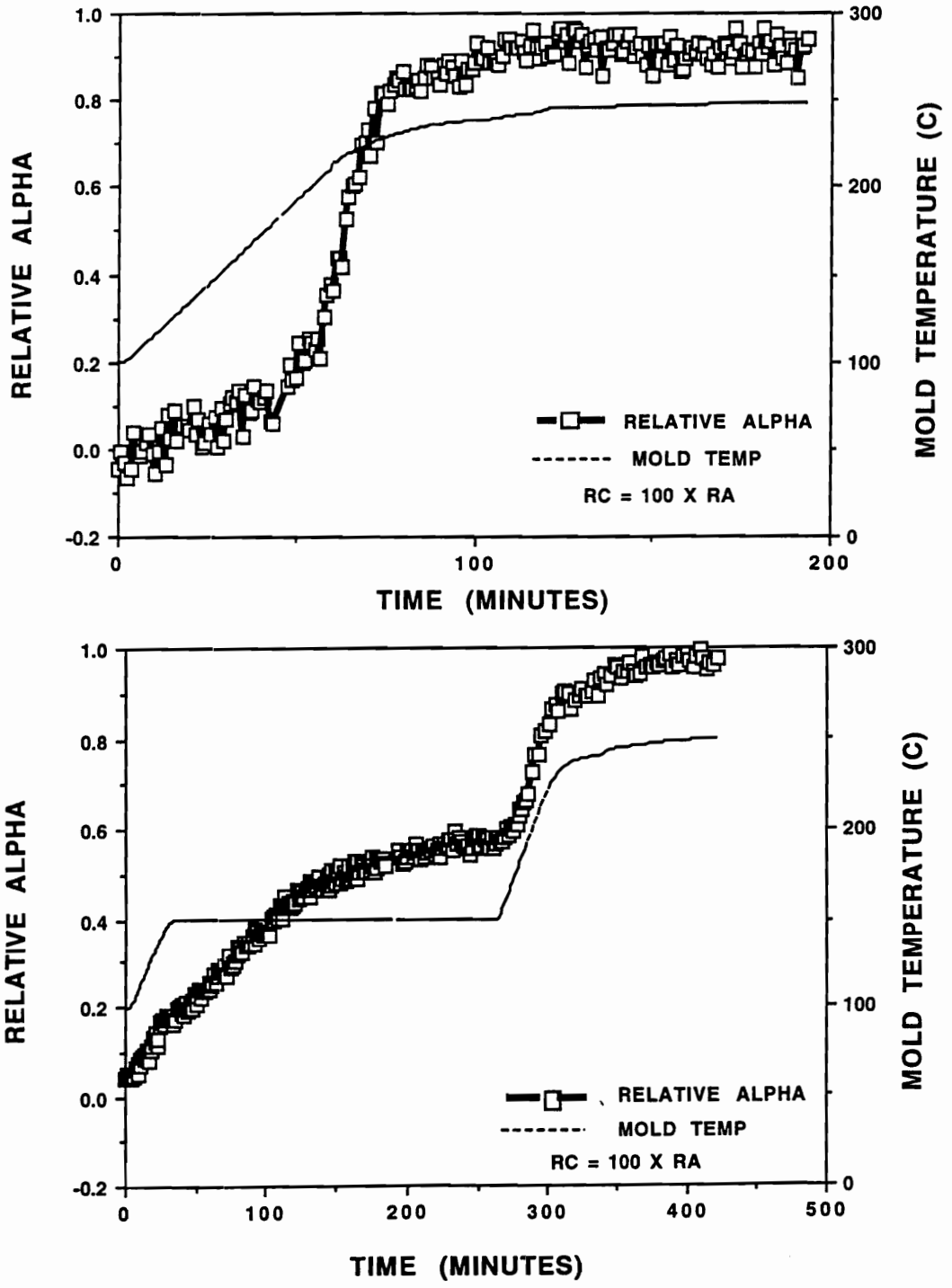

Figure 4.10. Real-Time Monitoring of Relative Degree of Cure (α_r) during the Cure of Resin Castings.

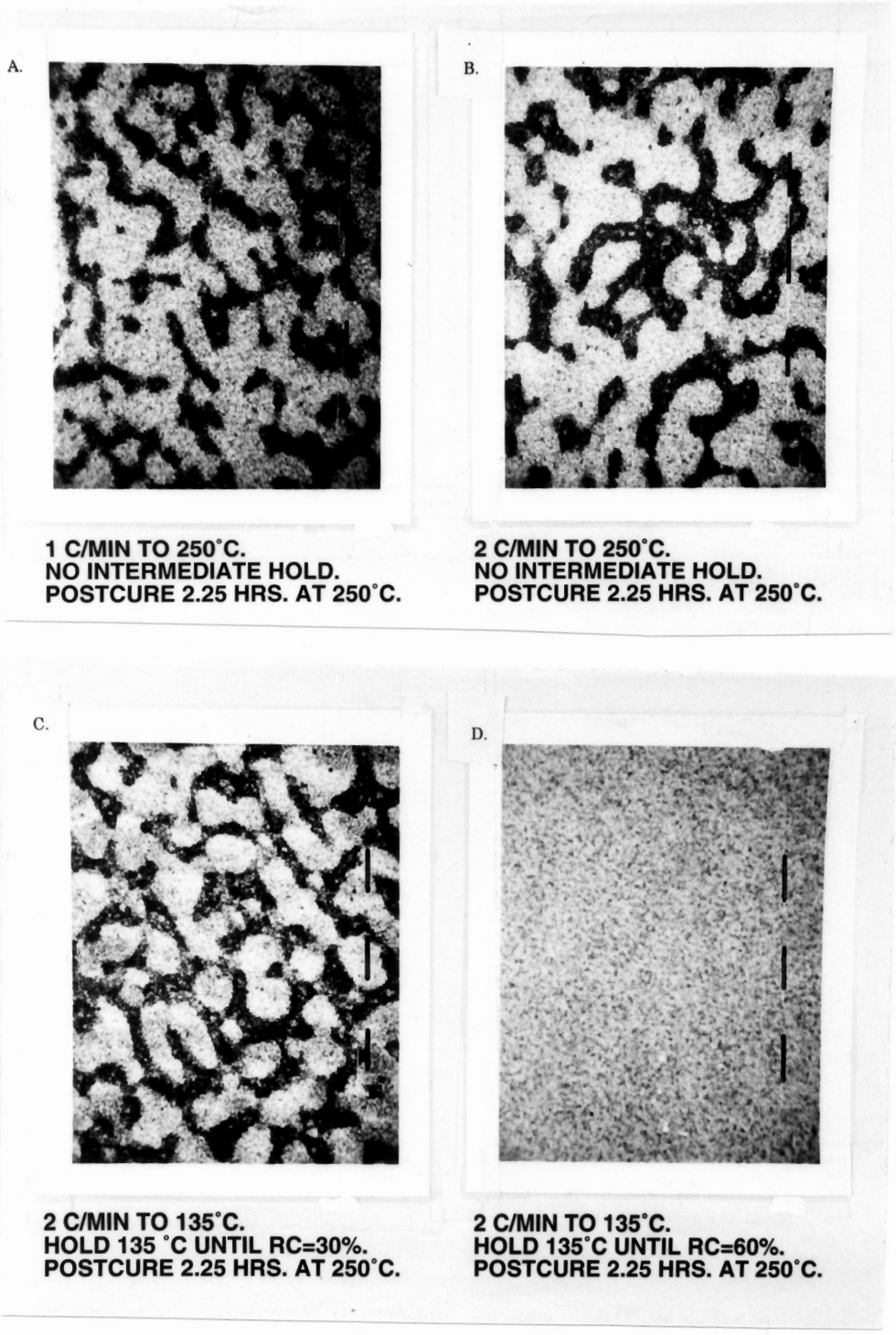

Figure 4.11. Morphologies Resulting from Interactive Cure Cycle Modifications. Black Bar is 0.5 microns.

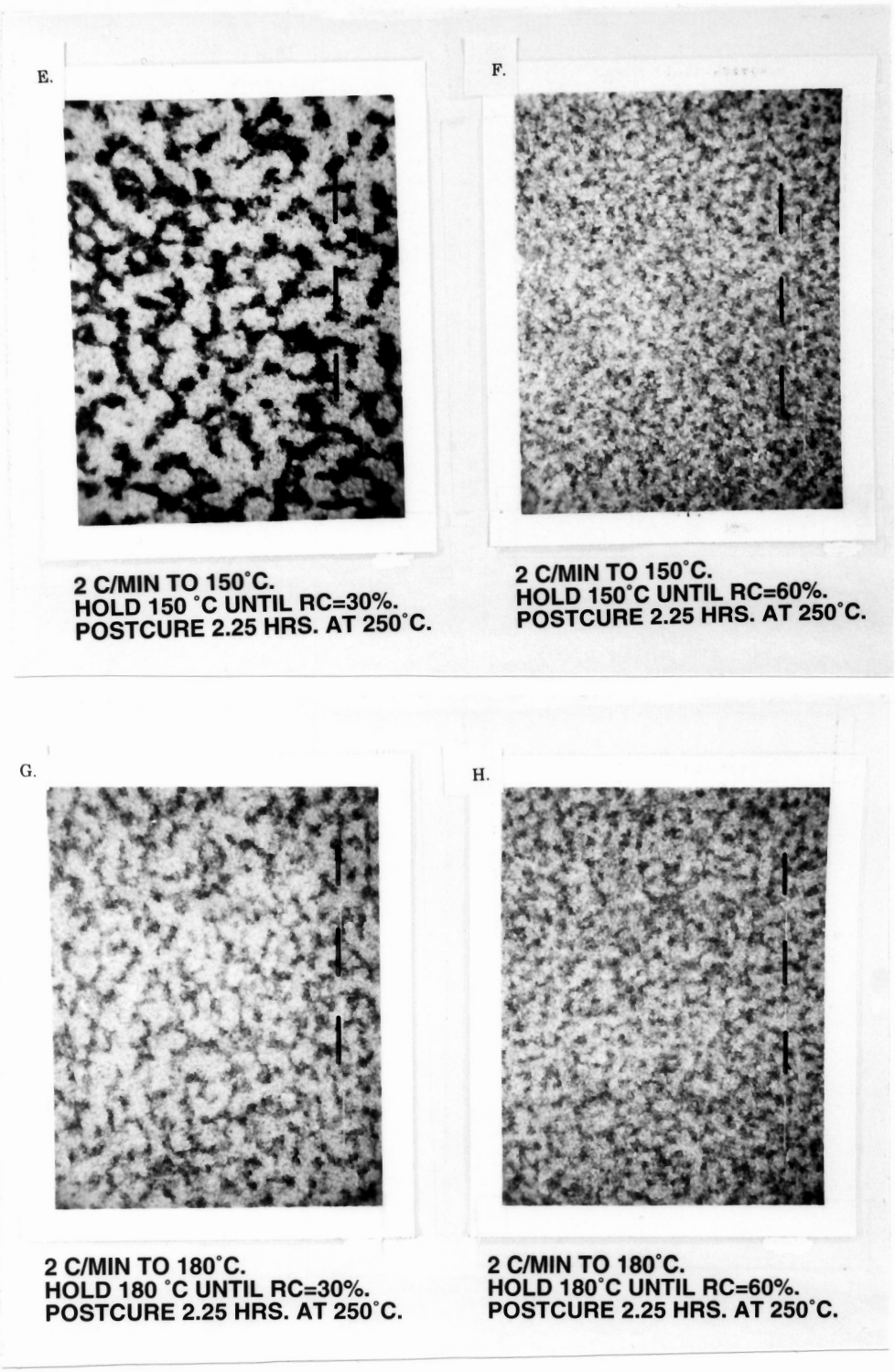

Figure 4.11. Continued

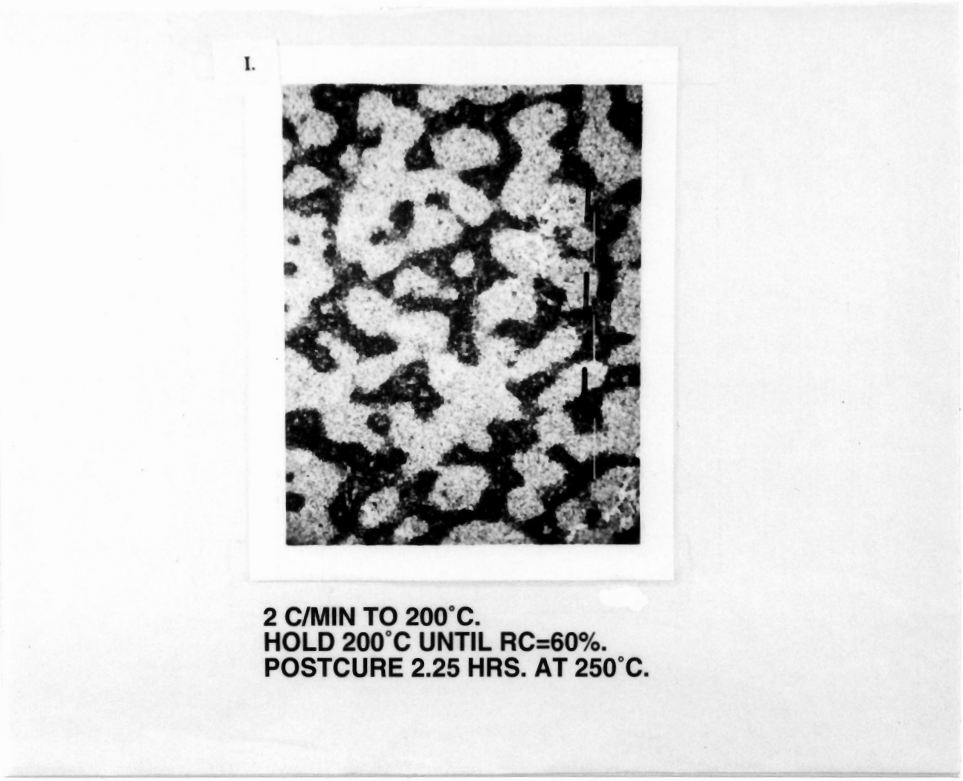

Figure. 4.11. Continued

dwells. These low levels of conversion were either inadequate to induce phase separation or to trap the fine microstructures. At 60% conversion (gelation), dramatic differences were observed as one would expect from the TTT diagram. The resin produced by the (ramped) control cycle, was visibly turbid, having well phase separated particles the size of the wavelength of visible light. Dwells to 60% conversion between 135 and 180°C trapped a very fine, mixed phase morphology which produced a transparent resin exhibiting little clearly definable structure at 25,000 X. For the 135°C dwell, even higher magnifications, did not produce a definite structure. At 150 and 180°C, the phases were slightly larger (approximately 0.15 microns) and slightly better defined (as far as concentration gradient between phases) than those at 135°C. Spinodal decomposition would begin with very small fluctuations in the concentrations in a homogeneous system. These concentration differences would become larger and larger eventually yielding an interlocked, phase separated system. The morphologies trapped at 60% conversion for 135, 150, and 180°C were those expected from early stages of spinodal decomposition.

At 180°C, there was less difference between the morphologies at 30% conversion and 60% conversion. This was probably due to the very, very rapid reaction at this temperature. The low conversion was achieved just after reaching 180°C; the 60% conversion very quickly after that. With the 200°C dwell, once again, the original morphology (control, no dwell) is restored. Visible fiber optic light transmission data (see Chapter 5) during the 2°C/minute control cycle showed a dramatic decrease in transmission between 180°C and 200°C, as would be expected from scattering due the formation of distinct, phase-separated, particles of the size of the wavelength of light. Both the control (and the 200°C isothermal dwell) resin castings were visibly turbid. While the earliest part of spinodal phase separation for the control morphology could not be seen with the light transmission method, one can say that between 180 and 200°C, the two phases became distinct enough to be observed. Therefore,

the dwell at 200°C, resulting after the particles were formed, had little effect. Light transmission for the 150°C dwell to 60% conversion displayed no drop in intensity, even as the cure was completed. This resin casting was optically transparent. In the 150°C dwell to 60% conversion, these phases remained small and relatively phase mixed and therefore could not be observed by light transmission. The fiber optic visible light transmission technique and the dielectric cure monitoring technique were used to provide physical data on the changes occurring during the cure of this system and are discussed in Chapter 5.

Despite the significant differences in morphology, all cure cycles produced similar thermal properties. Assuming no trapped cyanate reactive groups, all specimens have achieved greater than 98% conversion by DSC, with no significant differences between the cure cycles. Likewise, weight losses in air for all cycles were similar. In dynamic (air) runs, a 5% weight loss was achieved between 432-439°C. The samples were fairly similar as studied by the DuPont DMA with a room temperature dynamic storage modulus (E') between 1×10^9 to $1 \times 10^{9.5}$ Pa and softening (as a drop in modulus) beginning around 250-260°C. It was difficult to determine the details of the glass transition peak with the DuPont DMA as some slippage occurred while going through the glass transition.

After three weeks, chloroform exposure samples were generally intact, although some crumbling was seen in weak areas. The samples did not seem unusually soft or swollen. There were too few samples and uptake values varied too widely for any sort of statistical analysis, especially when corners were falling off some of the specimens. For a total of four specimens (three clear, one cloudy) the uptake values varied from 38 - 85% with no clear trend.

While it is attractive to generate a series of controlled morphologies, the real issue to the end user is whether these different morphologies produce different properties. Using an untoughened epoxy, Brett (4-1) showed the sensitivity of lap shear strength to cure profile and that an isocure state did not necessarily

produce the same properties. He attributed the differences the various curing reactions that had been proposed for epoxy cures. Manzione, Gillham, and MacPherson (4-15 - 4-16), Yamanaka, Takagi, and Inoue (4-26 - 4-27) and others have demonstrated differences of 0-50% in mechanical properties for rubber or thermoplastic toughened epoxies, most of the differences on the order of 0-30%.

To evaluate the effects of the morphology produced in these studies with the fiber optic sensor, Srinivasan later (2-100) made a series of K_{IC} specimens with uninstrumented dwells at 140, 160 and 180°C. The morphologies produced confirmed the trends in morphologies originally observed in the instrumented cycles. The toughness, as measured by K_{IC} dropped 20% for the finer morphologies produced by the isothermal dwells.

Although these drastic changes in morphology seem to result in only moderate changes in some of the mechanical and thermal properties, durability issues have not been addressed. Based on the changes in morphology induced in these processing studies, Ward (4-39) has proposed a series of double cantilever beam durability tests to determine the effects of changes in morphology on durability and the capability to customize the durability by changing the morphology.

Other researchers at Virginia Tech have been processing graphite (AS4) fiber reinforced composite panels using the 25% model thermoplastic toughened cyanate for mechanical testing purposes and modeling. The processing of these laminates had been optimized for consolidation and fiber volume (60-65%) by the incorporation of a isothermal dwell at 160°C for 1.5 hours. Based on the resin studies, one would expected that the processing dwell would result in a smaller, mixed morphology and an associated drop in properties related to toughness. Resin rich areas of a 16 ply quasi-isotropic lay-up panel processed in this manner were examined by staining and transmission electron microscopy at 12,500 and 25,000 x. Figure 4.12 shows the transmission electronmicrographs of the morphology of a resin rich region in the

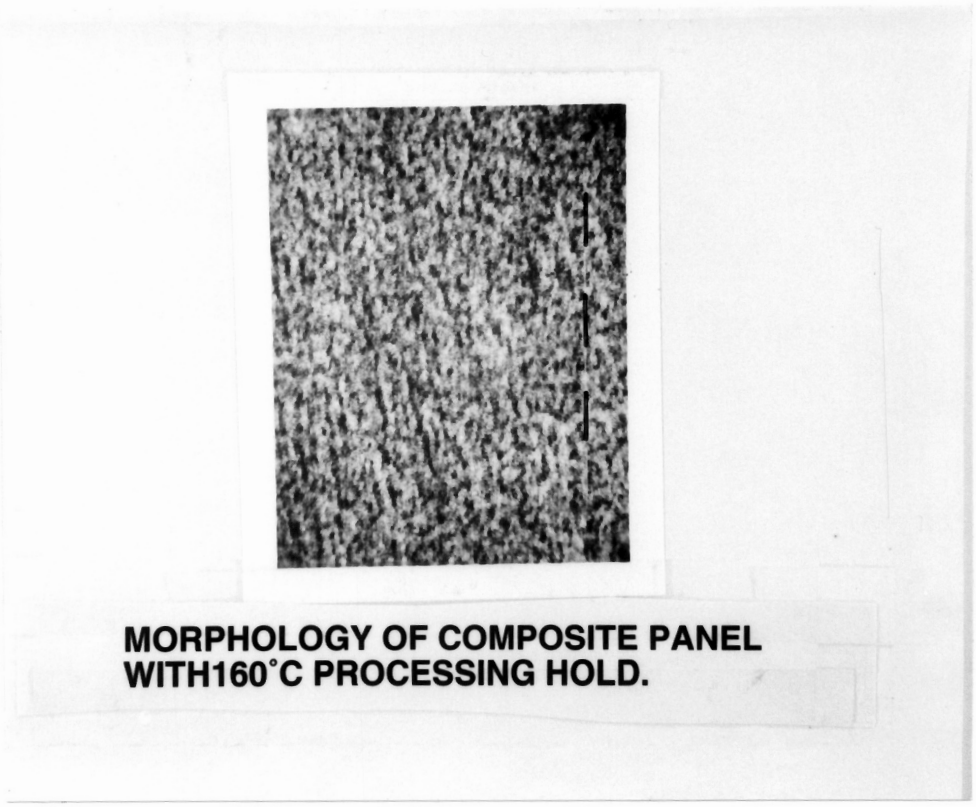

Figure 4.12. Morphologies of a Composite Panel with a 160°C Dwell. Black Bar is 0.5 microns.

composite panel. at a nominal 25000 x. The black bar is 0.5 microns. The composite panel showed a very indistinct, small (less than 0.2 micron), morphology that would be expected to result from the intermediate temperature dwell. Only preliminary data was available on these panels since the mechanical testing phase of the program has just begun. This panel was initially examined due to a suspected drop in impact propagation energy (lower than untoughened epoxy) for these panels. If the low properties are confirmed, it will be recommended that the cure cycle be changed (if it can be from a processing standpoint) to eliminate any extended isothermal dwells below 200°C. If a dwell must be incorporated, then the dwell advances the resin no further than 30%, since the 30% conversion appears to be low enough either to not induce phase separation or trap the small particles. Intelligent modification of this processing cycle with the on-line sensors and sensor combinations demonstrated in this study would be an excellent test of the applicability of these sensors to realistic production situations.

4.5 CONCLUSIONS AND SUMMARY

Intelligent, interactive manipulation of processing cycles, based on in-situ, real-time FTNIR fiber optic monitoring of network formation in a reactive thermoplastic toughened cyanate, has trapped a series of novel morphologies by gelation. Extremes in morphologies were produced within reasonable cure cycle variations. The same sort of changes in morphologies were found in a composite laminate which had had an intermediate temperature dwell introduced for processing purposes. Samples had similar degrees of cure (based on DSC), thermoxidative stability, dynamic Young's modulus, and T_g.

The effects on mechanical properties are still uncertain, and the full implications are still under study. Srinivasan has shown (2-100) that the finer morphology can, indeed, reduce the neat resin toughness by about 20% for this system. These morphologies were unintentionally produced in a graphite reinforced composite test laminate by a processing hold. The composite laminate was suspected

to have low impact strength although further mechanical testing is still in progress. A study has been undertaken to determine if these changes in morphology have any affect in the long term durability of adhesive joints. An exciting observation was that these changes were intentionally induced with no formulation changes, simply by the modification of the cure cycle based on real-time chemical conversion feedback from the FTNIR fiber optic sensor. The implementation of combined sensors for simultaneous in-situ real-time monitoring of chemical and physical changes demonstrated in Chapter 5, should have a significant impact on processing technology.

4.5 REFERENCES

4-1. C. L. Brett, Adhesion - 3, K. W. Allen, ed. Applied Science Publishers, London, p. 53-64 (1977).

4-2. E. Butta, G. Levita, A. Machetti, and A. Lazzerri, Polymer Eng. and Sci., 63-73 (1986).

4-3. S. Montarnal, J. P. Pascault, H. Sauterne, "Controlling Factors in the Rubber toughening of Unfilled Epoxy Networks: Application to Filled Systems" in Rubber-Toughened Plastics, Advances in Chemistry Series 222, C. K. Riew, ed. ACS USA (1989).

4-4. O. Olabisi, L. M. Robeson, M. T. Shaw, Polymer-Polymer Miscibility, Academic Press, New York, 1979.

4-5. D. R. Paul, "Polymer Blends: Phase Behavior and Property Relationships" in Multicomponent Polymer Materials, Advances in Chemistry Series 211, D. R. Paul and L. H. Sperling, eds., 2-15 (1986).

4-6. L. H. Sperling, "Recent Developments in Interpenetrating Polymer Networks and Related Materials," in Multicomponent Polymer Materials, Advances in Chemistry Series 211, D. R. Paul and L. H. Sperling, eds., p. 21-46 (1986).

4-7. T. K. Kwei and T. T. Wang, "Phase Separation Behavior of

Polymer-Polymer Mixtures, "Multicomponent Polymer Materials, Advances in Chemistry Series 211, D. R. Paul and L. H. Sperling, eds., p. 141-185 (1986).

4-8. R. S. Stein, "Optical Behavior of Polymer Blends, "in Multicomponent Polymer Materials, Advances in Chemistry Series 211, D. R. Paul and L. H. Sperling, eds., p. 393-444 (1986).

4-9. D. R. Paul, J. W. Barlow, and H. Keskkula, "Polymer Blends," in High Performance Polymers and Composites, J. I. Kroshwitz, ed. Wiley and Sons, Inc., USA, p. 797-859, (1991).

4-10. A. Echte, "Rubber-Toughened Styrene Polymers: A Review, in Rubber-Toughened Plastics, C. K. Riew, ed., ACS Advances in Chemistry Series, Vol. 222, p. 15-66, (1989).

4-11. A. J. Kinloch, Relationship Between the Microstructure and Fracture Behavior for Rubber-toughened Polymers, in Rubber-Toughened Plastics, C. K. Riew, ed. ACS Advances in Chemistry Series Vol. 222 p. 67-92 (1989).

4-12. Y. Huang and A. J. Kinloch, J. Mat. Sci. 27, 2753-2762 (1992).

4-13. Y. Huang and A. J. Kinloch, J. Mat. Sci. 27, 2763-2769 (1992).

4-14. Y. Huang and A. J. Kinloch, Polymer, Vol. 33, No. 6, 1330-1333 (1992).

4-15. T. Manzione, J. K. Gillham, and C. A. McPherson, J. of App. Poly, Sci., Vol. 26, 889-905 (1981).

4-16. T. Manzione, J. K. Gillham, and C. A. McPherson, J. of App. Poly, Sci., Vol. 26, 907-919 (1981).

4-17. L. C. Chan, J. K. Gillham, A. J. Kinloch, and S. J. Shaw, Rubber-Modified Epoxies: Cure transitions, and Morphology," in Rubber-Modified Thermoset resins, C. K. Riew and J. K. Gillham, eds., Advances in Chemistry Series, 208, ACS, 235-260 (1983).

4-18. L. C. Chan, J. K. Gillham, A. J. Kinloch, and S. J. Shaw,

Rubber-Modified Epoxies: Morphology, Transitions, and Mechanical Properties" in Rubber-Modified Thermoset Resins, C. K. Riew and J. K. Gillham, eds., Advances in Chemistry Series, 208, ACS, 2261-279 (1983).

4-19. R. J. J. Williams, J. Borrajo, H. E. Adabbo, and A. J. Rojas, "A Model for Phase Separation During a Thermoset Polymerization, in Rubber-Modified Thermoset Resins, C. K. Riew and J. K. Gillham, eds, Advances in Chemistry Series, 208, ACS, 195-213 (1983).

4-20. A. Vasquez, A. J. Rojas, H. E. Adabbo, R. Borrajo, and R. J. J. Williams, Polymer, Vol. 28, 1156-1164 (1987).

4-21. J. Borrajo. C. C. Riccardi, S. T. Moschiar, and R. J. J. Williams, "Effect of Polydispersity on the Miscibility of Epoxy Monomers with Rubbers," in Rubber-Toughened Plastics, ACS Advances in Chemistry, Vol. 222, C. K. Riew, ed. USA, (1989).

4-22. D. H. Verchere, J. P. Pascault, S. M. Moschiar, C. C. Riccardi, and R. J. J. Williams, ACS PMSE Preprints, Vol. 63, pp. 99 -103 (1990).

4-23. D. Verchere, J. P. Pascault, H. Sautereau, S. M. Moschiar, C. C. Riccardi, and R. J. J. Williams, J. App. Poly. Sci. vol. 42, 701-716 (1991).

4-24. S. M. Moschiar, C. C. Riccardi, R. J. J. Williams, D. Verchere, H. Sautereau, and J. P. Pascault, J. App. Poly. Sci. Vol. 42, 717-735 (1991).

4-25. D. Verchere, J. P. Pascault, H. Sautereau, S. M. Moschiar, C. C. Riccardi, and R. J. J. Williams, J. Appl. Poly. Sci. Vol. 43, 293-304 (1991).

4-26. K. Yamanaka and T. Inoue, Polymer, 30, 662-667 (1989).

4-27. K. Yamanaka, Y. Takagi, and T. Inoue, Polymer, 30, 1839 -1844 (1989).

4-28. T. Ohnaga, J. Maruta, and T. Inoue, Polymer, Vol. 60 1845-1850 (1989).

4-29. H. S.-Y. Hsich and W. J. Howard, ACS PMSE Preprints, Vol. 63, 127-131, (1990).

4-30. H S.-Y. Hsich, Poly. Eng. and Sci., Vol. 30, No. 9, 493-511 (1989).

4-31. H. S.-Y. Hsich, J. of Mat. Sci. 25 1568-1584 (1990).

4-32. H. S.-Y. Hsich, Part II, J. of Mat. Sci, 26, 3209-3222 (1991).

4-33. H. S.-Y. Hsich, Advances in Polymer Technology, Vol. 10, No. 3, 185-203 (1990).

4-34. A. J. Ryan, Polymer, Vol. 31, 707-712 (1990).

4-35. D. H. Kim and S. C. Kim, Poly. Eng. and Sci. Vol. 31, No. 5, 289-298 (1991).

4-36. Y. S. Lipatov, JMS - Rev. Macromol. Chem. Phys., C30(2), 209-232 (1990).

4-37. J. L. Hedrick, Dissertation, Virginia Tech, 1985.

4-38. S. C. Liptak, Dissertation, Virginia Tech, 1993.

4-39. T. C. Ward, CASS/CCMS Review 1993.

4-40. G. Wisanrakkit and J. K. Gillham, "The Glass Transition as a Parameter for Monitoring the Isothermal Cure of an Amine-Cured Epoxy System," from Polymer Characterization, Advances in Chemistry Series Vol. 227, C. D. Craver and T. Provder, eds, p. 143-166 (1990)

4-41. J. C. Hedrick, N. M. Patel, and J. E. McGrath, "Toughening of Epoxy Resin Networks with Functionalized Engineering Thermoplastics, in ACS Advances in Chemistry Series No. 233, C. Keith Riew and A. J. Kinloch, eds., 293 - 304 (1993).

4-42. S. P. Wilkinson, S. C. Liptak, J. J. Lesko, D. A. Dillard, J. Morton, J. E. McGrath, and T. C. Ward, "Toughened Bismaleimides and Their

Carbon Fiber Composites for Fiber Matrix Interphase Studies," in Proceedings of the Sixth Japan-U.S. Conference on Composite Materials, 240 -249 (1992).

4-43. S. A. Srinivasan and J. E. McGrath, High Perform. Polym., Vol. 5, 259-274 (1993).

4-44. S. C. Liptak, S. P. Wilkinson, J. C. Hedrick, T. C. Ward, and J. E. McGrath in "Electromagnetic (Microwave Processing Effects on Terminally Reactive and Non reactive Engineering Polymer Systems," in Radiation Effects on Polymers, R. L. Clough and S. W. Shalaby, eds,., ACS, Washington, DC., 364-383 (1991).

CHAPTER 5

SIMULTANEOUS REAL-TIME, IN-SITU CHEMICAL AND PHYSICAL MEASUREMENTS

5.1 INTRODUCTION

The logical extension of the in-situ, real-time FTNIR fiber optic monitoring technique is to combine this chemical sensor with an in-situ physical sensor. Small implantable microdielectric sensors have been used by a number of authors (5-1 - 5-27) to monitor the physical changes occurring during the cure of thermosetting resins. Recently, Maistros, et al. (5-25) and MacKinnon, et al. (5-26), have used a dielectric sensor to observe phase separation in toughened epoxies. The combination of the chemical information from the FTNIR fiber optic sensor with the physical information from the dielectric sensor would seem ideal for monitoring the changes occurring during the cure of toughened thermosets. This chapter covers the simultaneous FTNIR fiber optic and the frequency dependent electromagnetic (dielectric) sensor and/or fiber optic visible light monitoring of the cure of a thermoplastic toughened dicyanate resin.

5.2 BACKGROUND

The morphology and network structure of a phase separated, toughened thermoset results from the chemical and physical changes occurring during the processing. Changing the cure profile of such a thermosetting resin can drastically alter the properties through changes in the network and morphology. A number of authors have proposed that changes in time, temperature, stoichiometry, and catalyst can be used to change the morphology. This literature was reviewed extensively in Chapter 4. Also, in Chapter 4, the use of real-time, in-situ monitoring of conversion to produce some of these morphologies was demonstrated. The following review will discuss some of the ways of obtaining the information on the physical

changes.

5.2.1 Dielectric cure monitoring

Microdielectric sensors based on interdigitating (comb) electrodes sensors (Figure 5.1) are available for in-situ monitoring. Numerous articles and reviews have appeared (5-3 -5-16, 5-28) on monitoring the cure of untoughened thermosetting resin systems. For mathematical details, one is referred to these articles. This review will deal primarily with what the information means and how this information will differ in a toughened system. Microdielectric sensors have been used to monitor cure (5-1 - 5-19, 5-24 -5-28), water concentration (5-15 - 5-16), phase separation (5-25 - 5-26), diffusion (5-15 - 5-16), and changes due to aging (5-15 - 5-16). Such sensors are beginning to be used in process control and for feedback information in "smart" processing (5-17 - 5-18).

The basics of dielectric cure monitoring are explained quite well by References 5-1, 5-4, 5-13 - 5-16, and 5-28. Figure 5.2 shows the dipoles and ions in an alternating electrical field during the cure of a thermosetting resin. In the uncured resin, the dipoles orient to follow the alternating field and the ions align along the electrodes, forming charged layers. With increasing viscosity, the response becomes slower. If the "relaxation time" of the molecules is longer than the cycle time (the time needed for the field to change polarity), the molecules will begin to lag behind the field (Figure 5.2-b). Since higher frequencies have faster cycle times, this effect will be seen first at the high frequencies and progress to lower frequencies. At a given frequency, the response time will become slower and slower until the dipoles cannot follow the field and the ions are immobilized. If the applied alternating voltage can be thought of as varying in a sinusoidal manner (as in Figure 5.3), the response at the other electrode will also be sinusoidal in nature but will differ from the applied voltage in amplitude and phase. The amplitude and phase lag will vary with the material (dielectric) between the two electrodes. Analysis yields the loss factor e" (5-1, 5-13 - 5-16):

e" = absolute sample loss factor/permittivity of free space

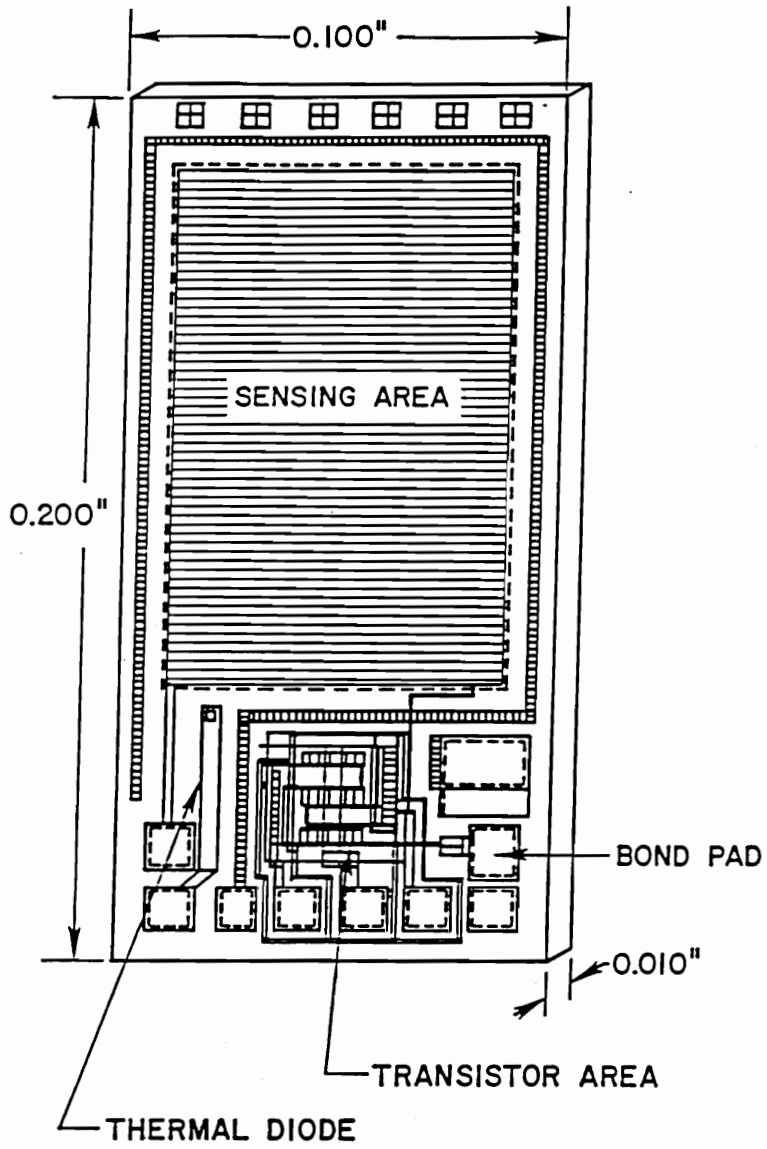

Figure 5.1. Implantable Microdielectric Sensor (5-13, 5-15).

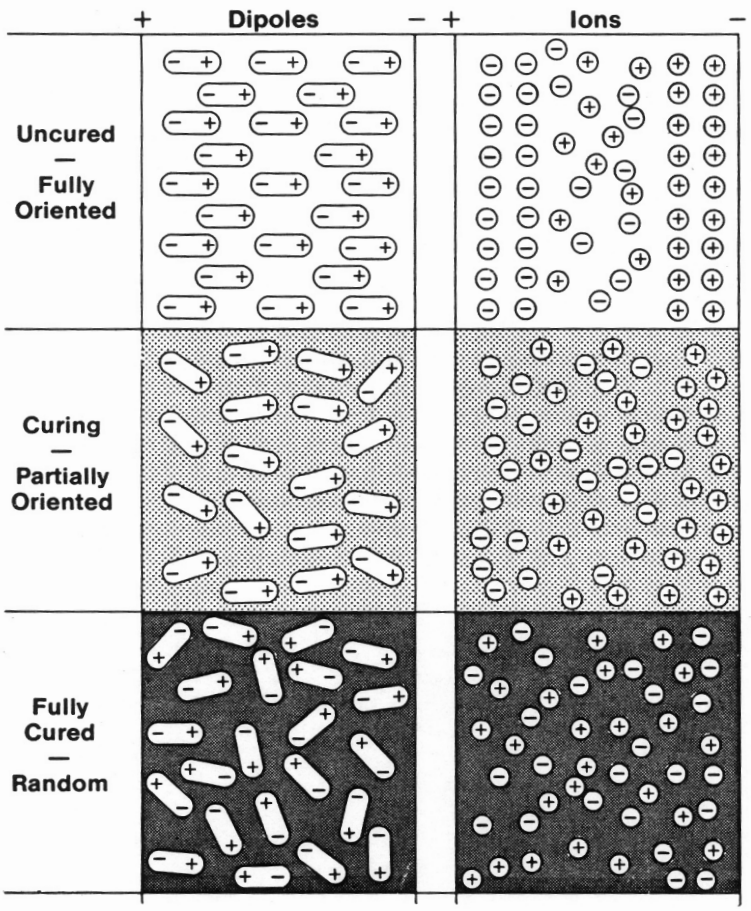

Figure 5.2. Behavior of Dipoles and Ions during Cure with an Applied Alternating Field (5-13).

= dipole term + σ / (ω * e_0)

σ = ionic conductivity

ω = w = angular frequency

e_0 = Permittivity of free space

e" = loss factor

The loss factor is associated with the energy dissipated as heat per cycle in aligning dipoles and moving ions. This is sometimes expressed in terms of ionic conductivity (5-1, 5-13 - 5-16) or as the loss factor times the angular frequency (5-1, 5-12). The ionic conductivity dominates the e" values at low frequencies and has been reported to scale with reciprocal viscosity prior to gelation (5-13 - 5-16). The ionic conductivity is a function of the resin viscosity, the extent of conversion, and the T_g of the material (typically shown by dipole peaks). It reflects the environment of the ions. If the viscosity is low, the ions will move, and the conductivity will be high. As the viscosity increases, the ion mobility decreases, as does the ionic conductivity. Isothermally (Figure 5.4), the loss factor will initially be high, decrease to a minimum then increase. The initial maximum is due to the initial mobility of the ions. As the mobility decreases, so does the ionic contribution to the loss factor. Eventually, the ionic contribution is less than the dipole contribution, and the loss factor increases. The loss factor will then peak as the dipole "reaches maximum lag behind the electrical field." Day (5-13 - 5-16) recommends using high frequencies at the beginning of cure and low frequencies at the end. Dipole peaks move to lower frequencies as cure proceeds (due to the advancing T_g). Figure 5.5 compares the loss factor to the viscosity for a typical cure cycle for catalyzed amine cured epoxy system.

The dielectric loss is much larger than the permittivity. The permittivity (e') is a measure of dipole alignment:

e' = absolute sample permittivity/permittivity of free space

= e' (dipole) + e' (background)

As heat is applied in materials with polar groups, the dipoles initially oscillate and permittivity goes up. The permitivitty then decreases to

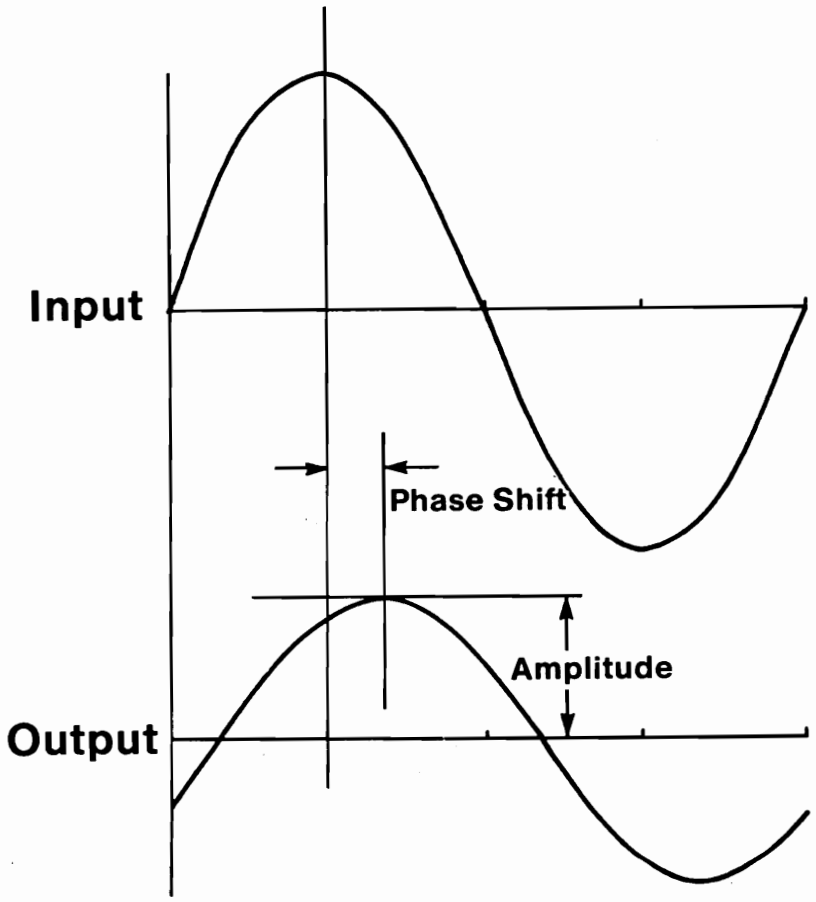

Figure 5.3. Applied Voltage and Response (5-13)

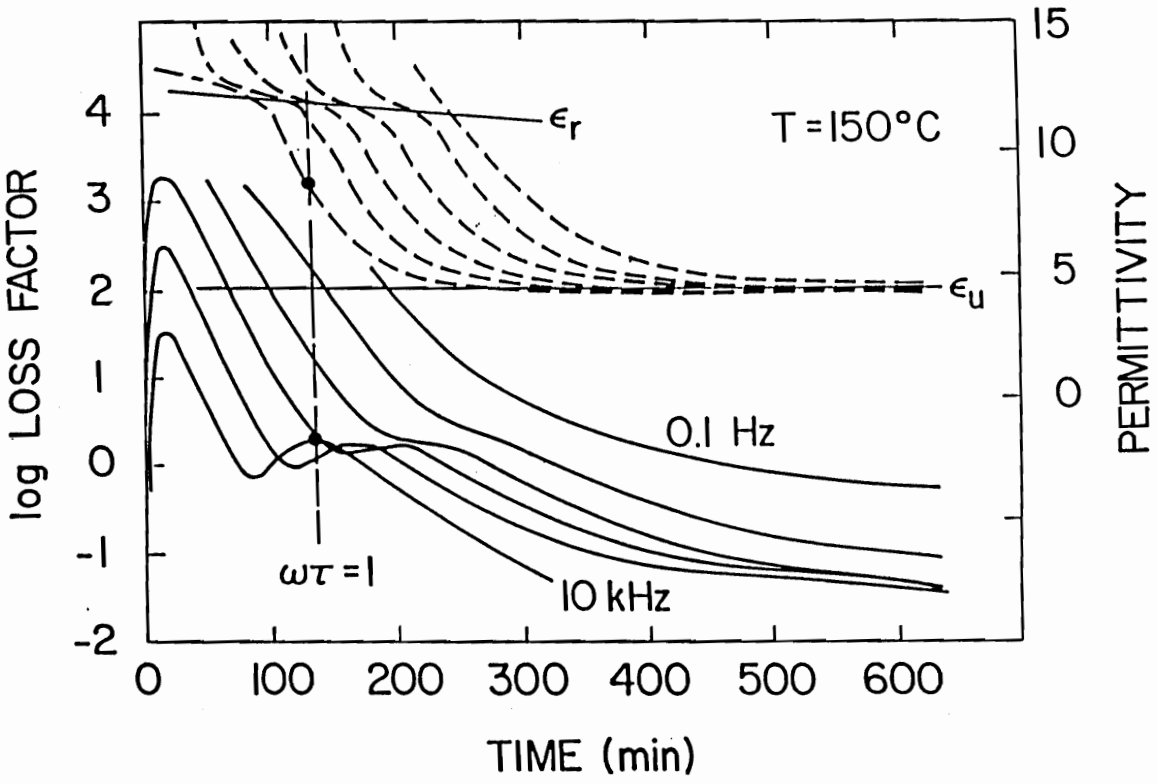

Figure 5.4. Dielectric Data for Isothermal Cure of an Epoxy (5-4).

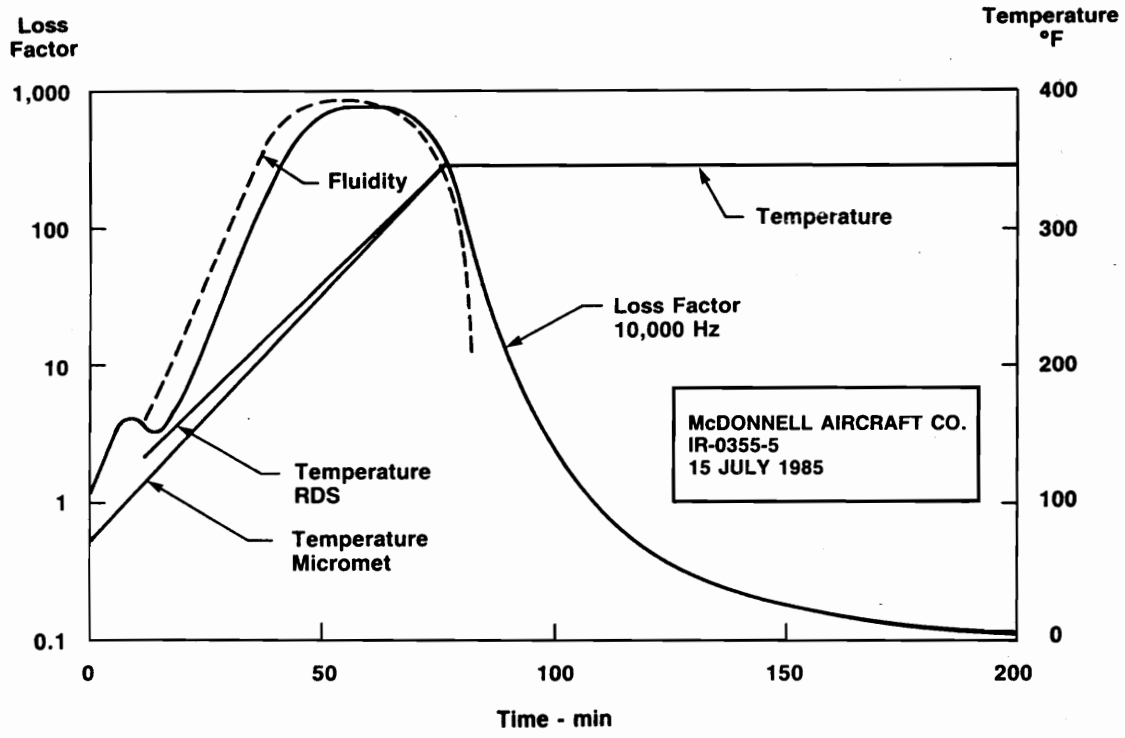

Figure 5.5. Dielectric Data during a Typical Cure for an Epoxy (5-13).

a lower plateau region (since dipoles cannot keep up with the polarization).

Electrode polarization may result in false e' and e" values. According to Day (5-13 - 5-16), electrode polarization is associated with high ionic conductivity. Under these conditions, ions may build up at the polymer-electrode interface, acting as a capacitor, and artificially producing a lower observed loss factor and a higher observed permittivity. Day states that "if e" * e_0 * ω does not change with frequency, then it is a measure of ionic conductivity." If e" * e_0 * ω does vary with frequency, there is dipole and/or electrode polarization.

Vitrification may or may not be seen as a dipole peaks in the loss factor. These were seen by Sheppard in the cure of a DGEBA epoxy (see Figure 5.5) but not seen by Bidstrup and Senturia (5-4) in the cure of a tetrafunctional epoxy. Vitrification was also observed in a photocurable acrylic by Zumbrum (5-19). Day, Sheppard, and Wall (5-11) proposed a method of real time determination of T_g during cure from multifrequency loss factor data for a diamine cured DGEBA resin based on a relationship originally proposed by Bidstrup. The ionic conductivity was related to T_g through a WLF relationship or a linear increase in log conductivity with T_g.

Recently, Ciriscioli and Springer (5-1) and Banhegyi, et al. (5-2) have reviewed and critiqued dielectric cure monitoring techniques addressing such issues as quantitative viscosity measurements and heterogeneous polymers. Ciriscioli and Springer took a "critical" look at the two most widely accepted ways of monitoring cure with microdielectric sensors, the method used by Senturia (5-3 - 5-10) and Day (5-13 - 5-16), the basis of the commercial systems from Micromet, and the approach used by Kranbeuhl (5-12), the basis for the commercial Dek Dyne systems. Rather interestingly, the authors concluded that either method yields similar ionic conductivity, that either method could determine the minimum viscosity and indicate the approach of the end of cure, but that neither could directly determine viscosity or degree of cure.

From theoretical equations, permittivity (e') and the loss factor (e") are expressed as:

$$e' = e_u + ((e_r - e_u)/(1 + (\omega * \tau)^2)) \quad (5\text{-}1)$$

$$e'' = ((\sigma/(\omega * e_0) + ((e_r - e_u) * \omega * t)/(1 + (\omega * \tau)^2))$$

τ = dielectric relaxation time

e_0 = permittivity of free space

Based on measurements of capacitance and conductance, "measured" or experimental permittivity (e'_m) and loss (e''_m) factors are obtained by the following calculations:

$$e'_m = C/C_0 \quad (5\text{-}3)$$

$$e''_m = G/(C_0 * 2p * f) \quad (5\text{-}4)$$

C = Capacitance

G = Conductance

f = frequency

m = measured

The actual permittivities can be calculated by dividing the measured values by the appropriate correction factors. If only the frequencies with little or no electrode polarization and dipole effects are used, the measured loss factor should be equal to the actual loss factor. Substituting the measured loss factor into equation 5-2 and rearranging yields:

$$e''_m * \omega = (\sigma/e_0) + ((e_r - e_u) * (\omega^2) * \tau)/(1 + (\omega * \tau)^2)) \quad (5\text{-}5)$$

σ = ionic conductivity

If the first term is much larger than the second, then the loss factor can be approximated by:

$$e''_m * \omega \sim \sigma/e_0 = \text{constant} \quad (5\text{-}6)$$

This is appropriate only for the frequencies where

$e''_m * \omega 1 = e''_m * \omega 2 = e''_m * \omega 3$, etc. = constant.

This is the approach used by Kranbeuhl. In fact, the data is often expressed as $e''_m * \omega$ or $e''_m * f$.

Day handles the situation by multiplying real loss factor by a correction factor (SF2) to give:

$$e''_m = SF2 * e'' \quad (5\text{-}7)$$

Substituting this into equation 5-2, letting SF2 = 1, and assuming that

the second term (again) is very small yields:

$$e''_m = \sigma/(\omega * e_0) \quad (5\text{-}8)$$

To assure that the second term is small, Day requires that:

$$e''_m >> (e_r - e_u)/2$$

or more specifically that the following equations must be satisfied:

$$R >> 1$$

$$1 < e'_m < 25$$

$$12 << e''_m << R$$

where R is a constant based on the geometry of the sensor and the resin. This yields

$$\sigma = \omega * e_0 * e''_m \quad (5\text{-}9)$$

Ciriscioli and Springer found that for the cure of a diamine cured epoxy, there was not a frequency that gave $e''_m * \omega$ = constant over the whole cure. As one would expect from the similarity of the equations, the methods gave very similar ionic conductivities, time at which the viscosity was minimum, and time when the rate of the increase in ionic conductivity with time was zero.

Ciriscioli and Springer also demonstrated that the ionic conductivity does not necessarily give the same viscosity and conversion values as that obtained by other means. Based on empirical kinetic equations from DSC and viscosity testing, the rate of cure and viscosity were calculated and compared with the dielectric data. Reciprocal ionic conductivity was compared with viscosity. Ciriscioli and Springer felt that the "ionic viscosity is not directly related to the viscosity" although it did show the same minimums and maximums and that the rate of ionic conductivity change with time is "not directly correlated to the actual rate of cure" although the rate of change goes to zero at about the same time as the cure rate goes to zero. Comparing a calculated DSC based degree of cure (α) with that obtained by integrating the $d\sigma/dt$ curves (in much the same way as one obtains α) produced differences between the ionic degree of cure and that from the DSC data. The authors suggest that "to determine the absolute values of viscosity and degree of cure it might be necessary to take into account additional parameters such

as temperature, dipolar mobility, and rates of permittivity, loss factor, and ionic conductivity." This author suggests that even this may be a bit too naive.

The data analyses used above are for homogeneous materials. In 1991, Bahegyi, et al. (5-2) reviewed the equations for mixed systems, and discussed experimental data for the interface, the effect of filler, water absorption, purity, and stress induced orientation. Calculations for the dielectric properties for non-homogeneous systems are often made based on some combination of property, shape factor, and volume fraction. The material can be treated as a statistical blend or as phase separated with one phase continuous (see References 5-2, 5-20 - 5-21, and 5-26 for equations). These equations may not be quantitatively useful for the irregular (most calculations are for spheres or ellipses), interlocked, co-continuous resin in this study as observed for MacKinnon, et al. (5-26) for the co-continuous formulation. Some of their generalities for spherical or elliptical particles will be summarized here. Under certain circumstances, when the concentration of the non-continuous phase is below the percolation limit and the non-continuous phase has a higher conductivity, an interfacial relaxation peak (a Maxwell Wagner Silas effect) may be seen at intermediate frequencies. Above the percolation threshold, the peak will most likely be "masked by the conductivity of the more conductive component". The effect may also be hard to determine if the relaxations of the individual phases overlap and/or obscure the relaxation. According to Banhegyi, this is hard to resolve, since "the apparent component relaxation strengths are (then) not linear functions of composition." Another possible complication is that the interfacial effects may also be obscured by space charge effects from the electrodes.

Banhegyi, et al. presented experimental data for several inhomogeneous systems. Of interest to this investigation is the observed phase separation of a 50/50 poly(benzimidazole) / poly(etherimide) (PBI/PEI) blend. A film was cast from solution, dried slightly below the boiling point of the solvent, and then heated.

Measurements were made between 0.02 - 100 KHz. Real (the authors refer to this as dispersion) and imaginary (loss) data was obtained. Initial heating produced two peaks, one at 140°C and 250°C (see Figure 5.6). The first peak was described as "virtually independent of the measuring frequency while the peak height increases with decreasing frequency". The authors attributed this first peak to water due to ambient storage. The higher peak was the T_g of the blend. At low frequencies, the blend T_g was complicated by electrode polarization (falsely yielding very high e' and e"). Continued heating produced a "break" in the e' and e" higher frequency curves between 340 and 350°C (where the blend is reported to phase separate). Subsequent heating resulted in loss of the water peak at 140°C, slightly reduced electrode polarization, and a clearer transition between 200 and 250°C. Varying compositions showed that the peak between 200 and 250°C (in the case of the 50/50 blend) was a composition dependent transition.

There has been rather limited information on the effects of phase separation on the dielectric cure data. In 1990, Lin and Hsieh (5-24) observed the cure of what they called a "toughened" bismaleimide. Although they mentioned thermoplastic toughening of bismaleimides, the formulation was not detailed other than as an experimental resin from their laboratory. The authors were not looking for phase separation. Evaluation of the data, in light of the Banhegyi, et al. article and later articles by Maistros, et al. and MacKinnon, et al, showed no obvious phase separation effect in the log e" data.

Maistros, et al. (5-25) showed a significant effect during the cure of a (reactive) rubber toughened epoxy. Highly thermoplastic loaded resins which may undergo spinodal decomposition, lower concentrations of rubber in epoxy are typically thought to undergo a binodal decomposition. The binodal decomposition results in the production of a small phase whose composition differs dramatically from that of the homogeneous mixture. This phase will then grow. In spinodal decomposition, the initial size of the phase is fixed. The

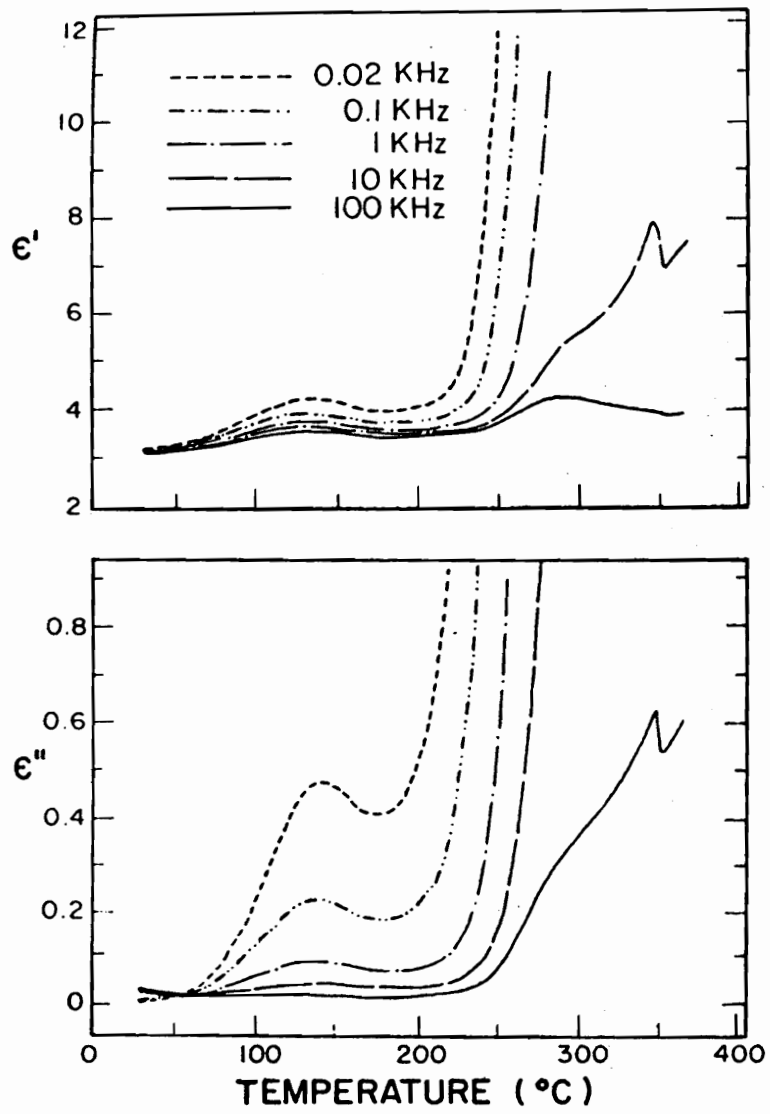

Figure 5.6. Dielectric Monitoring of Phase Separation in a PBI/PEI Blend (5-2).

concentration differences between the phases are initially very subtle. This may explain some of the differences in magnitude of the effect observed by Maistros and coworkers and that observed by MacKinnon, et al. (5-26). Maistros, et al. observed an extra low frequency maximum in the permittivity which corresponded to an increase in turbidity (see Figure 5.7). This peak was unusual and implied an "increase in polarizability...due to a new relaxation process." They attributed this peak to an interfacial polarization (a Maxwell-Wagner-Silas effect) due to phase separation. Mathematical derivations covered by Maistros, et al. are discussed in more depth in two papers by North, Pethrick and Wilson (5-20 - 5-21). The effect was significantly different for different frequencies, being most evident for low frequencies (Figure 5.8). There was also a very high initial values of e' and e" due to electrode polarization. Electron microscope examination of the toughened resin showed 0.5 micron diameter particles.

MacKinnon, et al. (5-26) examined the dielectric effects of phase separation during the cure of a fairly highly (20 -25%) thermoplastic loaded epoxy. The effect was much smaller than that observed by Maistros, et al. (5-25) and could only be resolved with computer subtraction above phase inversion. Electron microscopy showed that below 20% thermoplastic, the continuous phase was thermoset rich with (0.4 micron) thermoplastic rich particles. The authors observed an intermediate " ribbon-like morphology" before generating a co-continuous phase at 20-25%. Above 25%, the continuous phase was thermoplastic rich with 0.2 micron thermoset rich particles. K_{IC} and G_{IC} increased after phase inversion.

The authors initially observed electrode polarization at low frequencies, resulting in a large dielectric loss at the beginning of the cure. Vitrification was seen as a peak in the loss at high frequencies and as a slight increment in the permittivity for the untoughened resin. Up to about 5% thermoplastic loading, little difference was seen from the untoughened formulation. More thermoplastic made it difficult to "resolve dipolar processes." This

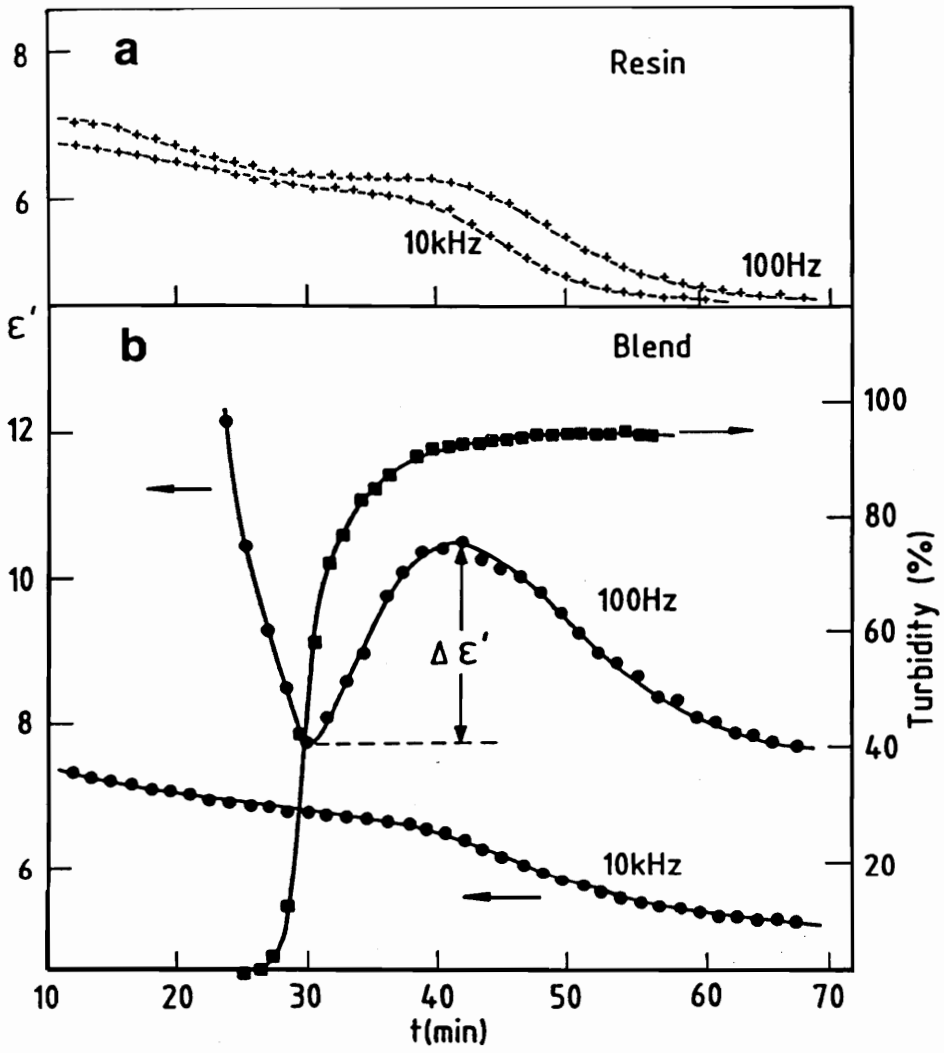

Figure 5.7. Dielectric Detection of Phase Separation in a Rubber-Toughened Epoxy (5-25).

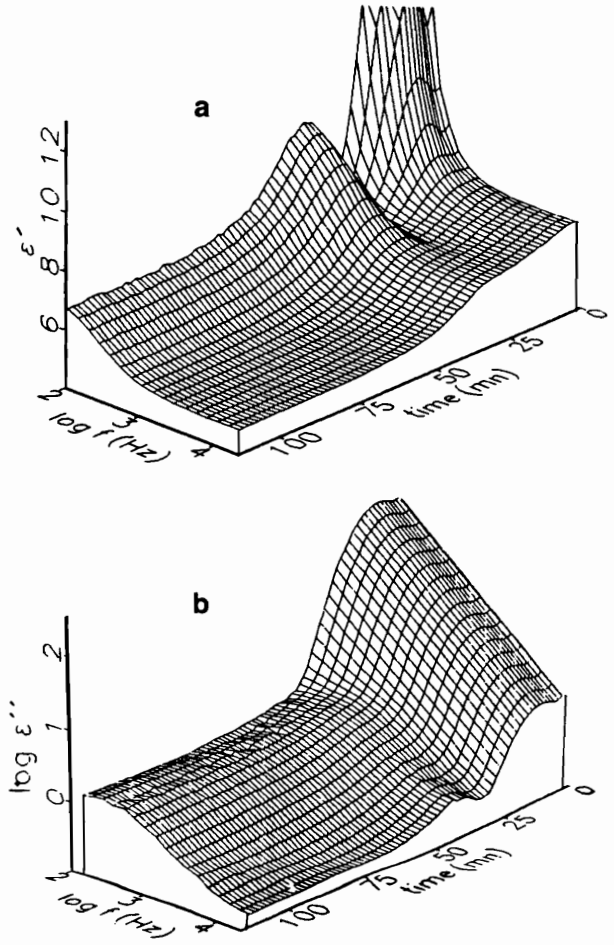

Figure 5.8. Frequency Dependence of Phase Separation Phenomena for the Rubber-Toughened Epoxy (5-25).

shoulder (see Figure 5.9) was eventually resolved into what the authors call a "distinct relaxation process independent of time of cure" above 26% thermoplastic. This effect is orders of magnitude more subtle than that seen by Maistros, et al. The dielectric data was fit to equations containing the shape as the only variable. The best fit a/b ratio (length/breadth) was calculated. For example, spheroids would have a = b, while ellipsoids would have b larger or smaller than a. Residual DC conductivity increased slightly with thermoplastic content up to 20%, then decreased with thermoplastic content. The epoxy was the more "conducting" phase. In the cured resin, the loss factor had a component due to dc conductivity and a loss component in the phase inverted systems. The authors attributed this loss to the Maxwell-Wagner-Silas (MWS) effect. The MWS effect required that higher conductivity (i.e. the epoxy) phase be "occluded" and preferably an "oblate spheroid." It was necessary to use a computer subtraction routine to resolve the MWS peak. This MWS peak was a function of thermoplastic content. Attempts to fit to a single phase model resulted in a poor fit. Above 20% thermoplastic, the two phase model gave a much better fit. Above 20%, a/b for the large volume fraction phase (the thermoset rich phase) decreased. The authors felt that this was consistent with a "more spherical form as the thermoplastic content is increased." The a/b for the thermoplastic rich phase increased up to 26-30%, then decreased.

Vitrification could be observed if the DC component was mathematically subtracted. Vitrification occurred later in the toughened formulations. After vitrification, the conductivity decreased. The conductivity decreased throughout the cure eventually reaching an asymptotic value. The thermoplastic acted as a diluent and delayed cure and increased gel time. The T_g of the cured toughened epoxy was lower than that of cured untoughened epoxy. The T_g of thermoplastic too close to that of the epoxy to be observed.

5.2.2 Optical methods

Phase separated blends are often optically turbid. Olabisi and

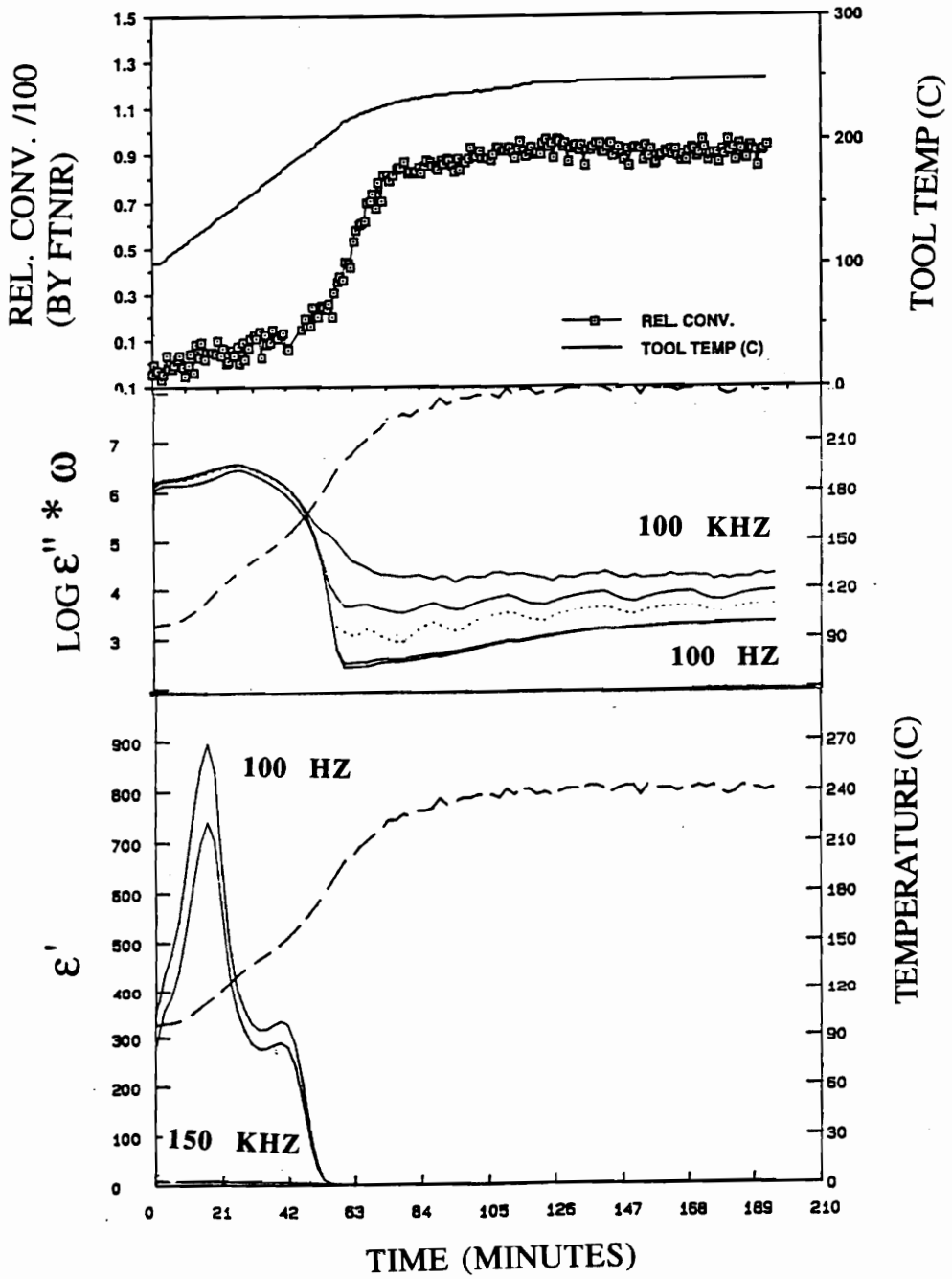

Figure 5.11. Simultaneous Conversion, Loss factor, and Permittivity during 2°C/minute Cure of the Toughened Cyanate.

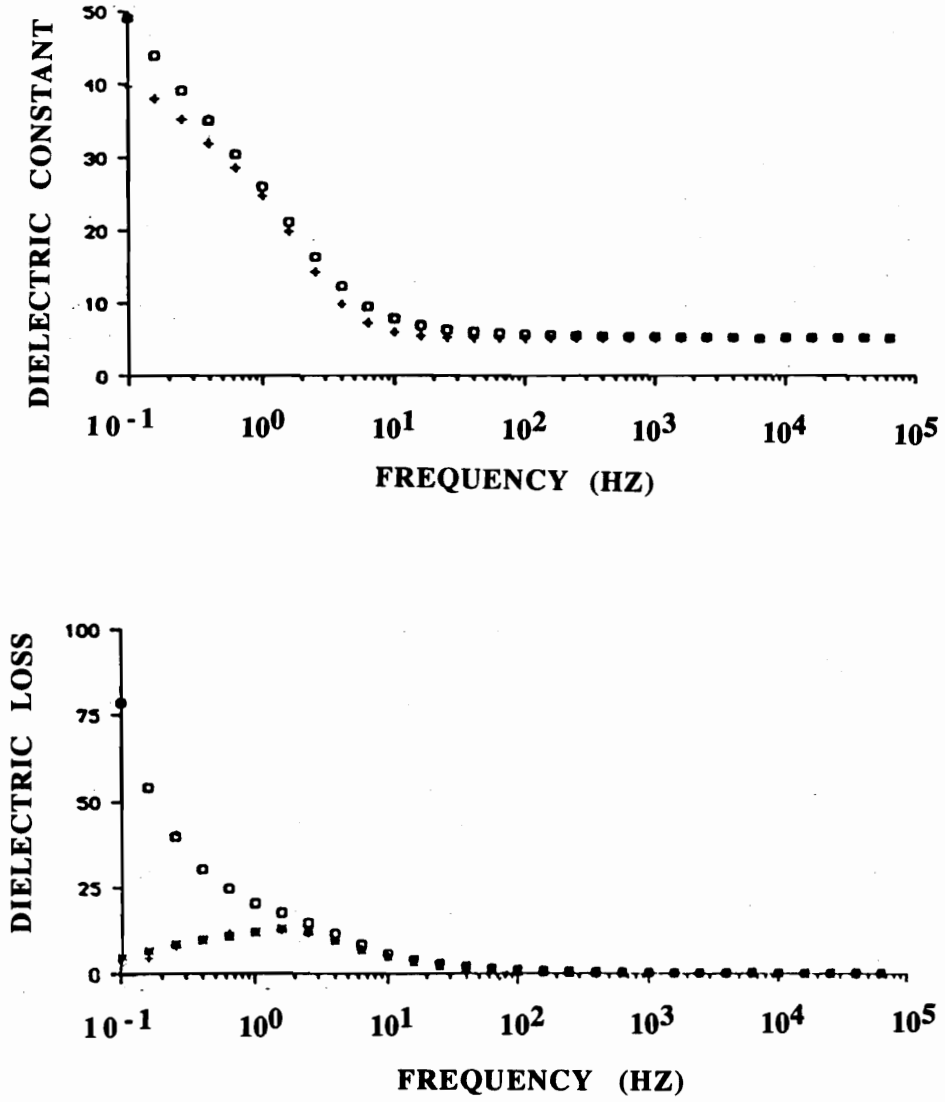

Figure 5.9. Dielectric Data during Cure a Polyethersulfone-Toughened Epoxy (5-26).

Robeson (4-4), referencing Gibbs, state that "by definition, stable homogeneous mixture is transparent, whereas, an unstable non-homogeneous mixture is turbid unless the components have the same refractive index." In other words, one way of determining a grossly phase separated system with significant differences in the refractive index of the phases would be to observe whether the resin was visibly transparent or not. A more quantitative method would be to measure the amount of light transmitted, although this would not be the most sensitive measure. More sensitive would be to measure the light scattered at some angle. Cloud points, "the point of incipient phase separation" (4-4), are often measured with a laser and photomultiplier detector measuring scattered light at 90 degrees to the incoming beam. For a spinodal decomposition, a definite "cloud point" would be hard to quantify since the change is gradual rather than significant. A very sensitive detector is also required since there is not very much light scattered at 90 degrees. The more sensitive method would be to measure the amount of light scattered, preferably as a function of the angle of transmission. This is used by a number of authors to confirm growth by spinodal decomposition (4-4, 4-8, 4-26, 4-27). For spinodal decomposition, the angle of the maximum of intensity would be constant. The value of the intensity would change.

Variable angle measurements at low scattering angles were not readily available. Cloud point methods were available but the data for the thermoplastic toughened resin were confusing. Since the desire was methods which could be used in-situ, transmitted visible light techniques were applied. The light put into a system should be the sum of the light transmitted and that lost or scattered due to turbidity. Although not as sensitive as the scattered data, gross changes can be detected by measuring the loss in the transmitted light. More specifically (4-8), for Rayleigh scattering of a spherical particle, the scattering varies with the square of the volume of the sphere and with the "square of the polarizability difference (or refractive index difference) between the sphere and its

surroundings. The scattering vanishes when refractive indexes are matched." As explained by Stein (4-8), citing Conaghan and Rosen, this can be expressed more quantitatively as:

$$\tau = N * \pi * R\text{^}2 * K \qquad (5\text{-}10)$$

$$\tau/\phi 1 = 3K/2d_p \qquad (5\text{-}11)$$

τ = turbidity

$\tau/\phi 1$ = specific turbidity

K = scattering coefficient

m_r = the refractive index ratio

α = reduced size

$\phi 1$ = particle size

d_p = particle diameter

If the particle is less than one tenth the wavelength of light

$$K = (32/27) * [m_r - 1]^2 * \alpha^4. \qquad (5\text{-}12)$$

The resin used in this study has been a toughened thermosetting cyanate resin which produced a highly interlocked, irregular morphology by an apparent spinodal decomposition. The equations say that the turbidity should be a function of size and of refractive index difference. At a given temperature in a spinodal decomposition, the size will be fixed at the beginning of the separation. If the size is adequate to scatter sufficient light, it will not do so until the refractive index differences are large enough to result in sufficient scattering. Initially, there is very little difference between the refractive indices of the phases formed by spinodal decomposition. This concentration (or refractive index) difference will grow as the decomposition proceeds. If the size is too small or the refractive index difference is not of sufficient magnitude (when the two phases are still phase mixed), there will be very little scattering. The method of detection (reduction of transmitted light) used in this study is not sensitive enough to detect low levels of light scattering. Therefore it will not see low levels of scattering due to small particles or phase mixed particles.

There appear to be two different instances of the use of fiber optic transmission or scattering in the literature. The first (2-7), as

described in Chapter 2, was the measurement of oil contamination in water. The particle size was determined by the scattering angle. The concentration was determined by intensity. More recently, the turbidity measurements made by Maistros, et al. (5-25) to confirm the dielectric observation of phase separation were obtained using some sort of fiber optic sensor. The measurements are described as being made simultaneously with the dielectric sensor and that light was transmitted "to and from the heated mould via optical fibers." No details of the actual design or measurements were presented.

5.3 EXPERIMENTAL

The resin was again the dicyanate of bisphenol A (BADCy) with 250 ppm aluminum acetyl acetonate (AlAcAc) and 2 pph nonyl phenol with or without 25% of a reactive thermoplastic. The resin was mixed at 104°C, degassed and then stored at room temperature in a desiccator until use. In general, fresh samples were made up weekly. Samples used for the simultaneous runs were less than 48 hours old.

The fiber optic sensor preparation is covered in detail in Chapter 2 and the Appendix. All data were obtained with a Nicolet 800 FTIR spectrometer with a CaF_2 beamsplitter, a tungsten halogen white light source, and a Nicolet fiber optic adapter with a dedicated, liquid nitrogen cooled InSb near infrared detector. The fiber optic adapter was attached to the mold in a programmable Fisher Isotemp Model 800 oven in the next room by two two-meter long pieces of polyimide coated, silica clad, low hydroxyl silica fiber (Polymicro Technologies TSP320450). The configuration was that described in Chapter 4 for the metal mold. Backgrounds were obtained with fibers touching. For sampling, a 1-2 mm gap was placed between the fiber ends and the fibers mechanically and adhesively restrained. Each data file consisted of 32 scans co-added together. Files were obtained approximately 50 seconds apart.

Dielectric data was obtained simultaneously at Virginia Tech with a Dek Dyne dielectric cure monitoring system borrowed from Professor D. Kranbeuhl at the College of William and Mary. An

interdigitated microdielectric sensor (FDEMS) on Kapton was placed into the mold about 1.5 cm from the fiber optic sensor (Figure 5.10). Either the stand alone sensor, the lap shear sensor or the mold with sensor can be readily modified for inclusion of the FDEMS sensor. Data were taken 0.1, 0.125, 1, 10, and 100 KHz for the simultaneous runs. Confirmation runs were later made with the Dek Dyne system at the College of William and Mary between .005 and 1000 KHz.

The visible fiber optic data were obtained by placing a United Detector Technology S370 Optometer at the end of the second fiber (using the same white light source and beam splitter used for the FTNIR spectroscopy and launching the light into the fiber through the Nicolet fiber optic adapter). An alternate solution to this would have been to multiplex the light coming out of the sample to both the InSb detector as well as the optometer to obtain truly simultaneous data. The light intensity at 650 nm was monitored as a function of time through the cure cycles. This data accumulation was not automated.

Cure cycles consisted of the control ramp (2°C/minute to 250°C with the postcure at 250°C for 2.25 hours) as well as the cycle with an intermediate interactive dwell at 150°C to a 60% relative conversion.

Scanning transmission electron microscopy was used to verify that the morphologies produced were consistent with that produced in Chapter 4.

5.4 RESULTS AND DISCUSSION

The in-situ FTNIR fiber optic and FDEMS (dielectric) sensor provided complimentary data. Figures 5.11 and 5.12 show the combined in-situ, real-time information from the simultaneous FTNIR and FDEMS dielectric runs. There were artifacts in the later portions of the simultaneous dielectric data, most likely due to loss of contact between the sensor and the resin due to resin shrinkage. Figures 5.13 and 5.14 show expansions of the data at 100 Hz for the first 100 minutes. During the 2°C/minute control ramp to 250°C, the log e" * ω values dropped slightly up to 120°C, most likely a viscosity minimum. Afterwards, the ionic conductivity decreased as the resin

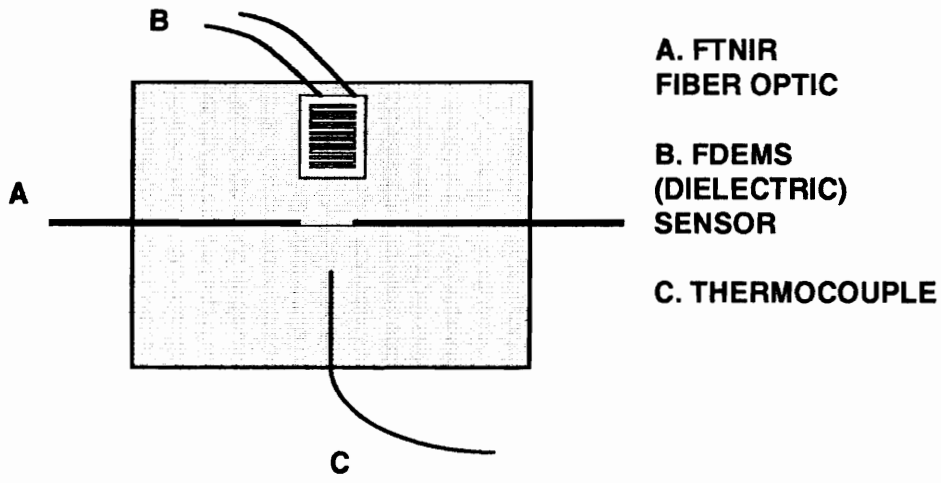

Figure 5.10 Sensor Placement for Simultaneous FTNIR Fiber Optic and FDEMS Dielectric Monitoring.

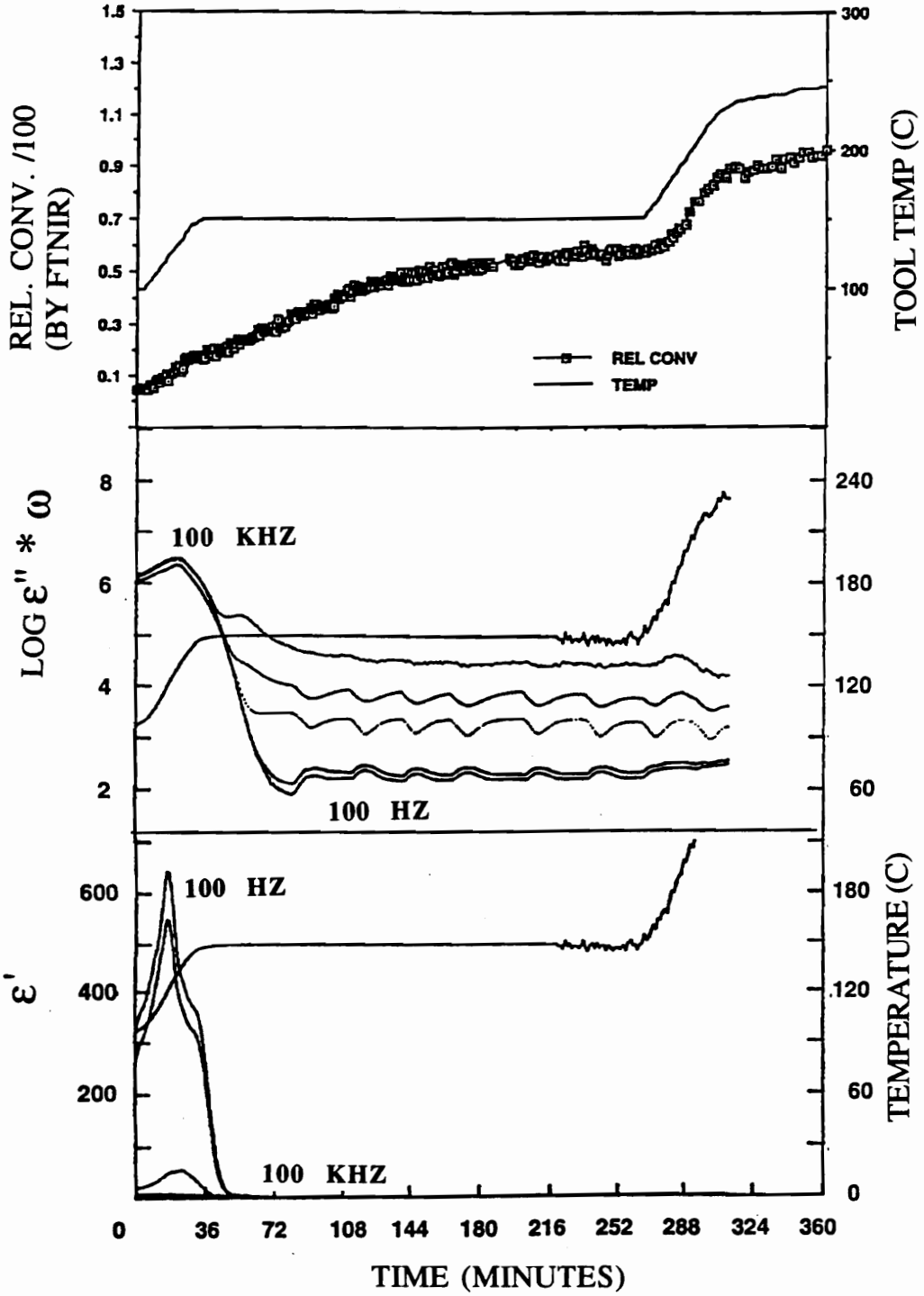

Figure 5.12. Simultaneous Conversion, Loss Factor, and Permittivity during 2°C/minute Ramp with 150°C Dwell for the Toughened Cyanate.

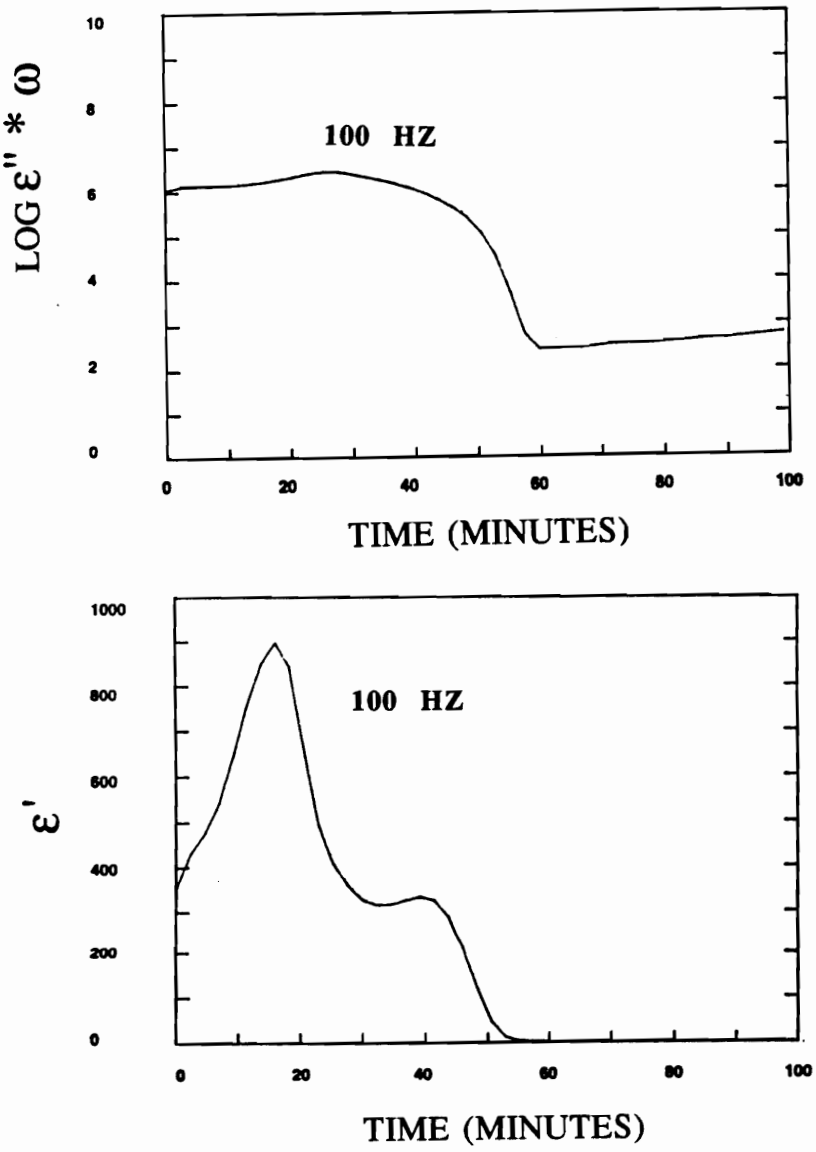

Figure 5.13. Expansion of Dielectric Permitivitty Data for a 2°C/minute Cure of a Toughened Cyanate.

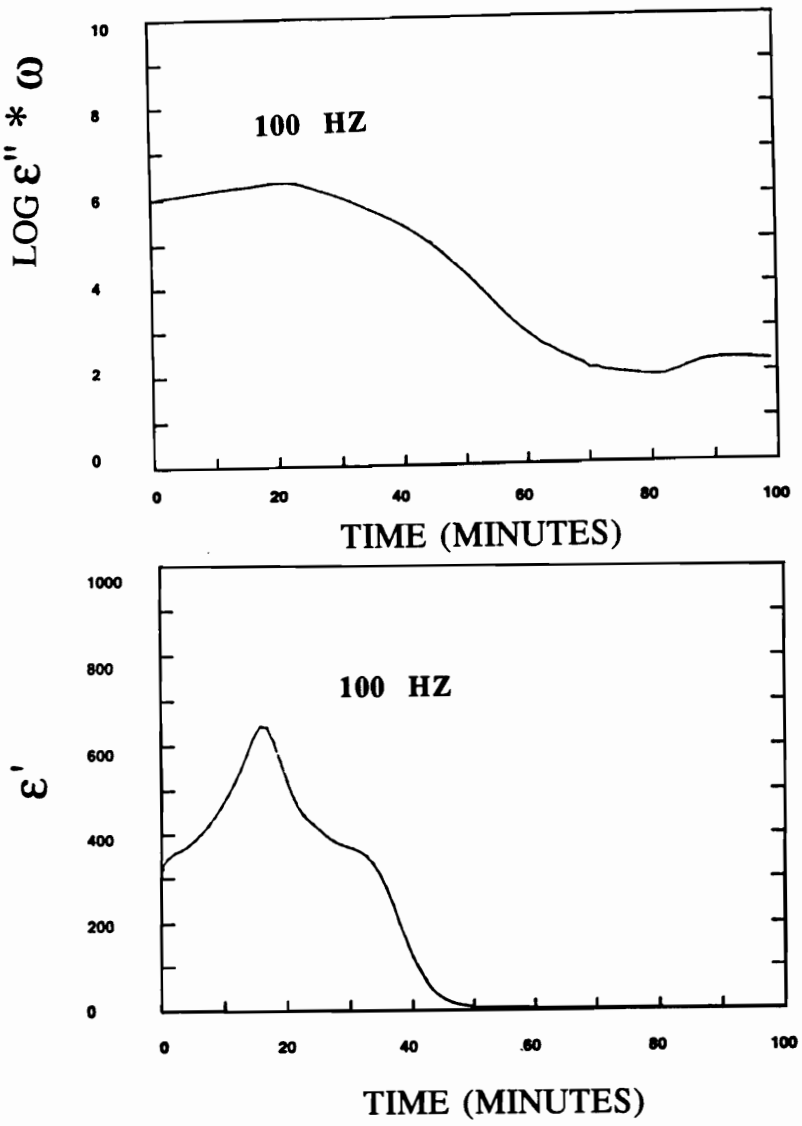

Figure 5.14. Expansion of Dielectric Loss Data during 2°C/minute Ramp with 150°C Dwell (for the Toughened Cyanate).

viscosity increased. In the simultaneous runs, the values leveled out, even appeared to be increasing at some frequencies slightly above 200°C. It was felt that the dielectric data above 200°C was an artifact. The rerun indicated a slight peak at about 200°C, followed by a gradual, asymptotic decrease. Initially, the log e" * ω curves overlapped well, but began to fan out about 160°C (see Section 5.2.1). The fiber optic conversion data provided further insight. There was very little reaction (less than 10%) up to the minimum viscosity. After the minimum viscosity, the increases in the crosslink density and the ionic viscosity (1/ionic conductivity) agree well up to the loss of the dielectric signal. Gelation (at α = 0.6) by the FTNIR measurement occurred at about 200°C. Vitrification, if the small peak in the e" * ω is vitrification, occurred very shortly afterwards. The permittivity data in Figures 5.11 and 5.12 were for the low frequencies (100 and 125 Hz). These graphs initially showed a fairly large electrode polarization (as seen by Maistros, et al. (5-25) and MacKinnon, et al. (5-26)) followed by a peak indicative of a phase separation that started at 145°C, reaches a maximum at 155°C, and returned to zero at about 180°C. In the rerun, the effect appeared to be masked somewhat more by the electrode polarization. The dielectric permittivity appears to "see" the phase separation earlier than optical methods (180 - 200°C) used for this study. The light transmission method used here would not be expected to see the beginning of a spinodal decomposition. Earlier spectroscopic data indicated a change in peak location for the aromatic peak (B2) at 5995 cm^{-1} between 180 and 200°C during the initial cure ramp. The area of the aromatic peak at 4675 cm^{-1} (B1) changes between 160 and 200°C. The transmission electron micrographs indicated that two distinctly different phases were produced between 180 - 200°C, but gave no indication of the onset of the phase separation.

The 2°C/minute ramp with 150°C dwell to 60% conversion cycle was selected because it produced a dramatically different morphology from the control (no dwell) cycle. As discussed in Chapter 4, the control cycle produced an optically turbid resin with

distinct 0.5-1 micron irregular thermoset-rich and thermoplastic-rich phases. The 150°C dwell, produced an optically transparent casting with much smaller, somewhat phase mixed particles. As the resin is heated, the ionic conductivity (e" * ω) went through a maximum, indicating a viscosity minimum around 120 - 130°C. After the beginning of the dwell, the ionic conductivity slowly decreased as the resin viscosity slowly increased. The changes should have become relatively asymptotic as the dwell continues (as was seen with the reruns). This was not seen in the simultaneous experiment. The simultaneous run once again appeared to contain some artifacts during the dwell not seen in the reruns. The e" * ω curves stay together for the first 40 minutes of the run, and then begin to fan out. The trimerization once again corresponds well with the viscosity, showing little reaction prior to the minimum viscosity and a slow increase after the dwell. The reaction rate slowed in the last hour of the dwell. The permittivity once again showed electrode polarization in the beginning of the run. A smaller maximum than in the control cycle was seen. This maximum began at 135-140°C, reached a maximum at the start of the dwell at 150°C, and dropped to zero approximately 15 minutes into the dwell. The actual area of the peak was approximately 20-30% the size of the peak in the control cycle. Once again, the dielectric technique appeared to detect the phase transition earlier than the optical techniques. The optical transmission stayed virtually level all during the dwell.

An attempt was made to determine FTNIR peak shifts during the mold runs. As explained in Chapter 3, there is too much noise with the combination of mold, oven, and longer fibers to distinguish the small changes in peak locations. Early isothermal heated cell runs at 135 and 160°C showed a moderate shift to lower wavenumbers for the B2 peak when the resin was held isothermally. B1 showed an even smaller shift. No distinct discontinuities were seen. Gelation (as measured by relative α = 0.6) occurred 200 minutes into the dwell. There might be a small bump in the log e" * ω curves after about 100 minutes into the dwell (as shown in the

reruns). It is uncertain whether this small peak reflects vitrification or not.

As shown in Figure 5.15 - 5.16 and briefly discussed above, visible fiber optic light transmission data during the 2°C/minute control cycle showed a dramatic decrease in transmission between 180 and 200°C, as would be expected from scattering due to the formation of distinct, phase-separated particle of the size of the wavelength of light. This resin casting was visibly turbid. Light transmission for the 150°C dwell to 60% conversion showed no such drop, even as cure was completed. This resin casting was optically transparent. The morphology produced by this resin formulation was indicative of a phase separation by spinodal decomposition. Typically, in spinodal decomposition, the sizes of the phases are determined at the beginning of the separation and remain constant. Changes occur in the concentration gradient between the two phases. Early spinodal decomposition would not produce a large enough difference in the refractive indices of the two phases to result in significant losses due to scattering even if the particles were the right size. The transmitted light technique was not sensitive to the early parts of the phase separation even if the particles were approximately the same size as the wavelength of the light seen by the detector. As the concentration differences in the two phases increased, the differences in the refractive indices would increase, eventually becoming large enough to produce scattering and the associated loss in transmitted light. Between 180 and 200°C in the control ramp, the phases became distinct enough to be observed by transmitted light. In the 150°C dwell to 60% conversion, no distinct particles of the appropriate size were formed. This is supported by the transmission electron microscope examination discussed in Chapter 4. The control ramp produced distinct (although irregular and interlocked) particles of 0.5 - 1.0 microns in diameter. The 150°C dwell produced very small particles, under 0.25 microns with possible phase mixing. The separation was also reflected in the dielectric permittivity measurements, although the permittivity

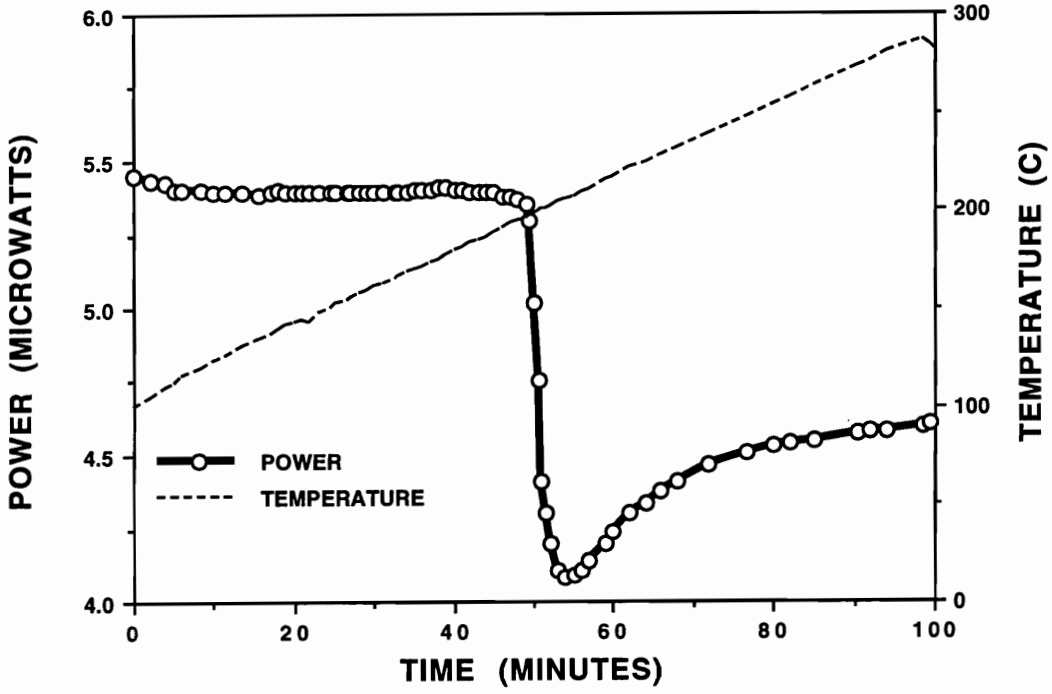

Figure 5.15. Optical Transmission at 650 nm during 2°C/minute Processing Cycle (Toughened Cyanate).

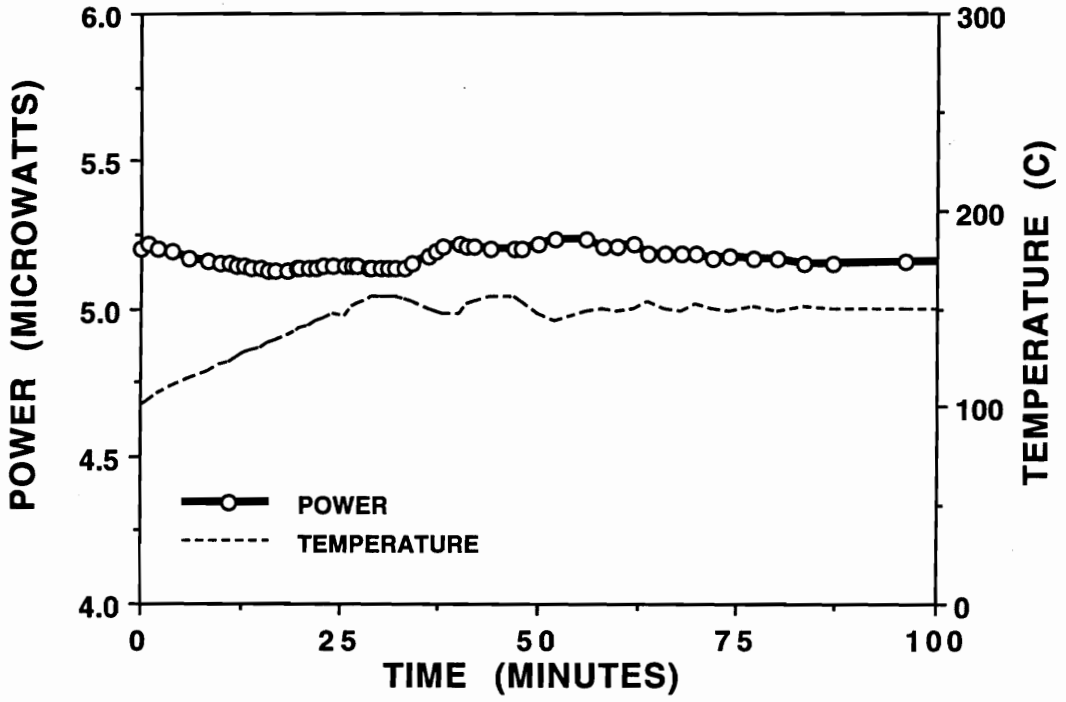

Figure 5.16. Optical Transmission at 650 nm for Processing Cycle with 150°C Dwell to 60% Conversion (Toughened Cyanate).

appears to be sensitive to earlier phase separation than transmitted light.

The preferred way to examine early phase separation (with light) would be low angle light scattering using a laser rather than white light source. A fiber optic sensor design was shown in Chapter 2 which was referred to as suitable for scattering experiments. This had a T-shaped groove with the fiber going to the detector at 90 degrees to the incoming light. Turbidity and cloud point measurements tend to look at scattering at 90 degrees. The 90 degree configuration was evaluated as the toughened resin was ramped a 2°C /minute. The Nicolet 800 tungsten halogen light source was not intense enough at a 90 degree scattering angle to detect anything but noise. Although there is a He-Ne laser used in the alignment procedures of there spectrometer, the amount of laser light goes into the sample chamber was very, very weak and not detectable. The ideal arrangement would be to have a lower angle (> 90 degrees) between the incoming light and the detector with either a stronger light source or a dedicated laser and/or a more sensitive detector. For simultaneous chemical and physical determinations, one would want to use the spectrometer white light source.

Combining these three sensors should provide simultaneous, real-time, in-situ monitoring of chemical and physical changes during the cure of a toughened or untoughened thermosetting resin. The inclusion of such a sensor would facilitate processing decisions and provide multiple feedback for computerized "smart" or expert systems. Using a 3 cm x 3 cm x 0.25 cm piece of aluminum in the appropriate position in a mold one could potentially, combine all these sensors. The 0.38 mm (wide) x 0.5 mm (deep) straight groove could be machined into the plate as described in Chapter 2. By obtaining integrated peak areas and peak locations, information on chemical reaction, temperature, T_g of the cured resin, and possibly phase separation can be obtained. Using the white light source, the chemical reaction could be monitored in the near-infrared with the spectrometer. Although gelation cannot be measured directly as a

physical event, the conversion at which gelation occurs can be calculated (and has been for many resins) or measured. This data can be used with the real-time conversion information as in Chapter 4. For the cyanate resin, as discussed in Chapter 3, the temperature could potentially be calibrated by the peak shift of the aromatic (backbone) peak at 4675 cm-1. Many high performance resins contain such aromatic ring structures in the backbone. Since the changes in the peak location are actually due to the changes in the density of the resin, a suitable calibration could provide density information. The peak shift at 6900 cm-1, at least phenomenologically, occurs at the same time as the formation of two distinct phases. Not detailed in Chapter 3, although rather obvious for from the discussions, one would expect slope changes or discontinuities as the resin is cooled down if one cures above the T_g or if vitrification is not reached and the resin goes through the T_g on the cool down. It is not known whether the change at "vitrification" during the processing would be too subtle to see or not.

The fiber coming out of the straight groove could multiplexed to a visible light detector. A multi-frequency detector would be preferable; however, a lot of information can be obtained from a fixed frequency visible or near visible detector as used in this study. The production of distinct (in terms of concentration gradients) particles in the latter portions of spinodal decomposition can be detected. The distinct particles produced by a binodal decomposition could be seen when they reach a given size. Particles the size of one micron are large enough to provide some toughening capability; therefore production of this size of particle may be critical in toughening applications. The refractive index of this material changes as it cures and should show a change in the slope or a discontinuity as it goes through T_g, whether this is by vitrification or when cooling. Refractive index is typically measured in the visible spectrum. This change would most likely affect the amount of visible light transmitted as measured by a fixed frequency detector. A multi-frequency detector could provide more information about the

cure chemistry. Most of these resins change color as they cure. The cyanate is initially colorless, becoming deep yellow-to-gold as the crosslinking reaction occurs, indicating that there should be reaction products absorbing in the visible region. Rather than transmission, a low angle or variable angle geometry with a multiplexer could provide information on the onset of phase separation and particle size. The dielectric loss factor would provide vital processing information such as the decrease in viscosity, the minimum viscosity, and vitrification information. The dielectric permittivity data should provide vital information about phase separation, although some of the effects may require computer enhancement.

5.5 CONCLUSIONS AND SUMMARY

Early cure monitoring looked at physical changes and tried to imply the chemistry associated with the changes. The FTNIR fiber optic sensor that has been demonstrated in this manuscript, eliminates the need to "imply" the chemical changes. The chemical changes do not tell the complete story of the curing resins any more than the physical changes did. What is required is a method of real-time simultaneous, in-situ monitoring of the chemical and physical changes. This capability has been successfully demonstrated by combining the FTNIR fiber optic sensor with a Dek Dyne remote microdielectric sensor and/or a multiplexing the light coming out of the fiber optic sensor to the FTNIR detector as well as a visible light detector. With this combination, one can potentially determine degree of conversion, gelation (as a constant degree of conversion), temperature, density, phase separation, vitrification, and (at least qualitatively) the viscosity changes. The dielectric technique seems more sensitive to the early phase separation while the optical techniques (transmission or peak shifts) seem more sensitive to the latter portions of the spinodal decomposition.

5.6 REFERENCES

5-1. P. R. Ciriscioli and G. S. Springer, 34th International SAMPE

Symposium, May 8th, p. 312-322 (1989).

5-2. G. Banhegy, P. Hedvig, S. Petrovic, and F. E. Karasz, Polym.-Plast. Tech. Eng., 30(2&3), 183 - 225 (1991).

5-3. N. F. Sheppard, Jr. and S. D. Senturia, Office of Naval Research, Contract N00014-84-K-0274, Task No. NR 039-260, Technical Report #3 (8/23/85).

5-4. Office of Naval Research, Contract N00014-84-K-0274, Task No. NR 039-260, Technical Report #4 (10/7/85).

5-5. Office of Naval Research, Contract N00014-84-K-0274, Task No. NR 039-260, Technical Report #5 (8/18/86).

5-6. S. A. Bidstrup, N. F. Sheppard. Jr., and S. D. Senturia, same contract, #6, 910/15/86).

5-7. W. W. Bidstrup and S. D. Senturia, same contract, #7, (11/15/86).

5-8. S. A. Bidstrup, N. F. Sheppard, Jr., and S. D. Senturia, same contract, #8, (11/15/86).

5-9. M. G. Allen and S. D. Senturia, same contract, #9, (11/15/86).

5-10. W. W. Bidstrup, S. A. Bidstrup, and S. D. Senturia, same contract, #10 (10/30/87).

5-11. D. R. Day, D. D. Sheppard, and A. S. Wall, 33rd International SAMPE Symposium, p. 603-613 (1988).

5-12. D. Kranbeuhl, D. Eichinger, D. Rice, H. Tulley, and J. Koury, 34th International SAMPE Symposium, p. 79 (1989).

5-13. "Principles of Dielectrometry," Micromet technical brochure.

5-14. Micromet Library Listing

5-15. "Review of Microdielectrometry," Micromet Instruments, Inc. User's Training Course -- Day One.

5-16. D. R. Day, "A Guide to the Theory and Operation of Micromet Instruments Low Conductivity Chip Sensor," (3/89).

5-17. D. R. Day, 33rd International SAMPE Symposium, March 7-10, 1988, p 594-601 (1988).

5-18. S. A. Johnson and N. K. Roberts, 34th International SAMPE Symposium, May 8-11, p. 373 - 384 (1989).

5-19. M. A. Zumbrum, "Characterization of Photocurable Networks in Real-Time and Post-Exposure," Dissertation, Virginia Tech, 1990.

5-20. A. M. North, R. A. Pethrink, and A. D. Wilson, Polymer, Vol. 19, August p. 913-922 (1978).

5-21. A. M. North, R. A. Pethrink, and A. D. Wilson, Polymer, Vol. 19, p. 923-930 (1978).

5-22. J. Daly and R. Pethrink, Polymer, Vol. 22, Jan, p. 37-42 (1981).

5-23. J. A. Sayre, R. A. Assink, and R. R. Lagasse, Polymer, Vol. 22, p. 87-94 (1981).

5-24. C.-R. Lin and P.-Y. Hsieh, 35th International SAMPE Symposium, p. 1233-1240 (April 1990).

5-25. G. M. Maistros, H. Block, C. B. Bucknall, and I. K. Partridge, Polymer, Vol. 33, Number 21, p 4471 -4477 (1993).

5-26. A. J. MacKinnon, S. D. Jenkins, P. T. Mcgrail, and R. A. Pethrick, Macromolecules, Vol. 25, 3492-3499 (1992).

5-27. N. F. Sheppard, Jr., Ph.D. Thesis, MIT (1986).

5-28 O. Olabisi, L. M. Robeson, and M. T. Shaw, Polymer-Polymer Miscibility, Academic Press, NY, 1979.

5-29 "Thermoset Process Cures: Controlling End-of-cure with Dielectric Sensors," Micromet Newsletter, Vol. 3, No. 3, Fall 1989.

CHAPTER 6
SUMMARY AND CONCLUSIONS

6.1 SUMMARY OF RESULTS

A practical, durable, inexpensive Fourier transform near infrared (FTNIR) fiber optic sensor was developed. The design was suitable for many applications, The cure of a model toughened cyanate as well as a commercial paste adhesive were followed with this sensor in the near-infrared. A mold was designed to incorporate the fiber sensor for composite application.

The growth of the normalized triazine (crosslink) peak appeared to follow second order kinetics. The normalized triazine peak reflected both chemical and physical changes due to changes in the aromatic reference peak. Analysis of the spectra showed significant changes in the aromatic peak size and location due to physical changes. Changes in peak in benzene peak locations may serve as an internal calibration for temperature and density and reflect the microenvironment of a specific chemical group. Conversion based on a calibrated triazine concentration did not appear to follow second order kinetics.

In-situ real-time monitoring of network formation in the toughened cyanate trapped a series of novel morphologies by intelligent, interactive manipulations of the processing cycles based on real-time conversion data. Extremes in morphology were produced within reasonable cure cycle variations. There is significant potential to intentionally modify the morphology in this system in a manner to customize properties. These changes were also observed in a graphite reinforced laminate.

Simultaneous, in-situ monitoring of chemical and physical changes during the cure of a toughened cyanate were successfully demonstrated using an FTNIR fiber optic sensor in combination with a microdielectric sensor and/or a visible fiber optic sensor. This combination of sensors will allow simultaneous monitoring of degree of cure, gelation, temperature, density, phase separation, vitrification,

and viscosity during cure.

6.2 NOVEL ACHIEVEMENTS

The following advancements have been made in this study:

- The crosslinking of a model dicyanate resin crosslink was monitored in the near-infrared.
- Differences were observed between kinetics based on normalized peak areas and those based on a calibrated triazine concentration.
- Aromatic peaks were observed to change with temperature and environment resulting in both frequency shifts and changes in absorbance.
- An implantable near infrared fiber optic sensor based on a grooved metal plate was designed as a stand alone sensor, as an integral part of a metal mold, and for adhesive test coupon geometries.
- This fiber optic sensor was used to follow the crosslinking of the model toughened resin as well as a commercial adhesive.
- In-situ, real-time monitoring of conversion with the fiber optic sensor was used to induce novel morphologies in the toughened dicyanate.
- Simultaneous in-situ, real-time dielectric and fiber optic spectroscopy were demonstrated to monitor the physical and chemical changes during the cure.
- Physical changes due to phase separation of the resin were observed with the fiber optic assembly by exchanging the near-infrared detector for a visible detector.

6.3 CONCLUSIONS

Cure of thermosetting resins can be monitored in-situ, in real-time with a simple, durable, inexpensive, fiber optic spectroscopic sensor in the near-infrared. This sensor provides sorely needed information to compliment the indirect physical information obtained

by commonly used dielectric cure monitoring. Combined, the techniques provide a much more complete story of the changes occurring during the cure. Neither tells the complete story by itself.

There is a lot of physical information available in the spectra. Analysis of peak shifts and changes in intensity provides a great deal of additional information on the temperature and possibly the environment (phase separation, vitrification, etc.) of the individual groups. These groups do not respond equally to these physical changes. These differences have to be considered during in-situ spectroscopic monitoring.

Simple transmission with fiber optics can provide useful information on phase separation when the wavelength of light is on the order of the size of the particle. In-situ variable angle scattering could provide a great deal more information about the growth of the morphology. In combination with the fiber optic spectroscopy and dielectric, this technique can provide an enormous amount of in-situ, real-time information (not previously available) on the cure of thermosetting resins, especially toughened ones.

The morphology of toughened systems can be intelligently modified based on this feedback. For time-temperature-path-dependent reactions (such as the cure of epoxies, bismaleimides, or certain other addition polyimides) the networks can also potentially be controlled by making the decision to preferentially induce one reaction (such as chain extension) over another reaction (such as crosslinking) based on the chemical changes observed with fiber optics.

With the intelligently induced changes in morphology come the potential for the design of a custom morphology to provide specific mechanical properties as suggested by Ward (4-39). This potential would extend to the design and control of optical and damping properties.

6.4 FUTURE WORK

This study has opened up a number of possibilities for future

work based on the control of the morphology and/or network. Ward has already begun work on the custom mechanical properties (4-39). As mentioned above, this same approach could be adapted to the custom design of optical and/or damping properties.

There is a desperate need for appropriate sensors to monitor the chemical and physical changes during the cure of thermosetting systems. The combined fiber optic/dielectric sensor would offer a wealth of information on the chemical, physical, and optical changes occurring during processing and allow an "intelligent" response to be made in real-time. To date, responses are only being made on very limited data, typically dielectric sensors and thermocouples.

There is a need for the understanding and modeling of the chemical and physical changes and the sensor responses. A lot of what has been observed qualitatively can and should be quantified and appropriate models developed to predict conversion, phase size etc. as a function of time, temperature, or X Y Z location based on the information from the combined sensors.

The fun has just begun!

CHAPTER 7
APPENDIX

Included in the Appendix are additional details on the manufacture of the fiber optic sensor, the Nicolet macro language programs used to obtain and analyze real-time cure data, and examples of the real-time data.

The fiber sensors were relatively easy to prepare. The polyimide coating was burned off in the area to be exposed (about 5-10 seconds with a conventional cigarette lighter). The char was carefully rubbed off with a Q-tip and alcohol. As shown in Figure 7.1 one side of the fiber was taped to a surface with masking tape. The other side is pulled in tension. A diamond scribe is carefully used to nick the exposed region while it is in tension, producing good optical ends. The ends were originally checked under the microscope but with enough experience the quality could be accessed visually.

The size of the metallic plate and groove were discussed in Chapter 2. Figure 7.2 provides further detail on the alignment and mechanical and adhesive restraint on the fibers. After the fibers are cleaned with alcohol, the free ends were inserted into the Nicolet fiber optic adapter. A small (approximately 0.5 inch) piece of capillary tubing was threaded on each sensor end. The tube was pushed back about 1 cm to expose the fiber ends. The fiber ends and tubes were placed in the groove as shown in Figure 7.2. The ends were aligned (gently touching) to maximize the FTIR interferagram. A background spectra was obtained with ends touching. The fibers were pulled back to give a 1-2 mm gap for sampling. The capillary tubes were lightly carefully!) crushed with the flat side of a microscope slide to hold the fibers in the groove. Room temperature epoxy was then applied at the intersection of the metal groove and capillary tube and at the exterior (not on the plate) intersection of the tube and fiber. The adhesive was allowed to cure at room temperature and then slowly ramped to 20°C above the expected testing temperature.

A number of Nicolet programming macros were written and revised over the course of the project. These macros are given in Tables 7.1 - 7. 6. Sample real-time conversion data from a 2 C/minute ramp is given in Table 7.7.

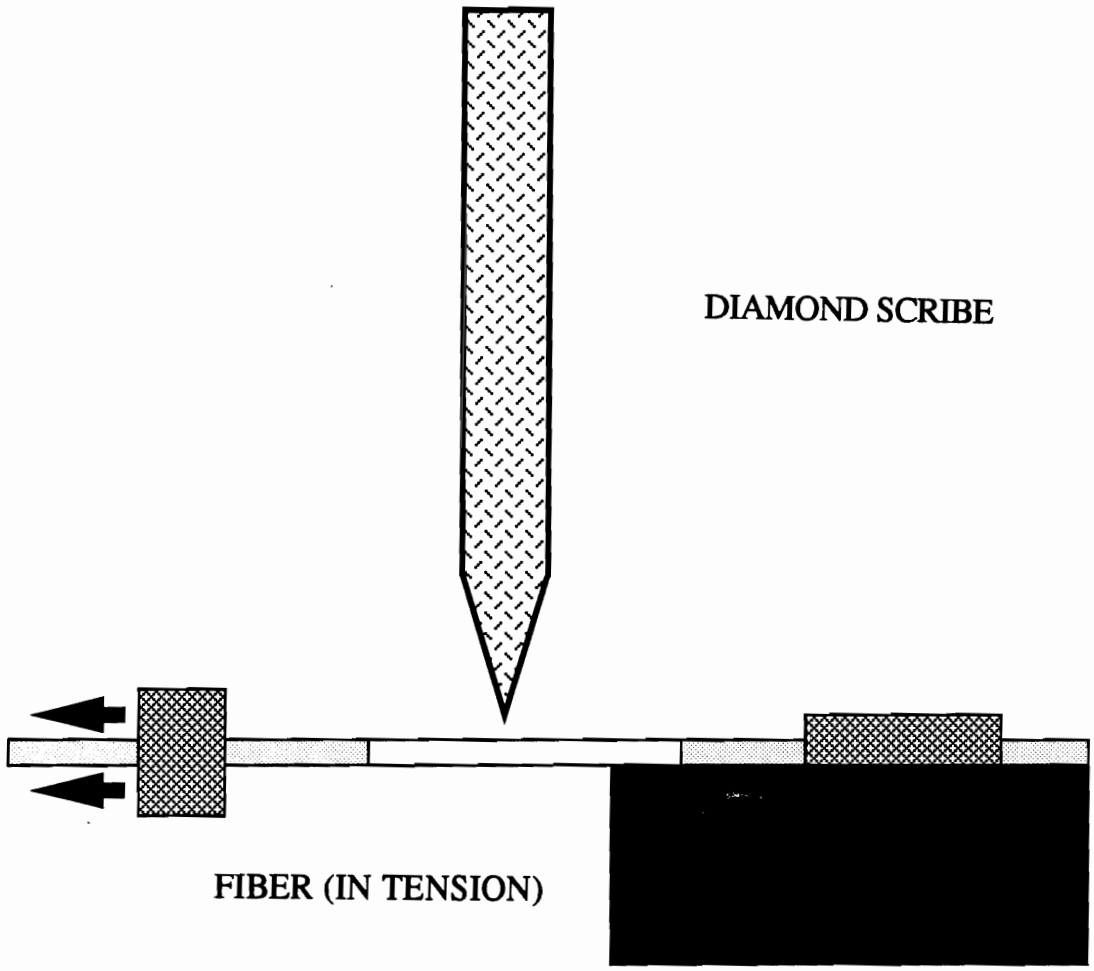

Figure 7.1 Preparation of optical ends for low-hydroxyl silica glass fiber optic.

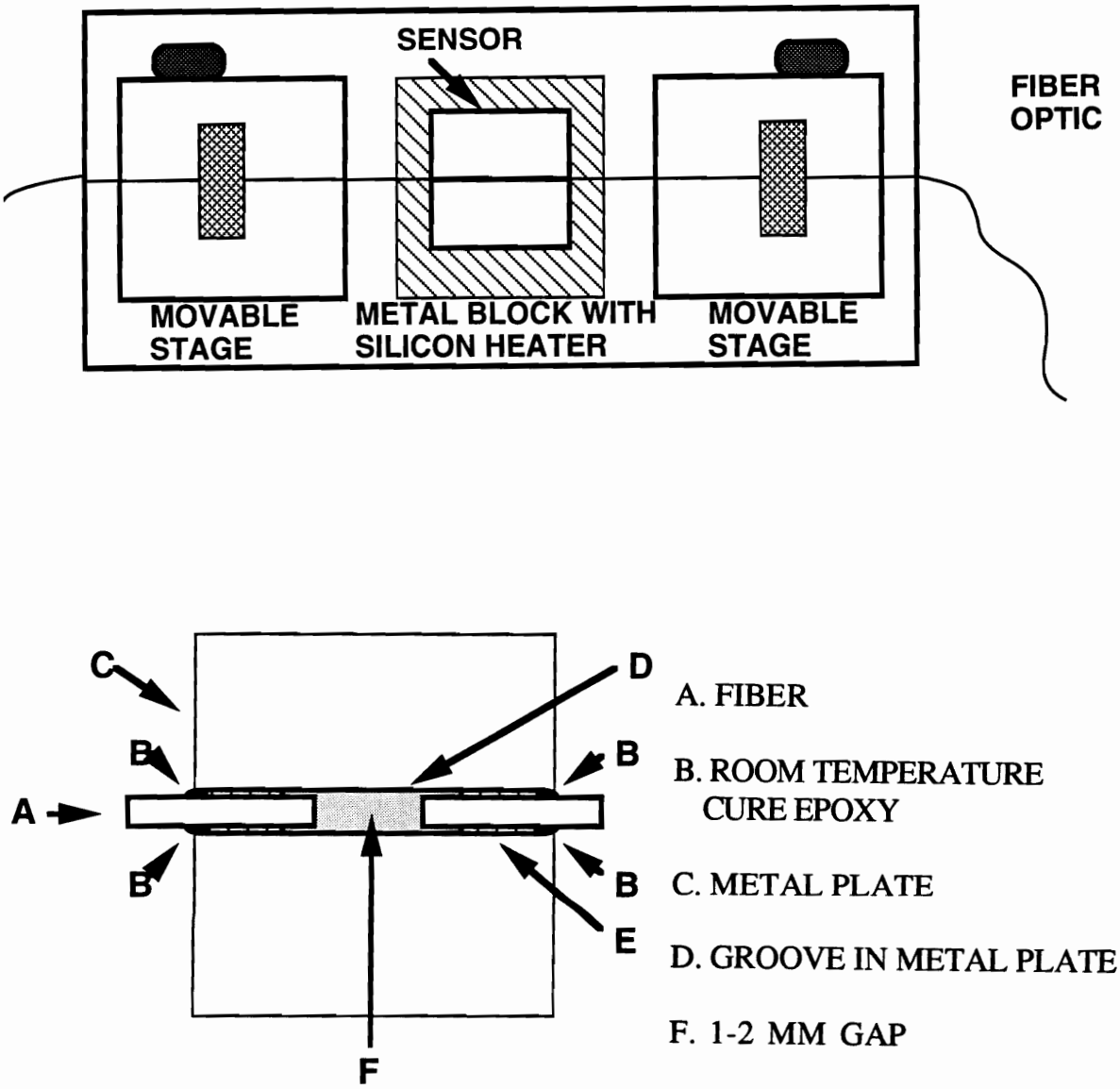

Figure 7.2 Mechanical and adhesive fastening of fiber optic in sensor.

Table 7.1 Nicolet Macro Language Program for Real-Time Data Analysis and Transfer to Compaq 386/40 (Normalized Triazine and Normalized Conversion).

```
OMD
ENTER # OF SCANS PER MEASUREMENT:
NSD
OMD
THIS MACRO TAKES APPROX 1 MEASUREMENT PER 1-1.5 MIN
OMD
TO CHANGE TIME, CHANGE VI0 IN MACRO
OMD
ENTER TOTAL # OF MEASUREMENTS:
QIT
OMD
ENTER STARTING FILE TO STORE DATA:
DFN
OMD
ENTER BACKGROUND FILE:
BFN
VI1=DFN
FORIII=1TILQIT
SCD
RAD
ABD
JC4
BAS=NO
FXF=4790
LXF=4645
SMD
VF0=FCD
FXF=4645
LXF=4580
SMD
VF1=FCD/VF0
VF2=VF1-0.41
VF3=VF2/0.34
M01
PRN DFN
STD
PRN VF1
PRN VF3
OMD
--------
M01
VI0=100
TEM=11
NPR
DFN=DFN+1
NXTIII
END
```

Table 7.2 Nicolet Macro Language Program for After the Fact Data Transfer to Compaq 386/40 (Normalized Triazine and Normalized Conversion

```
OMD
DATA TRANS TO COMPAQ
ENTER STARTING FILE:
SRT
OMD
ENTER ENDING FILE:
QIT
DFN=SRT
FOR III=SRT TIL QIT
BAS=NO
FXF=4790
LXF=4645
SMD
VF0=FCD
FXF=4645
LXF=4580
SMD
VF1=FCD/VFO                    (1)
VF2=VF1-.42
VF3=VF2/0.32
M01
PRN DFN
STD
PRN VF1                        (2)
PRN VF3                        (3)
OMD
----------
M01
DFN=DFN+1
NXT III
END
```

"0.42" is the normalized, integrated shoulder area at 104°C
"0.32" is the difference between the normalized, integrated area at 104° C and that at 270°C during a 2 C/minute ramp.

Table 7.2. Cont'd.

To get areas of triazine peak and benzene peak, make the following substitutions:

Substitute VF1=FCD at (1)
Substitute PRN VF0 at (2)
Substitute PRN VF1 at (3)

Table 7.3 Nicolet Programming Language Macro for Near-Infrared Baseline Correction

```
RFN=4
FCR=1
FCS=1
FXF=9100
LXF=3845
OMD
AUTOBASELINE 9100 TO 3845
SRT
QIT
TEM=DFN
DFN=SRT
FOR III=SRT TIL QIT
PRN DFN
OFN=DFN
MOR
DFN=RFN
XSP=9100
XEP=6400
SLG
XSP=6400
XEP=5500
SLG
XSP=5430
XEP=5160
SLG
XSP=5160
XEP=4930
SLG
XSP=4930
XEP=4784
SLG
XSP=4784
XEP=4510
SLG
XSP=4510
XEP=3948
SLG
XSP=3948
XEP=3957
SLG
XSP=3957
XEP=3845
SLG
SFN=OFN
DIF
DSS
DFN=OFN+1
NXT III
DFN=TEM
END
```

Table 7.4 Nicolet Programming Language Macro for Real-Time Near-Infrared Baseline Correction (called out as "JC4")

```
FCR=1
FCS=1
FXF=9100
LXF=3845
TEM=DFN
RFN=4
OFN=DFN
MOR
DFN=RFN
XSP=9100
XEP=6400
SLG
XSP=6400
XEP=5500
SLG
XSP=5430
XEP=5160
SLG
XSP=5160
XEP=4930
SLG
XSP=4930
XEP=4784
SLG
XSP=4784
XEP=4510
SLG
XSP=4510
XEP=3948
SLG
XSP=3948
XEP=3957
SLG
XSP=3957
XEP=3845
SLG
SFN=OFN
DIF
DSS
XSP=6400
XEP=3900
DFN=TEM
ASD
DSD
END
```

Table 7.5 Nicolet Programming Language Macro to Turn Printer On or Off (called out as "M01")

This macro is included in the preprogrammed Nicolet Macro Library as M01 and, therefore was not listed.

Table 7.6 Nicolet Programming Language Macro for Mid-InfraRed Baseline Correction

```
RFN=4
FCR=1
FCS=1
FXF=4000
LXF=772
OMD
AUTOBASELINE 4000 TO 800
SRT=31
QIT=105
TEM=DFN
DFN=SRT
FOR III=SRT TIL QIT
PRN DFN
OFN=DFN
MOR
DFN=RFN
XSP=3802
XEP=3216
SLG
XSP=3216
XEP=2770
SLG
XSP=2770
XEP=2495
SLG
XSP=2495
XEP=2114
SLG
XSP=2114
XEP=1843
SLG
XSP=1843
XEP=1704
SLG
XSP=1704
XEP=1430
SLG
XSP=1430
XEP=1035
SLG
XSP=1035
XEP=996
SLG
XSP=996
XEP=899
SLG
XSP=899
XEP=772
SLG
SFN=OFN
DIF
DSS

DFN=OFN+1
NXT III
DFN=TEM
END
```

Table 7.7 Real-Time Data Obtained During a 2°C/Minute Cure Ramp

	TIME (MIN)	NORM TRIAZ	REL. CONV.	TOOL TEMP (C)
1	0.000	0.394	-0.046	100.000
2	0.850	0.409	-0.004	100.000
3	1.733	0.399	-0.032	100.000
4	2.600	0.388	-0.065	100.366
5	3.450	0.395	-0.045	101.999
6	4.317	0.423	0.037	103.663
7	5.200	0.404	-0.017	105.360
8	6.067	0.404	-0.018	107.025
9	6.917	0.409	-0.003	108.658
10	7.800	0.416	0.016	110.355
11	8.667	0.422	0.036	112.020
12	9.517	0.406	-0.013	113.653
13	10.400	0.391	-0.054	115.349
14	11.283	0.408	-0.006	117.046
15	12.167	0.426	0.047	118.743
16	13.033	0.399	-0.033	120.408
17	13.883	0.437	0.080	122.041
18	14.750	0.419	0.026	123.706
19	15.633	0.441	0.091	125.403
20	16.500	0.416	0.019	127.067
21	17.367	0.426	0.048	128.732
22	18.217	0.429	0.055	130.365
23	19.083	0.428	0.054	132.030
24	19.967	0.426	0.046	133.727
25	20.833	0.443	0.098	135.392
26	21.700	0.422	0.034	137.057
27	22.550	0.433	0.068	138.690
28	23.417	0.411	0.002	140.354
29	24.300	0.414	0.013	142.051
30	25.167	0.430	0.060	143.716
31	26.017	0.421	0.032	145.349
32	26.883	0.435	0.074	147.014
33	27.767	0.411	0.004	148.711
34	28.633	0.442	0.093	150.376
35	29.483	0.417	0.019	152.008
36	30.367	0.433	0.069	153.705
37	31.233	0.445	0.103	155.370
38	32.100	0.451	0.120	157.035
39	32.950	0.447	0.108	158.668
40	33.817	0.456	0.136	160.333

Table 7.7 Continued

	TIME (MIN)	NORM TRIAZ	REL. CONV.	TOOL TEMP (C)
41	34.683	0.419	0.027	161.998
42	35.583	0.453	0.126	163.727
43	36.450	0.438	0.082	165.392
44	37.333	0.440	0.087	167.088
45	38.200	0.459	0.143	168.753
46	39.067	0.449	0.115	170.418
47	39.950	0.446	0.106	172.115
48	40.817	0.451	0.120	173.780
49	41.683	0.456	0.134	175.445
50	42.567	0.432	0.066	177.142
51	43.433	0.431	0.061	178.806
52	47.350	0.459	0.143	186.330
53	48.217	0.476	0.193	187.995
54	49.083	0.464	0.159	189.660
55	49.933	0.466	0.164	191.293
56	50.800	0.493	0.243	192.958
57	51.683	0.478	0.199	194.655
58	52.550	0.480	0.205	196.320
59	53.417	0.496	0.253	197.984
60	54.267	0.493	0.243	199.617
61	55.150	0.488	0.231	201.314
62	56.017	0.497	0.255	202.979
63	56.883	0.480	0.206	204.644
64	57.733	0.513	0.304	206.277
65	58.617	0.529	0.351	207.974
66	59.483	0.538	0.377	209.638
67	60.350	0.533	0.363	213.593
68	61.200	0.559	0.439	214.525
69	62.083	0.558	0.435	215.665
70	62.950	0.552	0.418	216.687
71	63.817	0.589	0.526	217.747
72	64.667	0.605	0.575	218.553
73	65.550	0.614	0.600	219.571
74	66.417	0.616	0.607	220.473
75	67.283	0.621	0.620	221.347
76	68.150	0.647	0.697	222.192
77	69.017	0.648	0.701	223.082
78	69.867	0.659	0.732	223.785
79	70.733	0.639	0.672	224.476
80	71.617	0.675	0.781	225.300
81	72.483	0.649	0.703	226.010
82	73.350	0.687	0.816	226.696
83	74.217	0.687	0.815	227.431
84	75.067	0.679	0.793	227.905

Table 7.7 Continued

	TIME (MIN)	NORM TRIAZ	REL. CONV.	TOOL TEMP (C)
85	75.950	0.688	0.819	228.603
86	76.817	0.695	0.838	229.191
87	77.683	0.699	0.851	229.833
88	78.533	0.697	0.844	230.288
89	79.400	0.705	0.867	230.731
90	80.283	0.690	0.823	231.317
91	81.150	0.693	0.831	231.794
92	82.017	0.691	0.827	232.250
93	82.883	0.692	0.828	232.765
94	83.733	0.698	0.847	233.094
95	84.600	0.689	0.821	233.412
96	85.483	0.700	0.853	233.877
97	86.350	0.709	0.880	234.236
98	87.217	0.707	0.875	234.658
99	88.067	0.700	0.852	234.895
100	88.933	0.699	0.849	235.121
101	89.817	0.695	0.838	235.498
102	90.683	0.710	0.882	235.772
103	91.550	0.703	0.861	236.031
104	92.417	0.712	0.889	236.357
105	93.267	0.708	0.876	236.415
106	94.150	0.700	0.854	236.717
107	95.017	0.692	0.830	236.834
108	95.900	0.712	0.889	237.108
109	96.767	0.694	0.837	237.283
110	97.633	0.705	0.869	237.445
111	98.500	0.706	0.870	237.679
112	99.350	0.710	0.884	237.731
113	100.217	0.727	0.932	237.859
114	101.083	0.715	0.897	237.891
115	101.967	0.714	0.894	238.086
116	102.833	0.722	0.919	238.183
117	103.700	0.711	0.885	238.000
118	104.567	0.712	0.887	239.000
119	105.417	0.713	0.891	239.000
120	106.283	0.710	0.881	239.000
121	107.150	0.716	0.901	239.000
122	108.000	0.729	0.938	240.000
123	108.867	0.729	0.938	240.000
124	109.750	0.722	0.919	240.000
125	110.617	0.724	0.922	240.000

Table 7.7 Continued

	TIME (MIN)	NORM TRIAZ	REL. CONV.	TOOL TEMP (C)
126	111.483	0.723	0.920	241.000
127	112.350	0.728	0.936	241.000
128	113.200	0.719	0.910	241.000
129	114.067	0.712	0.888	242.000
130	114.933	0.725	0.927	242.000
131	115.783	0.737	0.963	242.000
132	116.650	0.723	0.922	243.000
133	117.517	0.714	0.894	243.000
134	118.367	0.723	0.920	243.000
135	119.233	0.727	0.932	244.000
136	120.100	0.717	0.902	244.500
137	120.967	0.719	0.910	244.795
138	121.817	0.718	0.907	244.846
139	122.683	0.734	0.953	244.898
140	123.550	0.739	0.968	244.949
141	124.417	0.728	0.935	245.000
142	125.283	0.734	0.952	245.051
143	126.133	0.711	0.886	245.100
144	127.000	0.738	0.964	245.150
145	127.867	0.736	0.959	245.200
146	128.733	0.727	0.933	245.250
147	129.583	0.734	0.952	245.298
148	130.467	0.707	0.874	245.347
149	131.350	0.724	0.924	245.397
150	132.217	0.728	0.934	245.445
151	133.100	0.730	0.943	245.494
152	133.983	0.722	0.917	245.542
153	134.850	0.731	0.945	245.590
154	135.733	0.702	0.858	245.638
155	136.600	0.724	0.922	245.684
156	137.483	0.722	0.916	245.731
157	138.367	0.727	0.931	245.778
158	139.233	0.732	0.948	245.824
159	140.100	0.732	0.948	245.870
160	140.967	0.718	0.907	245.915
161	141.817	0.719	0.908	245.959
162	142.683	0.727	0.933	246.003
163	143.567	0.733	0.951	246.048
164	144.433	0.716	0.899	246.092
165	145.317	0.724	0.923	246.137
166	146.200	0.727	0.932	246.181
167	147.067	0.717	0.902	246.224
168	147.983	0.710	0.882	246.269

VITA

Janis Michelle Brown was born in Dallas, Texas on April 13, 1955, the only child of Patsy and Bill Brown. Janis was valedictorian of her high school class and graduated from the University of Texas at Arlington in May 1977 with a Bachelor of Science in Chemistry. Immediately after finishing her B.S., she began night school at that university working on her M.S. in Chemistry which she completed in May 1983. Janis tried several jobs right out of school, but eventually settled down at General Dynamics/Ft. Worth Division, where she spent ten years in a Materials and Processes Group. Before taking academic leave from GDFW, she was an engineering specialist with a variety of responsibilities including evaluating conventional composites for hypervelocity applications and high temperature organic matrix composites for airframe applications. With her background in chemistry and characterization, her favorite part of working with the composites were the structure-property and processing-property relationships. She has extended that work here at Tech in her research of the use of cure monitors in toughened systems. Janis has recently accepted a job with Hughes Missile Systems Company in Tucson, Arizona.

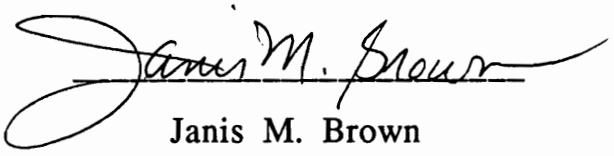

Janis M. Brown